

AN INTERNALLY REFERENCED LEAKY WAVEGUIDE SENSOR FOR  
MONITORING OF PH

THOMAS WENSLEY

A thesis submitted to the University of Birmingham for the degree of

DOCTOR OF PHILOSOPHY

School of Chemistry

College of Engineering and Physical Sciences

University of Birmingham

November 2022

UNIVERSITY OF  
BIRMINGHAM

**University of Birmingham Research Archive**

**e-theses repository**

This unpublished thesis/dissertation is copyright of the author and/or third parties. The intellectual property rights of the author or third parties in respect of this work are as defined by The Copyright Designs and Patents Act 1988 or as modified by any successor legislation.

Any use made of information contained in this thesis/dissertation must be in accordance with that legislation and must be properly acknowledged. Further distribution or reproduction in any format is prohibited without the permission of the copyright holder.

# ABSTRACT

Leaky waveguide (LW) sensors have the potential to offer label-free, low-cost and long-term continuous monitoring of pH, particularly in situations in which contaminants or additives may hinder sensor functionality or where maintenance is difficult. The pH of water supply and wastewater treatment affects a range of industrial, household and environmental factors, and one of its requirements is compatibility with the presence of free chlorine. In this project, a polyion hydrogel sensor for near-neutral pH detection is developed, additionally incorporating a compatible, chemically inert waveguide for common-path, automatic internal referencing and correction for matrix effects.

To meet this need, leaky waveguides (LW) were developed from porous polyacrylamide hydrogels. Fabrication of the sensor hydrogel from linear polymer or dissolved monomer were shown to provide suitable LWs of mesoporous structure and refractive index sensitivities in the 130-150 degrees per refractive index unit (RIU) range. Fresnel diffraction was also observed around the leaky mode. Addition of ionisable copolymers to the gel were shown to provide pH-dependent swelling detectable by monitoring of the leaky mode, and a linear range of up to 5 pH units was demonstrated.

Additionally, a polysaccharide-based sensor design was constructed using agarose and chitosan as respective pH-inert and -sensitive polymers. Multi-layered waveguides capable of sustaining independent leaky modes were produced by sequential deposition of the polysaccharides. A combined, common-path LW sensor, one of the first of its kind, was produced and a sensitivity of 0.280 degrees/pH unit and a typical linear range of pH 4-8 demonstrated. By substituting agarose for linear polyacrylamide, a sensitivity of 0.273 degrees/pHU was achieved.

A fully synthetic waveguide was developed through incorporation of *N,N*-dimethylamino moieties into the hydrogel using an acrylate and acrylamide comonomer as the linking group. The former provided superior initial sensitivity at 0.132 degrees/pHU and a neutral pH range suitable for environmental monitoring but suffered from leaching and degradation while in prolonged use. The acrylamide comonomer provided a stable pH-sensitive waveguide of sensitivity 0.091 degrees/pHU and a typical linear range of pH 4-8. Easier incorporation of the latter comonomer indicates the acrylate monomer forms crosslinked microparticles during polymer formation.

For the first time, multi-layered synthetic waveguides for pH sensing were then produced by adapting the method for polysaccharide waveguides, with deposition of linear polyacrylamide onto a cast waveguide of higher density. The internally referenced sensor retains a pH sensitivity of 0.091 degrees/pHU, and a tested range of pH 4-8. Sensitivity to selected interferants was also assessed for both single-layer and internally referenced dimethylamino-bearing leaky waveguides. In both states the sensor was shown to be susceptible to dye staining and interference from monovalent salt solutions but effectively eliminated nonspecific interactions.

# ACKNOWLEDGEMENTS

I would like to thank my supervisor Ruchi Gupta for her advice and support, and for the opportunity to work at a postgraduate level. The only reason I was able to work on this project is because she saw promise in an undergrad. This project would never have been possible without generous funding from the EPSRC and Process Instruments Ltd. In addition, PI's Craig Stracey and especially Nick Goddard offered advice, technical support, much of the special software used in the project, and the occasional reality check in pre-Covid times. Ultimately our whole research group has a lot to thank Nick for over the past few years.

My sincerest thanks go to the members of Gupta Group for numerous shared hardships of the waveguide and interferometer variety. I would especially like to thank Elisabetta Labella for her optimism and professionalism, Nicola Toole and Hazel Dixon for letting me lean on their chitosan expertise when synthetic polymers were failing us, and postdoctoral researchers Firoj Ali, Anil Pal and Sameh el Sayed for their steady support and practical advice when I needed it most. I am also grateful to the AFC staff and the technical and building managers in the School of Chemistry, particularly Trevor Hardy for countless odd-jobs and practical advice around the laboratory.

Special thanks go to numerous friends, both in person and virtual, for being with me in what gradually became a dark period in my life. The ever-wonderful May Roepstorff, to whom I owe everything, and also to Astra, Sam and Laurent for being around from the start and a constant source of creativity, and for being among the first to hear some important news and help me understand what it meant. Delyth, Dan, Joshua, Louen and co for the community I've had the rare privilege of helping them build, and well as their warmth and the unending supply of high-quality art and fox photos. Cosmo and Stirling for both their respect and enthusiasm in countless small ways, even if

they had to fight to understand what everyone else was doing at first. I would also like to thank my many other friends who preferred to stay anonymous in this section – this will result in solitary.

Finally, I cannot begin to express my gratitude to my family. Mum for the dreaded phone calls and always providing a chance to natter, as well as frequent reality checks when I needed them most over the years. Dad and Julia for their selfless and loving help and, knowing what stress can do, always being ready to give me an opportunity to decompress. My brother Matthew (ooh look a bear!), whose honest and rational advice I can always count on. My grandfather Eric for his patience and kind words. And finally, my grandparents Derek and Gerry Wensley, who together remain the model of faith and kindness I try to aspire to.

And lastly, to almighty God, before whom all of my best efforts equate to nothing but whose selfless love has touched me nonetheless.

# TABLE OF CONTENTS

Chapter 1. Introduction and Literature Review.....	19
1.1. Introduction .....	19
1.2. Optical Sensors.....	21
1.2.1. Examples of Optical Sensors .....	22
1.2.2. Developments of Interest .....	25
1.3. Free Chlorine Sensors .....	27
1.4. Chlorine Sensors in the Literature .....	29
1.4.1. Issues with Chlorine Detection .....	32
1.4.2. The Traditional Methods for Chlorine Detection.....	32
1.4.3. Electrochemical Chlorine Detection.....	34
1.4.4. Optical Chlorine Detection .....	35
1.5. pH Sensors.....	38
1.6. pH Sensors in the Literature .....	40
1.6.1. Means of Sensing pH.....	45
1.6.2. pH-Sensitive Dyes.....	46
1.6.3. Fluorescent pH Sensors.....	48
1.6.4. Chemomechanical pH Sensors.....	49
1.7. Project specification and objectives .....	53
1.8. Thesis Outline.....	54
Chapter 2. Theory of Waveguide Optics .....	55
2.1. Introduction .....	55
2.2. Optical Waveguides .....	55
2.2.1. Refraction and Snell's Law .....	55
2.2.2. The Guided Mode .....	58
2.3. Maxwell's Equations .....	60
2.3.1. Underpinning Equations .....	61
2.3.2. Arrangements of Maxwell's Equations .....	67
2.3.3. Electromagnetic Waves.....	71
2.4. Optical Waveguides and Related Phenomena.....	73
2.4.1. The Goos-Hänchen Effect.....	73
2.4.2. The Evanescent Field.....	74
2.4.3. Surface Plasmon Resonance .....	75
2.4.4. Fresnel Reflections and the Leaky Waveguide .....	76
2.5. Summary .....	79
Chapter 3. Preliminary Studies for the Synthesis of pH-Sensitive Reference Hydrogel Waveguides ....	80
3.1. Introduction .....	80

3.2.	Casting Methodology and Assay .....	80
3.2.1.	Chemicals and Materials .....	81
3.2.2.	Experimental Procedure .....	81
3.2.2.1.	The Leaky Waveguide Testing Apparatus .....	82
3.2.2.2.	Cast Production .....	84
3.2.2.3.	Metal-Clad Leaky Waveguides (MCLW) .....	88
3.2.2.4.	Waveguide Operation and Testing .....	88
3.2.3.	Results and Discussion (Casting) .....	90
3.2.3.1.	Leaky Waveguide Production .....	90
3.2.3.2.	Refractive Index Sensitivities of Cast Films .....	94
3.2.3.3.	Porosities of Cast Films .....	95
3.3.	Linear Polymer Production and Characterisation .....	98
3.3.1.	Chemicals and Materials .....	98
3.3.2.	Experimental Procedure .....	99
3.3.3.	Results and Discussion .....	102
3.3.3.1.	Production and Testing of Spincoated Waveguides .....	104
3.3.3.2.	RI Sensitivity of Spincoated Waveguides .....	106
3.3.3.3.	Porosity and Other Tests for Spincoated Waveguides .....	108
3.4.	pH Sensitivity of Waveguides .....	110
3.4.1.	Chemicals and Materials .....	111
3.4.2.	Experimental Procedure .....	111
3.4.3.	Results and Discussion .....	112
3.4.3.1.	pH Sensitivity of Reference Polymer .....	112
3.4.3.2.	Provision of Acidic Functional Groups .....	114
3.4.3.3.	N-Aminopropyl Methacrylamide Copolymer .....	116
3.4.3.4.	N,N-( Dimethylamino)ethyl Methacrylate Copolymer .....	118
3.4.3.5.	Response Intensity of pH-Sensitive Polymers .....	119
3.5.	Summary .....	120
Chapter 4. pH Sensitivity of Polysaccharide and Internally Referenced Polysaccharide Leaky Waveguides 122		
4.1.	Introduction .....	122
4.2.	Materials .....	123
4.2.1.	Chemicals and Materials .....	123
4.2.2.	Instrumentation .....	124
4.3.	Experimental Procedure .....	124
4.3.1.	Polymer Deposition .....	124
4.3.2.	Sample Preparation .....	127
4.4.	Results and Discussion .....	128



4.4.1.	Single-Layer Agarose Waveguides .....	128
4.4.2.	Single-Layer Chitosan Waveguides .....	132
4.4.3.	Stacked Polysaccharide Leaky Waveguide .....	137
4.4.4.	Internally Referenced pH Sensitivity and Buffer Selection .....	140
4.4.5.	Synthetic Reference Material .....	143
4.4.6.	Summary .....	146
Chapter 5.	Developing Synthetic Leaky Waveguides for pH Sensing .....	147
5.1.	Introduction .....	147
5.2.	Materials and Methods .....	147
5.2.1.	Chemicals and Materials .....	147
5.2.2.	Instrumentation .....	148
5.3.	Experimental Procedure .....	149
5.3.1.	Polymer Casting .....	149
5.3.2.	Sample Preparation and Storage .....	151
5.4.	Results and Discussion .....	152
5.4.1.	Optimisation of DMAEMA .....	152
5.4.2.	Sensor Longevity .....	159
5.4.2.1.	Understanding Sensitivity Loss .....	160
5.4.3.	Adopting DMAPMAM .....	161
5.4.3.1.	Longevity and Repeatability .....	166
5.4.3.2.	Sensitivity with Buffer Strength .....	169
5.4.4.	Effects of Interferants .....	170
5.5.	Summary .....	179
Chapter 6.	An Internally Referenced Synthetic Leaky Waveguide .....	180
6.1.	Introduction .....	180
6.2.	Materials .....	181
6.2.1.	Chemicals and Materials .....	181
6.2.2.	Instrumentation .....	181
6.3.	Experimental Procedure .....	182
6.3.1.	Polymer Casting .....	182
6.3.2.	Sample Preparation .....	183
6.4.	Results and Discussion .....	184
6.4.1.	Stacked co-DMAPMAM Waveguide Fabrication .....	185
6.4.2.	pH Sensitivity of Stacked Sensor .....	188
6.4.3.	Internal Referencing and Eliminating RI Interference .....	191
6.4.4.	Chemical Interferants .....	192
6.5.	Summary .....	198
Chapter 7.	Conclusions and Future Work .....	200

7.1.	Introduction .....	200
7.2.	Conclusion.....	200
7.3.	Future Work .....	203
7.3.1.1.	References .....	207

# LIST OF FIGURES

Figure 1.1 - N,N-Diethyl-p-phenylenediamine, a common free chlorine sensitive dye.....	33
Figure 1.2 - o-phenylenediamine, a free chlorine sensitive dye related to DPD (above). .....	34
Figure 1.3 - Sample dye structures. a: phenolphthalein, a phthalide dye. b: pararosaniline, a triarylmethane dye. c: fluorescein, a fluoran dye. d: methyl red, an azo dye. ....	47
Figure 1.4 - Fluorescein isothiocyanate (FITC), a common pH-sensitive fluorescent dye. ....	49
Figure 2.1 - refraction occurring where $n_1 < n_2$ . Note the shortening of apparent wavelength as the ray enters the denser medium. ....	57
Figure 2.2 - model of Colladon and Tyndall's demonstrations of a waveguide. The light angle exceeds $\theta_C$ at each boundary, resulting in reflection that guides the light ray down the waterspout.....	58
Figure 2.3 - Constructive interference of a guided mode, with emphasis on wavefronts. For purposes of illustration, the effects of $\phi$ have been disregarded for this cartoon. ....	60
Figure 2.4 – Demonstrations of the dependence of the cross-section of an area intersecting an magnetic field undergoing flux, upon the emf experienced upon that area. ....	63
Figure 2.5 - Visualisation of spatial terms used in Equation 2.8, specifically closed loop C, open area A and the vector from the surface $dS$ .....	65
Figure 2.6 - Left: Visualisation of spatial terms used in Equation 2.11, specifically closed loop C, open area A and the vector from the surface $dS$ . Right: The same conditions when applied to one half of a charging capacitor. Note the presence of a B field between the capacitor. ....	66
Figure 2.7 – Visualisation of electromagnetic wave, travelling in direction x, with transverse E and B.....	72
Figure 2.8 - excerpt from the original paper, <sup>149</sup> showing displacement of the reflected light (T). In the above equation, $\Delta x$ represents distance of displacement QS.....	74
Figure 2.9 - Demonstration of Fresnel reflection. As incident angle increases, a greater proportion of light is reflected, and the blue/yellow chequered pattern becomes more clearly visible. Inset: a cartoon of Fresnel reflection. A broader line indicates a greater relative proportion of the incident light. ....	77
Figure 3.1 - Diagram of leaky waveguide (LW) apparatus. ....	83
Figure 3.2 - Photograph of leaky waveguide apparatus interior while in use. ....	83
Figure 3.3 - Glass functionalisation agents. Allyltrimchlorosilane (ATCS) may bond readily with silanol groups but can polymerise or form multiple layers if an oxygen source is introduced. Chloro(dimethylvinyl)silane (CDMVS) may less efficiently coat a silica surface due to steric hindrance but suffers no risk of multilayers or 3d structures forming. ....	85
Figure 3.4 - The favoured backbone polymer for waveguide production acrylamide, alongside its compatible short-chain crosslinker equivalent methylenebis(acrylamide) (bis).....	86

Figure 3.5 - Ammonium persulphate (APS) and N,N,N',N-tetramethyl ethylenediamine (TEMED), a common pair of activation reagents for free radical polymerisation of acryl-bearing monomers. Upon combination, the persulphate ion cracks the TEMED over the C-C central bond to provide an available free radical.....	86
Figure 3.6 - Casting arrangement for polyacrylamide LW production. ....	87
Figure 3.7 - Cartoon of single-layer cast leaky waveguide layout .....	88
Figure 3.8 - annotated image of a leaky waveguide, taken by attached CCD. ....	91
Figure 3.9 - Cast polyacrylamide waveguides by photoresist spacer of size (a) 5.5 $\mu\text{m}$ , (b) 4.5 $\mu\text{m}$ , (c) 2.0 $\mu\text{m}$ . (d) cast polyacrylamide waveguide by microspheres of median size 1.1 $\mu\text{m}$ . Scale bars are 2° (vertical) and 2cm (horizontal).....	91
Figure 3.10 - Predicted reflection characteristics of waveguide, following data recovered from Figure 3.9d as model. Note the waveguide thickness required to replicate a waveguide fabricated at 1.1 $\mu\text{m}$ thickness. ....	93
Figure 3.11 - Refractive index sensitivities of polyacrylamide cast gels produced with photolithographic or microsphere spacers .....	95
Figure 3.12 - PEG permeation capacity, for polyacrylamide cast gels produced with photolithographic or microsphere spacers. "Normalised response" here means the waveguide response for the indicated polymer as a function of its expected sensitivity by refractive index alone.....	98
Figure 3.13 - Cartoon of spun single-layer waveguide layout .....	100
Figure 3.14 - <sup>1</sup> H NMR spectra of acrylamide copolymers. Solvent peak at 4.7 ppm removed for clarity. (a) Polyacrylamide co-allylamine polymer. (b) Polyacrylamide co-N-aminopropyl methacrylamide polymer. (c) polyacrylamide-(N,N-dimethylamino)ethyl methacrylate copolymer. Presence of broad asymmetric doublets at 1.5 ppm (polymer backbone CH <sub>2</sub> ) and 2.1 (acrylamide CH) indicate acrylamide units; presence of indistinct peak at 1.2 (methyl CH) indicates methacrylate or methacrylamide units.....	103
Figure 3.15 - FTIR spectra of acrylamide homopolymer, plus 30:1 statistical copolymers of, Polyacrylamide co-N-aminopropyl methacrylamide and polyacrylamide-(N,N-dimethylamino)ethyl methacrylate. Spectra are offset to provide legibility.....	103
Figure 3.16 – Photodiode-detection scan of metal-clad leaky waveguides. Enhanced intensity indicates a resonance angle.....	105
Figure 3.17 – waveguide appearance with (a) and without (b) dye addition.....	105
Figure 3.18 - PEG sensitivity of spun polyacrylamide co-allylamine, 250 ppm GA, 4000 rpm spin speed. Calues are calculated by sensitivity relative to glycerol, calculated by response/RI.....	109
Figure 3.19 - retention of bovine serum albumin on spun polyacrylamide gel. Vertical lines represent initiation of buffer wash and the point where all free BSA is evacuated. Subsequent tailing of response represents gradual loss of bound BSA. ....	110
Figure 3.20 - pH response profiles of cast and spun polyacrylamide leaky waveguides. Agarose (from Chapter 4) included for reference. ....	113

Figure 3.21 - Acrylic acid, a pH-responsive acidic monomer very similar in structure to the acrylamide backbone..... 115

Figure 3.22 - Effects of nitrous acid treatment on the pH sensitivity curves of spun polyacrylamide waveguides. Spun polyacrylamide co-acrylic acid included for comparison. Note strength of nitrous acid treatment, given in the legend. .... 116

Figure 3.23 - pH sensitivity curves of spun acrylamide copolymers containing molar ratios of 1/10 acrylic acid, 1/30 N-aminopropyl methacrylamide and 1/30 N,N-(dimethylamino)ethyl methacrylate..... 117

Figure 3.24 - pH-sensitive copolymers N-aminopropyl methacrylamide (NAPMAAm) and (N,N-dimethylamino)ethyl methacrylate (DMAEMA). Note the presence of the ester linkage in the latter, rather than a secondary amide..... 118

Figure 4.1 - Chemical structures of the repeating units of agarose and chitosan. Note the presence of primary amine group in the structure of chitosan..... 122

Figure 4.2 - Cartoon of polysaccharide-based leaky waveguide layouts in this chapter. Single-layer waveguides (a) followed the configuration of spun waveguides in the above chapter. Stacked leaky waveguides (b) use the reference material below – this may be agarose or (later) polyacrylamide. .... 126

Figure 4.3 –Leaky waveguide on glass (left) and metal-clad leaky waveguide (right) for selected agarose reference material. Scale bars are 2° (horizontal) and 2cm (vertical). .... 129

Figure 4.4 - pH sensitivity of agarose reference gel, using MCLW in place of LW..... 130

Figure 4.5 - RI sensitivity of agarose single-layer gel, as determined with glycerol solutions. .... 131

Figure 4.6 - sample image of chitosan waveguide output. Scale bars are 2° (horizontal) and 2 cm (vertical). ..... 133

Figure 4.7 - pH sensitivity of chitosan waveguide..... 134

Figure 4.8- RI sensitivity of chitosan single-layer gel, as determined with glycerol solutions..... 135

Figure 4.9 – Porosity assay, normalised with relative RI sensitivity of single-layer polysaccharide gels to PEG standards as described in Section 3.2.3.3. No negative responses were found, unlike polyacrylamide gels in the previous chapter, indicating a lack of nonspecific absorption between PEG and polysaccharides. .... 136

Figure 4.10 - Output image for agarose-chitosan stacked waveguide. Due to larger area covered by the two modes, the TIR is visible as a straight line at the far left of the image. .... 137

Figure 4.11 – Refractive index sensitivity of the stacked polysaccharide waveguide ..... 138

Figure 4.12 - Porosity assay, with relative RI sensitivity of stacked polysaccharide waveguides to PEG standards..... 139

Figure 4.13 - pH sensitivity of stacked agarose-chitosan stacked waveguide ..... 141

Figure 4.14 - pH sensitivity of stacked agarose-chitosan stacked waveguide with comparative running buffers. Internally referenced ‘difference’ data shown for clarity. .... 143

Figure 4.15 - Sample image of spun polyacrylamide-chitosan waveguide. Scale bars are 2° (horizontal) and 2cm (vertical). .... 144

Figure 4.16 - pH sensitivity of stacked polyacrylamide-chitosan stacked waveguide with comparative running buffers., comparing phosphate buffer (left) and pH-adjusted HEPES buffer (right) solutions. ....	144
Figure 5.1 - Cartoon of cast pH-sensitive leaky waveguide layout used in this chapter. ....	150
Figure 5.2 - Examining possible relationships between total monomer fraction and bisacrylamide content, for co-DMAEMA gels.....	156
Figure 5.3 - Examining possible relationships between total monomer fraction and copolymer ratio, for co-DMAEMA gels .....	156
Figure 5.4 - pH sensitivity curve of co-DMAEMA cast waveguide, formulas 6.4 and 6.5 (defined in description). Note difference in overall response over pH 8-10 range. ....	157
Figure 5.5 - Losing pH sensitivity in co-DMAEMA waveguides through immersion in water.....	159
Figure 5.6 - Appearance of a co-DMAEMA waveguide before (a) and after (b) water immersion. Note the migration of resonance angle from the TIR, and the expanding area of noise in the intervening space. .	160
Figure 5.7 - Prior comonomer (N,N-dimethylamino)ethyl methacrylate (DMAEMA, left) alongside newly introduced monomer N,N-(dimethylamino)propyl methacrylamide (DMAPMAM, right). Note the slightly longer pendant group length along with the switch from ester linkage to an acrylamide linkage similar to the structure of the base polymer.....	162
Figure 5.8 - pH sensitivity slopes for assayed co-DMAPMAM waveguides, ordered in terms of polymer backbone units per dimethyl moiety.....	165
Figure 5.9 - Extended immersion of co-DMAPMAM waveguide under pH 7 running buffer. Bubble in flow cell until approx. 180 minutes. Initial response of 0.0 degrees represents a 10 mM NaCl charging/stabilisation solution applied before the running buffer, in order to ensure proper filling of the delivery capillary tubes and flow cell before data acquisition could begin.....	167
Figure 5.10 - cyclic treatment of waveguide between pH 4 and 7 running buffers, 8 repetitions. Note the reduced apparent response of repetitions 6-7. Initial response of 0.0 degrees represents a 10 mM NaCl charging/stabilisation solution applied before the running buffer, as above. ....	168
Figure 5.11 - pH response of co-DMAPMAM Waveguides at different buffer concentrations.....	169
Figure 5.12 - Selected interferant studies performed upon cast co-DMAPMAM waveguides. Black dot indicates reference material (cast polyacrylamide) ran in parallel. ....	175
Figure 5.13 - Base structure of humic acids, a form of biomolecule associated with soils and tree roots. Note the proliferation of carboxylic groups. ....	178
Figure 5.14 - Waveguide after humic acid treatment. Brown discolouration most visible at original location of flow cell inlet, upper centre of image.....	178
Figure 6.1 - The layout of the DMAm-PAAm stacked leaky waveguide as tested in this chapter.....	187
<i>Figure 6.2 - pH sensitivity curve of internally referenced co-DMAPMAM waveguide .....</i>	<i>189</i>
<i>Figure 6.3 - pH sensitivity curve of waveguide at the pH 6.5-7.5 region .....</i>	<i>189</i>
Figure 6.4 - effect of glycerol-doping pH buffers for co-DMAPMAM stacked waveguides.....	191

Figure 6.5 - Sodium chloride interferent studies performed on (a) internally referenced and (b) separate single-layer leaky waveguides..... 194

Figure 6.6 - Urea interferent studies performed on (a) internally referenced and (b) separate single-layer leaky waveguides. .... 194

Figure 6.7 - Aluminium sulphate interferent studies performed on (a) internally referenced and (b) separate single-layer leaky waveguides..... 195

Figure 6.8 - Calcium chloride interferent studies performed on (a) internally referenced and (b) separate single-layer leaky waveguides..... 196

Figure 6.9 - Humic acid interferent studies performed on (a) internally referenced and (b) separate single-layer leaky waveguides. .... 197

Figure 7.1 - Demonstration of the layout of a hypothetical multianalyte stacked leaky waveguide, using pH and free chlorine sensitivity as model analytes..... 204

# LIST OF TABLES

Table 1.1- selected drinking water quality standards as set by EU Council Directive 98/83/EC, Amended 2005 .....	20
Table 1.2- Selection of chlorine sensors, their working principles and their advantages and disadvantages .....	29
Table 1.3 - Selection of pH Sensors, their working principles and their advantages and disadvantages.....	40
Table 3.1 - Photolithographic spin conditions for cast film fabrication.....	85
Table 3.2 - Hydrodynamic radii of polymers used to probe for waveguide porosity and protein compatibility. ....	89
Table 3.3 – Materials and proportions used in initial linear polymer manufacture, along with.....	101
Table 3.4 – Sensitivities of selected polyacrylamide co-allylamine leaky waveguides. All errors represent 1 standard deviation. ....	107
Table 5.1- Formulation of co-DMAEMA waveguides. A star * indicates a bulk gel formed, but with poor or no shape-retaining ability. ....	153
Table 5.2 - Formulation of co-DMAPMAM waveguides, initial test parameters. A star * indicates a bulk gel formed, but with poor or no shape-retaining ability. A waveguide profile of 'n/a' indicates no waveguide could produced. ....	163
Table 5.3 - Tabulated summaries of the effects of total monomer and DMAPMAM fraction upon the range of sensitivity (a) and the linear sensitivity slope over that range (b). A greener colour indicates more ideal properties, a broader range in table a and greater sensitivity in table b. ....	164
Table 6.1 - Spin characteristics of PAAm reference layer for stacked co-DMAPMAM waveguides. Sample agarose-chitosan waveguide provided as an image comparison. ....	186



# DEFINITIONS AND ABBREVIATIONS

LW	Leaky waveguide
RI	Refractive index
RIU	Refractive index units
pHU	pH units
TOC	Total organic carbon
HPLC	High performance liquid chromatography
DPD	N,N-Diethyl-p-phenylenediamine
RSD	Relative standard deviation
DNA	Deoxyribonucleic acid
QDs	Quantum dots
g-CNQDs	Graphitic carbon nitride quantum dots
SPR	Surface plasmon resonance
FACTS	Free available chlorine test by syringaldazine
FAS	Ferrous ammonium sulphate
SACD	Super audio compact disk
TIR	Total internal reflection
FTIR	Frustrated total internal reflection
TE	Transverse electric polarised light
TM	Transverse magnetic polarised light
Bis	<i>N,N</i> -methylenebisacrylamide
TEMED	<i>N,N,N',N'</i> -tetramethyl ethylenediamine
APS	Ammonium persulphate
APTES	(3-Aminopropyl) triethoxysilane

ATCS	Allyltrichlorosilane
PEG	Poly(ethylene glycol)
CDVMS	Chloro(dimethyl)vinylsilane
CCD	Charge-coupled device
MCLW	Metal-clad leaky waveguide
cryo-SEM	Cryo-Scanning Electron Microscopy
APMA	<i>N</i> -aminopropyl methacrylamide
BSA	Albumin from bovine serum
RB4	Reactive blue 4
DMAEMA, DMA	( <i>N</i> -dimethylamino)ethyl methacrylate
GA	Glutaraldehyde
PAAm	Polyacrylamide
FTIR-ATR	Fourier transform infrared spectroscopy
NMR	Nuclear magnetic resonance
FITC	Fluorescein isothiocyanate
$pK_a$ , $pK_aH$	Acid dissociation constant, the $pK_a$ of conjugate acid
PAAm-Ac	Poly(acrylamide co-acrylic acid)
PAAm-NP	Poly(acrylamide co-APMA)
PAAm-DM	Poly(acrylamide co-DMAEMA)
HEPES	4-(2-hydroxyethyl)-1-piperazineethanesulfonic acid
DMAPMAm, DMAm	( <i>N</i> -dimethylamino)propyl methacrylamide
DDLW	Dye-doped leaky waveguide

# Chapter 1. INTRODUCTION AND LITERATURE REVIEW

## 1.1. Introduction

Covering a broad scope of analytes relating to chemical, physical and microbial or microbiological features,<sup>1</sup> the supply, state and discharge of water affects a range of household uses as well as recreation, environmental monitoring, agricultural and industrial processes and wastewater management and treatment.<sup>1-4</sup> In particular, the provision of potable water is of fundamental importance not only in ensuring water quality but also to maintain public confidence in their water supply.<sup>5-7</sup>

In a modern context, growing populations as well as increasing environmental awareness have created greater demand while limiting public support for the development of traditional water supply infrastructure.<sup>7</sup> This increase in stress leads in turn to an increased reliance on finite and ecologically vulnerable freshwater resources,<sup>8</sup> and has led to the ongoing development of a host of water treatment systems and processes to maximise water sources while maintaining stringent restrictions on water quality parameters.<sup>6,7,9</sup>

In the UK (and indeed in Europe at large) the highest quality of water is considered essential, with high utility costs to households considered acceptable for the quality of product. The introduction of comprehensive numerical standards for water safety in the UK began with the 1980 European Drinking Water Directive, a break from earlier measures that required such measures as chlorination, microbiological testing and that the water be 'wholesome'.<sup>7</sup> Today, water quality regulations follow EU Council Directive 98/83/EC and its derivatives, which sets out 26 chemical,

18 physical or aggregate, 2 radiological and 7 microbiological parameters as well as specifying the sampling frequency.<sup>10</sup>

In the United Kingdom, water supply legislation is and remains based on the European Council Directive 98/83/EC and at the time of writing is unaltered by the UK leaving the EU.<sup>11</sup> Certain parameters are provided in **Table 1.1**, below

*Table 1.1- selected drinking water quality standards as set by EU Council Directive 98/83/EC, Amended 2005*

<b>Parameter</b>	<b>Limit (mg/l except where stated)</b>	<b>Notes</b>
Turbidity	Acceptable to Consumers	No abnormal change.
Colour	Acceptable to Consumers	No abnormal change.
pH	6.5 – 9.5	Should not be corrosive.
Lead	10 µg/l	Not necessary if TOC is analysed.
Iron	200	
Aluminium	200	
Cadmium	5	
Arsenic	10	
Nitrate	50	12.5 µg/l if bottled.
Sulphate	250	Should not be corrosive.
Bromate	10	Measured if taken from surface water.
Cyanide	50 µg/l	
Polyaromatic Hydrocarbons	0.1 µg/l	
Total Organic Carbon	--	No abnormal change.
Vinyl Chloride	0.5	Should not be corrosive.
Total Pesticides	0.5	For 10 <sup>4</sup> m <sup>3</sup> /day.
Trihalomethanes	100 µg/l	

One of the most common tools for directing the analysis of water quality is the Standard Methods for the Examination of Water and Wastewater, published and maintained by the American Public Health Association.<sup>6</sup> Based originally on a 1905 committee report on standard methods of water analysis,<sup>12</sup> this resource collates the more established and trusted methodologies for assessing water quality and so is often used to describe yardstick tests against which new analyses or devices are tested.<sup>13-16</sup>

Unfortunately, many water quality monitoring systems are plagued by common issues – they may be difficult to integrate, reliant on off-line sample collection and analysis, or reliant on expert users and too expensive to operate widely.<sup>1</sup> Of note is the analysis of free chlorine, an extensively used disinfection agent, where the majority of methods are either off-line and laboratory based or require the addition of chemical reagents or labels.<sup>17</sup>

The aim of this chapter is provide a brief summary of the state of literature regarding pH and chlorine sensing (with particular interest given to the research unit's specialisation in soft materials, specifically hydrogels),<sup>18-21</sup> and ultimately to demonstrate the need for an integrated, label-free, continuous-monitoring sensing scheme for pH and free chlorine.

## **1.2. Optical Sensors**

Sensors consist of two general components. The receptor or recognition element produces a measurable effect in response to the analyte, be it the colour in a dye,<sup>22, 23</sup> the strength<sup>24-26</sup> or quenching<sup>27</sup> of fluorescence in a fluorescent dye, the resistivity of a conductive material,<sup>28</sup> or a size<sup>29</sup> or optical density<sup>30</sup> response. The transducer converts and amplifies the receptor response into an observable signal for the reporter to quantify, such as absorbance spectroscopy,<sup>4</sup> refractometry,<sup>31</sup> or electrical current<sup>32</sup> or voltage.<sup>28</sup> A third stage responsible for signal processing, the reporter, may also be considered. While largely electronic in nature,<sup>33</sup> A visual form of identification<sup>22, 34, 35</sup> may be encountered where simplicity and ease of use is the goal.<sup>36</sup>

Sensors tend to be classed by their transduction method, with electrochemical and optical designs remaining prominent. Electrochemical sensors were prominent in early benchtop sensor design,<sup>37,</sup>

<sup>38</sup> and remain in very wide use due to the ease of transducer-reporter interfacing.<sup>39</sup> Optical sensors are widely researched and versatile<sup>40</sup> and often require no direct contact with the sample.<sup>39</sup> Optical sensors include both spectroscopic and visual identification systems.<sup>40</sup> Other transduction families, such as mass-sensitive materials, acoustic<sup>39</sup> and chemomechanical,<sup>29</sup> all exist, however they are less widely investigated. Typically silica and certain polymers are favoured for sensor construction, permitting high attainable refractive index and high transmittance with good clarity of signal.<sup>41, 42</sup>

### **1.2.1. Examples of Optical Sensors**

For the sake of brevity and focus, only the sensor type preferred by the research group (optical sensors) shall be briefly discussed immediately below. Where other sensors are discussed further into this chapter, and a rundown of the structure and mechanisms of waveguides (particularly slab waveguides) is given in the following chapter, less information will be required below.

Interferometric sensors employ two coherent light beams to detect small changes in refractive index through the sample. The combination of the two beams, sensor and reference, reveals an interference pattern that shifts as optical conditions in the reference channel change.<sup>43</sup> The layout and structure of a sensor can vary considerably within the realm of interferometry. Interferometers commonly use two channels and either allow light to diverge naturally after sensing (Young type) or be recombined into a single channel for transduction (Mach-Zehnder type).<sup>44</sup> However, they may use a pair of stacked planar waveguides and monitor emerging light,<sup>45</sup> monitor the phase change encountered during backscattering or diffraction,<sup>46</sup> or utilise reflection from the end of an optical fibre<sup>47</sup> or between two closely spaced surfaces.<sup>48</sup> Due to their ability to directly monitor small changes in the analyte without particular need for sample treatment or labelling reagents,<sup>43</sup> interferometers have found broad use in biosensing applications.<sup>45-48</sup>

Diffraction gratings, first encountered by developing photographic media in a gel through which standing waves had been reflected<sup>49</sup> and then refined through holography,<sup>50</sup> have come into their own as a sensor by combination with soft materials. Photonic structures such as gratings allow visually-distinguishable color changes that can be quite dramatic, allowing the semi-quantitative determination of chromophore-based colorimetric sensors without chemically susceptible dyes.<sup>51</sup> optical fibres, a common approach to sensor design,<sup>41</sup> are favoured particularly for grating sensors<sup>31</sup>,

52

Related to diffraction gratings in underlying function, crystalline colloidal arrays mimic the underlying structural colour and diffraction characteristics found in opals.<sup>51</sup> Like other diffraction based photonic sensors such as gratings and holograms, offers colorimetric and reversible sensing technology<sup>53</sup> by assembling charged monodisperse microparticles into regular structures with tunable periodicity and so optical properties.<sup>54</sup> Typically formed from polystyrene or poly(methyl methacrylate),<sup>51</sup> with functional recognition groups such as crown ethers<sup>55</sup> or an analyte-binding enzyme<sup>56</sup> incorporated within the bulk hydrogel. The sensing group may also be a copolymer incorporated into the polymer backbone of the colloid.<sup>57-59</sup> As the target analyte interacts with the recognition group buried inside the hydrogel, a change in hydrogel volume or refractive index is induced, thereby changing the optical properties of the crystalline array as a whole and so changing the diffraction colour.<sup>54, 60, 61</sup>

Surface Plasmon Resonance sensors are one of the most widely used label-free detection devices particularly for biosensing applications,<sup>17, 30, 53</sup> but also small charged molecules such as ammonia<sup>62</sup> or fluoride.<sup>63</sup> The theory of SPR is described in the following chapter, but briefly, the sensor measures small changes in surface refractive index occurring at the surface of a metal film where

electromagnetic waves, or surface plasmons, are driven by illumination at a specific wavelength and incident angle defined in part surrounding environment, particularly in the evanescent field.<sup>64</sup> SPR sensors are typically use noble metal nanostructures, producing sharp and easily monitored spectral absorption peak,<sup>53, 65</sup> however precisely applied gold<sup>17, 30, 66</sup> or silver<sup>62, 63</sup> thin layers are often required to permit measurable surface plasmon effects.

SPR may also be achieved with nanoparticles around the size of the wavelength in place of a thin film, combining the advantages of SPR and nanoparticle or photonic sensor construction.<sup>51</sup> While the particles may be incorporated into hydrogels and used as a matrix-sensitive component,<sup>67, 68</sup> more recently gold nanorods have been used as the core of a polymer nanofibre to permit SPR sensing down the length of the optical fibre<sup>69, 70</sup> or construction of additional structures such as microcavities.<sup>71, 72</sup>

Additionally, the mechanical flexibility of a soft material allows polymers to swell and deswell in response to stimuli, an alternative form of detection mechanism.<sup>41</sup> While the merits and drawbacks of a purely chemomechanical sensing scheme are discussed in Section 1.6.4 below, it is worth noting that a sensing scheme using electroosmotic pressure,<sup>31, 52</sup> complexation<sup>73</sup> or similar gel swelling/deswelling methods can be paired with other means of transduction to gain the sensitivity and continuous monitoring capacity of an optical sensor<sup>74</sup> while retaining a specific physical sensing scheme. Through a swelling-based sensing scheme, conditions from humidity<sup>65, 74-76</sup> to light exposure<sup>77</sup> can be measured. Because soft materials tend to be porous at the microscopic scale, and can provide a scaffold onto which recognition elements can be attached<sup>41</sup> or encapsulated,<sup>78, 79</sup> with suitable decoration or preparation of the bulk polymer a relatively large 3d volume may elicit a response for otherwise space-limited sensing schemes.<sup>31, 73, 77</sup>



## 1.2.2. Developments of Interest

While not within the scope of this thesis, a popular area of interest for sensor development remains minimally invasive diagnostic monitoring<sup>80</sup> at the point of care.<sup>51, 81</sup> Wearable or implantable sensors are also a promising area of development<sup>41</sup> owing to the flexibility<sup>82</sup> and low toxicity possible with polymer networks, especially hydrogels decorated with hydrophilic functional groups that facilitate biocompatibility.<sup>83, 84</sup> In particular hydrogels, which due to their water/scaffold makeup are nontoxic but also resist tissue damage due to their resemblance to the extracellular matrix<sup>85, 86</sup> and also are biodegradable once their function is fulfilled<sup>87, 88</sup> with programmable degradation time.<sup>89</sup> Mechanical deformation can also be used as part of the function of the sensor, such as monitoring the bend of a joint.<sup>36</sup>

More specific to optics, Fibre type sensors give excellent light-guiding performance and with polymer construction, also offer mechanical flexibility.<sup>41</sup> This flexibility creates opportunities for physically resilient sensors, with some sensors able to withstand elongation by 700%<sup>90</sup> and still operate. Waveguide optical technology may also be used to develop or repair an optical component of a sensor in situ – Kwok et al<sup>91</sup> employed a polymer optical fibre to deliver blue light without leakage to selectively induce scleral photochemical crosslinking in the eye of rabbit, itself a promising treatment for myopia.

As mentioned in more detail below in Section 1.6.2, the bulk optical response may utilise the porous material of a hydrogel as both a scaffold and sensing medium to readily allow simple visual qualitative response such as changes in colour or appearance of the bulk gel<sup>92</sup> and can be combined with properly calibrated transducers<sup>93</sup> or even readily available equipment such as smartphone cameras<sup>35, 93</sup> for superior sensitivity, but lack the high sensitivity of optical confinement schemes such as those below.<sup>64</sup> Absorption-based sensors are however sensitive to uneven colour

development or outside conditions such as light quality, although standardisation of colour shift with techniques such as an insensitive reference dye may be used.<sup>94</sup> The popularity of waveguide optics in sensors, discussed below, helps to account for this.

There is currently a relative scarcity of sensors capable of independently detecting multiple varieties of metal ions,<sup>64</sup> however use of quantum dot fluorescence<sup>25, 93</sup> and complexation<sup>64</sup> has grown popular. Metal-organic-frameworks as optical sensors have also seen interest as an effective sensing method for dyes and biological molecules, as well as metal ions.<sup>25, 95-97</sup> In the following section the state of literature for the chlorine ion is discussed.

One emerging sensor type of note is the leaky waveguide, explained in some more detail in Section 2.4.4 below. A model optical leaky waveguide consists of a slab waveguide with a reduced refractive index difference between waveguide (where the light is contained) and substrate (transparent structural material upon which the waveguide is sited).<sup>98, 99</sup> Typically, optical waveguides require coupling and decoupling methods such as prisms with optically matched interfaces to allow light to enter and exit, however a leaky waveguide allows the lossy mode to decouple gradually through partial transmission at the waveguide-substrate boundary.<sup>100</sup> A prominent advantage to leaky waveguides is that the waveguide occurs in a relatively low-index state, permitting porous, soft or biocompatible materials to be used.<sup>101</sup>

While leaky waveguide sensors may utilise SPR and achieve sensing through the evanescent field, analogous to attenuated total reflection,<sup>100</sup> sensors also exist which incorporate recognition elements into the waveguide directly to achieve bulk sensing.<sup>98</sup> These waveguides are also relatively rapid to manufacture, taking a single step, and can match holographic structures for sensitivity.<sup>101</sup> Optical leaky waveguides are also an actively developing field, with the recent discovery<sup>98</sup> and utilisation

of exponentially decaying interference fringes at the resonance angles of lossy modes with sufficiently low refractive index contrasts. These diffraction-based leaky waveguide sensors offer improved sensitivity<sup>99</sup> as well as requiring no specific visualisation component such as dyes.<sup>19, 99</sup>

### 1.3. Free Chlorine Sensors

For preventative disinfection, the dosage of **chlorine** is of paramount importance. In the least harmful of cases, either too little<sup>7</sup> or too much<sup>40</sup> chlorine in water supply will lead to an unpleasant taste or odour. Too-low available chlorine risks interference of disinfection from other variables in wastewater quality, such as suspended solids,<sup>102</sup> ultimately producing insufficient ability to neutralise pathogenic bacteria<sup>103</sup>. Too-high chlorine levels creates harmful haloalkanes such as chloroform, a carcinogen.<sup>103</sup>

Chlorine sensing is therefore of great interest to governments, and both upper and lower boundaries for chlorine content have put in place. The appropriate free chlorine level is 2-3 mg/L by the World Health Organisation, or a maximum of 4 mg/L under US standards.<sup>40, 104</sup> The small acceptable range of 2 mg/L free chlorine (or 0.038  $\mu\text{M}$  HOCl) coupled with the typically changeable conditions of wastewater, together pose a significant challenge to the water treatment industry.

For chlorine, numerous methods exist for sensing such as amperometry, potentiometry, spectroscopy, colorimetry, chemiluminescence, titrimetry, as well as more laboratory-bound methods such as HPLC, stopped-flow spectrometry, membrane introduction mass spectrometry and electro-spray ionization mass spectrometry.<sup>105-107</sup> **Table 1.2** Error! Reference source not found. offers a few examples of relatively current developments in chlorine sensing. The latter 4 especially

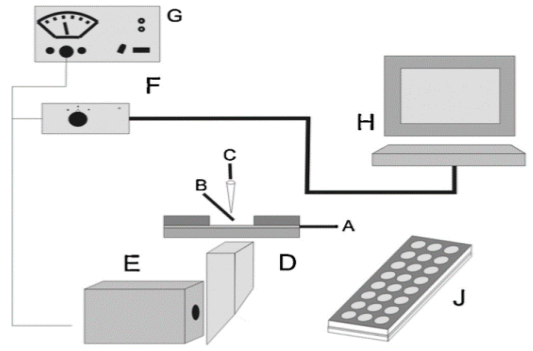
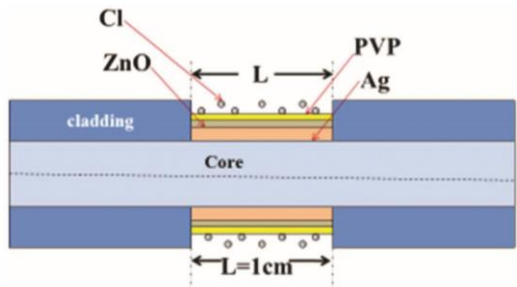
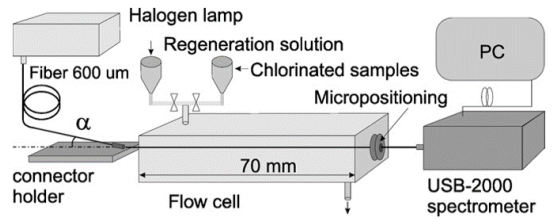
require expensive instruments and expert operators, severely limiting their employment in common environments.<sup>105</sup>

## 1.4. Chlorine Sensors in the Literature

Table 1.2- Selection of chlorine sensors, their working principles and their advantages and disadvantages

Reference	Year	Method	Principle	Schematic	Strengths	Limitations
Chlorine - Electrochemical						
T. Soundappan, K. Haddad, S. Kavadiya, R. Raliya & P. Biswas, <i>Appl Nanosci</i> , 2017, 7, 645-653	2017	Amperometric	monitoring of voltammetric reduction peak of chlorine on film.		<10 sec response, 0.1-10.08 mg/L effective range, resistant to ~1 mM of numerous cations	noble metal electrodes tend to be high-cost, not tested for continuous use
P. Salazar, M. Martín, F.J. Carcía-García, J.L. González-Mora & A.R. González-Elipe, <i>Sens Actuat B</i> , 2015, 213, 116-123	2015	Amperometric	Amperometric response from chlorine/prussian blue redox reaction.	Glassy carbon electrodes (GCEs, 3 mm diameter), USA. Electrochemical measurements were performed with a DRP-STAT400 potentiostat. For all electrochemical measurements, an Ag/AgCl (3 M KCl) and a Pt wire were used as reference and counter electrodes, respectively. Sensors placed in 25 ml of stirred phosphate buffer, pH 5.5, with 1 M KCl. -0.1 V applied. chlorine aliquots added to alter solution strength, response measured after each stage.	9 µg/L - 10 mg/L effective range	noble metal electrodes tend to be high-cost
L.H.H. Hsu, E. Hoque, P. Kruse & P.R. Selvaganapathy, <i>Appl Phys Lett</i> , 2015, 106, 063102	2013	Potentiometric	phenyl capped aniline tetramer is oxidised by free chlorine, modifying resistivity of nanotube.		rapid reversibility (time not given), 0.06-60 mg/L effective range	sensor lifetime of only 30 hr, sensor must be refreshed by applying negative current

Reference	Year	Method	Principle	Schematic	Strengths	Limitations
Chlorine - Optical						
R.A. Potyrailo, W.G. Morris, R. Wroczynski, L. Hassib, P. Miller, B. Dworken, A.M. Leach, S. Boyette & C. Xiao, <i>Sens Actuat</i> , 2009, 136, 203-208	2009	Colorimetric	Ratiometric colorimetric response between sensing cyanine dye and reference methylene blue.		requires pathlengths of ~10 μm, low cost sensor	relatively high (0.3 mg/L) limit of detection, solely off-line detection
Y. Xiong, J. Tan, C. Wang, J. Wu, Q. Wang, J. Chen, S. Fang & M. Duan, <i>Sens Actuat B</i> , 2017, 245, 674-682	2017	Evanescent field	sample + DPD injected into capillary around optical-fibre, detection by SPR spectroscopy.		high sensitivity (LoD 1.5 μg/L), resistant to 100-2000 mg/L of numerous cations	low linear range at 5-400 μg/L, requires DPD injection
J. Xu, K. Feng & M. Weck, <i>Sens Actuat B</i> , 2011, 156, 812-819	2011	Evanescent field	cyanuric acid reversibly binds free chlorine, detected by evanescent field interferometry.		good reproducibility, on-line analysis suitability	consistently reported only around 60% of values of DPD titrations in real samples
Y. Tang, Y. Su, N. Yang, L. Zhang & Y. Lv, <i>Anal Chem</i> , 2014, 86, 4528-4535	2014	Fluorometric	in pH >9 solutions, hypochlorite ion (ClO⁻) produces luminescence from g-CNQDs.		durable and non-toxic QD, resistant to interference from up to 10³ quantities of anions, 50 μg/L - 50 mg/L effective range	cannot detect HOCl, requires impractically high pH for waste/potable water applications

Reference	Year	Method	Principle	Schematic	Strengths	Limitations
M. Szili, I. Kasik, V. Matejec, G. Nagy & B. Kovacs, <i>Sens Actuat B</i> , 2014, 192, 92-98	2014	Fluorometric	luminol is oxidised to diazoquinone by $\text{ClO}^-$ , then reacts with $\text{H}_2\text{O}_2$ to luminesce as aminophthalate.	 <p>Fig. 1. Instrumental setup: (A) PL film on ITO glass; (B) sample compartment; (C) pipette or capillary tube for sample; (D) prism; (E) photomultiplier; (F) amplifier; (G) power supply; (H) computer; and (J) cells in the PVC-body on PL coated ITO glass.</p>	shelf life of 3-12 months, 0.1-1000 mg/L effective range	not continuous measurement, unstable at high pH, high RSD at around 6%
R. Tabassum & B.D. Gupta, <i>Analyst</i> , 2015, 140, 1863-1870	2015	Refractometric	influence of chlorine on dielectric PVP film, detected by SPR as refractive index shift.		0.5-5 mg/L effective range, pH-independent response	detects only $\text{Cl}_2$ , no examination of sensor specificity
I. Kasik, J. Mrazek, O. Podrazky, M. Seidl, J. Aubrecht, P. Tobiska, M. Pospislova, V. Matejec, B. Kovacs, A. Markovics & M. Szili, <i>Sens Actuat B</i> , 2009, 139, 139-142	2009	Refractometric	influence of chlorine on o-phenylenediamine layer, detected by SPR as refractive index shift.		Response time of around 3 seconds, reasonable sensitivity (LoD 0.14 mg/L)	sensor must be maintained at pH 1, performance degrades after 5-7 cycles

### **1.4.1. Issues with Chlorine Detection**

In water, free chlorine does not exist as the chloride ion, but instead takes the form of hypochlorous acid HOCl and the hypochlorite ion  $\text{OCl}^-$ , in a proportion that is a function of temperature and pH.<sup>103</sup> The range of transition between the two forms is around pH 5-10 - assays that detect  $\text{OCl}^-$  may fail to do so with HOCl, and vice versa, meaning knowledge of pH is of considerable importance when detecting free chlorine.<sup>103, 108</sup>

Traditional chlorine assays (outlined below) have tended toward non-continuous measurement, either due to a titrimetric process,<sup>109</sup> requiring frequent calibration or employing exhaustible reagents.<sup>40</sup> This is an issue as chlorine is unstable in solution,<sup>6, 110</sup> meaning any method that requires storing or transporting samples before analysis risks reporting an inaccurate result, as well as the contamination risks associated with sample storage.<sup>40, 109</sup> Additionally, an initially fast and reversible reaction on the clean sensor surface may become irreversible as the surface becomes contaminated.<sup>109</sup>

There is therefore a clear need for long-lived and reliable chlorine sensors capable of continuous chlorine measurement.

### **1.4.2. The Traditional Methods for Chlorine Detection**

Long-standing methods of detecting residual or total chlorine have remained in use, both as a validated and accepted analytical process<sup>6</sup> and as a benchmark for comparison with new sensor technologies.<sup>32</sup> These include Iodometric titration,<sup>6, 110</sup> amperometric titration,<sup>109</sup> potentiometric



sensing, DPD redox or colorimetric analysis and syringaldazine (FACTS) titration,<sup>109</sup> although FACTS has fallen out of favour<sup>110</sup> due to non-reproducibility and stability issues.<sup>9</sup>

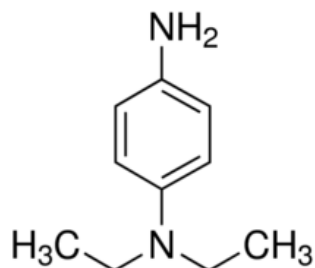


Figure 1.1 - *N,N*-Diethyl-*p*-phenylenediamine, a common free chlorine sensitive dye

Most commonly used is the *N,N*-diethyl-*p*-phenylenediamine (DPD) redox assays originally developed by Palin.<sup>37, 109, 111</sup> DPD (**Figure 1.1**) remains ever popular as an operationally simple near-line analysis tool, and follows two internationally recognised methodologies.<sup>9</sup> In the first, oxidation of DPD by chlorine at around neutral pH produces a magenta-coloured Würster dye, a relatively stable free radical species,<sup>9</sup> which may be visually identified or monitored photometrically.<sup>6</sup>

In the second method, DPD is oxidised by free chlorine species to produce the *Würster dye*. Titration with a ferrous ammonium sulphate (FAS) reducing agent is then performed, which reverts the dye to colourless DPD.<sup>9</sup> The visually unmistakable endpoint of the FAS titration helps to insulate this method from user error.<sup>6</sup> However, it is vulnerable to interference from iodine and bromine as well as manganese<sup>40</sup> and copper.<sup>103</sup>

Research surrounding DPD as a sensor continues, however, including within optical sensors. The high sensitivity (a 1.5 ppb limit of detection in one case)<sup>17</sup> and selectivity of DPD colorimetry are attractive, while trends in analyser miniaturisation and low-cost systems offer a variety of ways to make use of absorbance or spectrophotometric transducers.<sup>17, 40</sup> As the reaction of DPD with

chlorine is non-reversible, continuous-measurement designs such as that recently proposed by Xiong, Tan *et al*<sup>17</sup> must introduce new indicator alongside the sample.

With a structure not dissimilar to DPD, *o*-phenylenediamine (*o*-PDA, **Figure 1.2**) may also serve as an optical chlorine indicator. Kasik, Mrazek *et al*<sup>66</sup> demonstrated a fibre optic sensor clad in indium-tin-oxide, onto which *o*-PDA is voltammetrically deposited, providing an effective receptor that is coupled to surface plasmon resonance (SPR) spectroscopy. A more recent sensor from the same institute traded *o*-PDA for polyluminalol, leading to a higher-throughput system with a slightly inferior (yet still remarkable) detection limit of 1.8 ppb.<sup>112</sup>

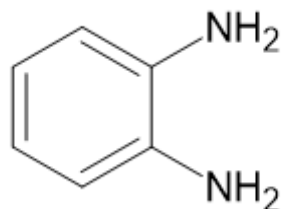


Figure 1.2 - *o*-phenylenediamine, a free chlorine sensitive dye related to DPD (above).

Overall, the automation of DPD-based chlorine detection provides high sensitivity and accuracy on demand, at the cost of frequent calibrations, expensive components, difficulty in miniaturisation, trace metal interference and the discharge of waste buffer that is considered environmentally harmful.<sup>40</sup> Due to the persistent need to inject or replenish the indicator, there is little place for DPD detection in online chlorine sensing.

### 1.4.3. Electrochemical Chlorine Detection

Electrochemical transduction systems are valued for their wide sensing range, good response, small minimum dimensions, low cost and ease of integration with electronic systems.<sup>40</sup> Such

properties synergise with microfabrication and microfluidic systems, and so benefit from the ongoing interest and research in those topics.<sup>29, 40</sup> The development of an electrochemical sensor often requires a suitably robust, sensitive and specific electrode for the selected analyte,<sup>32</sup> although sensors are often hampered by a need for expensive noble metal reference electrodes.<sup>113</sup>

For example, by depositing the inorganic dye Prussian blue (doped with a cationic surfactant) onto a glassy carbon electrode, Salazar, Martin *et al*<sup>32</sup> improved upon a sensor originally demonstrated 5 years earlier.<sup>114</sup> The sensor produced correlated favourably with DPD colorimetry and was sufficiently stable both in storage and over successive uses, but having only being tested for stability over 3 weeks, the long-term reliability of the sensor is not entirely known.<sup>32</sup>

While the typical potentiometric chlorine sensor employs a set of electrodes, other alternatives are being investigated. For example, Hsu, Hoque *et al*<sup>28</sup> developed a short-lived but sensitive free chlorine sensor by monitoring the resistance change of single-wall carbon nanotubes functionalised with a phenyl-capped aniline tetramer. Oxidation of the aniline by chlorine converts the carbon nanotube-aniline into a less resistive state, which is readily detected as a change in current. However, the receptor must be regenerated by manually applying a negative voltage to the electrode.

#### **1.4.4. Optical Chlorine Detection**

The optical detection of chlorine is diverse, as an ever-growing number of sensors and transducers may be interfaced in a variety of combinations, as shown in Error! Reference source not found.**Error! Reference source not found..**

One optical sensor in everyday, non-scientific use is a CD or DVD drive – a laser interrogates at one or more wavelengths, and a light-sensitive transducer retrieves data from the result. This was clearly demonstrated in 2009 by Potyrailo, Morris *et al.*,<sup>115</sup> using a super audio compact disk (SACD) and a computer CD-DVD reader to monitor both a chlorine-sensitive dye and a reference dye printed on the disk. As a technology, the idea of moving from sample to final product in one modular, low-cost and ubiquitously analysable microfluidic system offers such ‘lab-on-a-disk’ sensors considerable promise,<sup>115, 116</sup> however the limited real estate within the disk limits its functionalities. More to the point, the inability to apply to continuous or on-line measurements to a disk held within a closed CD tray pose considerable problems and limit the uptake of the technology.<sup>116</sup>

As small sensor dimensions become ever more highly regarded in sensor design,<sup>32</sup> spectroscopy becomes more difficult to accomplish. The sensitivity of absorption spectroscopy scales with the path length (the distance the beam travels within the sample), as described by the Beer-Lambert law,<sup>117</sup> so the path length must be preserved in order to ensure performance. This may be performed simply by directing the incident beam down a capillary tube, but also by utilising total internal reflection (described below). As light reflects losslessly against the cladding of a fibre-optic capillary, it travels a total distance greater than the length of the capillary, offering greater path lengths for the same capillary size.<sup>117</sup>

Total internal reflection also offers certain exclusive sensing techniques. SPR occurs when light is entirely reflected on a metal-dielectric interface, creating an exponentially decaying (evanescent) field that propagates into and through the metal cladding into the sample beyond. As the refractive index of the sample changes, the evanescent field and in turn the reflectivity to the incident light is affected.<sup>30</sup> The short distance the evanescent field travels can be utilised by fixing an analyte such as a capture antibody<sup>118</sup> to a sensing region, where a sensing fibre-optic wire interacts with a

sample-carrying capillary.<sup>30</sup> Tabassum and Gupta<sup>30</sup> utilised this design of sensor to produce a reusable and low-cost online chlorine sensor with sufficient sensitivity for water supply applications.

Xu, Feng & Weck<sup>13</sup> demonstrated a chlorine sensor that employs interferometric sensing to normalise refractive index measurement, and integrated this system into a field testing kit for chlorine sensing of industrial chiller water. Of interest however is that their sensor only reported ~60% of the values found by DPD colorimetry, a difference which the authors tentatively attributed to combined chlorines, such as chloramine.

Chemiluminescence has certain advantages over colorimetric sensors. It is sensitive, has no issues with background scattering of light, and can be versatily applied to various analytes.<sup>103</sup> The very small quantity of analytes required for a response lends chemiluminescence to miniaturised analyses.<sup>117</sup> One of the more common luminescent materials is luminol<sup>103</sup>, which fluoresces in the presence of hypochlorite<sup>112</sup> and can be polymerised to form a more easily manufactured thin film.<sup>108, 112</sup>

Luminescence may also be performed with lower-cost and less toxic nanoscale materials such as certain quantum dots.<sup>103</sup> By doping a nanoparticle with a luminescence-quenching material,<sup>119</sup> or by fabricating a quantum dot with sensitivity to a certain analyte, sensitive and highly specific sensors can be manufactured. In the case of a widely discussed paper by Tang, Su *et al*,<sup>103</sup> a graphitic carbon nitride quantum dot manufactured by a one-pot, one-stage synthesis was shown to luminesce in the presence of free chlorine, with a limit of detection of 20 nanomoles.

## 1.5. pH Sensors

Free chlorine expression is affected by **pH**, as are a range of factors such as microbiological growth, precipitation, coagulation, disinfection and plumbosolvency (attack of plumbing and pipework by corrosive water).<sup>7, 12, 120, 121</sup> The ability to monitor and ultimately react to pH changes are critically important in a host of circumstances. In an industrial setting, the impact pH has on the efficiency and yield of chemical processes makes it of essential importance to food, pharmaceutical and manufacturing.<sup>2-4</sup> A shift in physiological pH can lead to premature ageing, cardiovascular damage and cancer.<sup>33</sup> Clinical monitoring of pH is also of interest, for example in the active development of smart dressings that track the progress of healing of a wound without disruptive removal and reapplication cycles.<sup>22</sup>

Within the context of water quality and wastewater treatment, pH affects a range of processes.<sup>120</sup> pH of filtered water is known to have an impact on filtration performance, while upon release into waterways, pH of soil has a considerable influence on crop growth.<sup>121</sup> Abnormal pH will exacerbate problems with water softening, precipitation, coagulation, disinfection and most obviously acid-base neutralisation,<sup>6</sup> while control and if necessary adjustment of pH will mitigate issues with iron and manganese removal, plumbosolvency (attack of plumbing systems by corrosive water) and microbiological contamination.<sup>7</sup>

Sensing for free chlorine requires on-line sensors that can account for the form ClOH is expressed in. This rules out the most common chemical assays as described below, especially N,N-Diethyl-p-phenylenediamine (DPD), which do not easily take to label-free means. An alternative, however, would need to incorporate an effective sensing scheme that can monitor and correct for the ionisation state of ClOH and ClO<sup>-</sup>. This necessitates pH sensing functionality. While pH monitoring is a well-served field in its own right, especially in terms of the label-free sensing

regime we seek to develop for chlorine, not every sensing scheme is both suitable for and compatible with the needs of chlorine detection. There is therefore a need to identify and develop a sensor capable of on-line monitoring of both pH and chlorine.

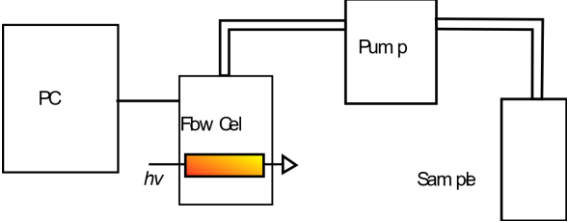
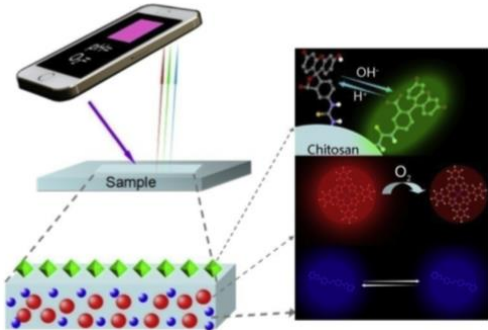
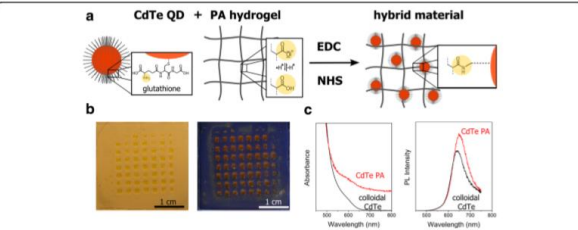
## 1.6. pH Sensors in the Literature

Table 1.3 - Selection of pH Sensors, their working principles and their advantages and disadvantages

Reference	Year	Method	Principle	Schematic	Strengths	Limitations
pH - Absorbance						
P. Kassal, M. Zubak, G. Scheipl, G.J. Mohr, M.D. Steinberg & I.M. Steinberg, <i>Sens Act B</i> , 2017, 246, 455-460	2017	Colorimetric	dye GJM-534 interrogated at 527 nm, detection by photodiode.		precise (0.05 pH units), low production cost.	accuracy of 0.08 pH units, narrow range of 6.4-8.4, dye substrates are limited
D. Kim, S. Lee, K. Lee, S. Baek & J. Seo, <i>Food Sci Biotechnol</i> , 2017, 26, 37-42	2017	Colorimetric	basic analytes penetrate a poly(ethylenetetrathalate) film to reach a dye-PVA-filter paper substrate. Visible colour change.		temperature independent, real-time analysis	very narrow linear range of 6-6.6, designed primarily for visual detection
R. Heydari, M. Hosseini, A. Amraei & A. Mohammadzadeh, <i>Mat Sci Eng C</i> , 2016, 61, 333-337	2016	Colorimetric	dye immobilised on thin film is interrogated at 490 nm, detection by photodiode.		reproducible, precise (RSD 0.9%), wide pH range of 3-10, resistant to 0.5 M NaCl	~1 min response, takes up large proportion of visible spectrum (250-550 nm)



Reference	Year	Method	Principle	Schematic	Strengths	Limitations
N. Chamkouri, A. Niazi & V. Zare-Shahabadi, <i>Spectrochim Acta A</i> , 2016, 156, 105-111	2016	Colorimetric	dye immobilised on thin film is interrogated at 539 nm, detection by photodiode.		wide pH range of 2-10, signal displayed no leaching or drift over 6 months, resistant to 0.5 M NaCl	1 min response, RSD of ~5%
A.Q. Maclin, M.D. Kim, S.A. Dergunov, E. Pinkhassik & E. Lindner, <i>Electroanal</i> , 2015, 27, 733-744	2015	Colorimetric	enclosed nanocapsules loaded with dye are planted inside an optical fibre and interrogated at 665 nm.		resolution of 0.03 pH units, stable over 4.5 years	narrow range of 7.3-9.3, variable gel diameter imparts imprecision, issues with light scattering
M. Hosseini, R. Heydari & M. Alimoradi, <i>Spectrochim Acta A</i> , 2014, 128, 864-867	2014	Colorimetric	dye immobilised on thin film is interrogated at 464 nm.		wide pH range of 4-12, precise (RSD 0.4%), resistant to 0.5 M NaCl	~1 min response

Reference	Year	Method	Principle	Schematic	Strengths	Limitations
S. Trupp, M. Alberti, T. Carofiglio, E. Lubian, H. Lehmann, R. Heuermann, E. Yacoub-George, K. Bock & G.J. Mohr, <i>Sens Actuat B</i> , 2010, 150, 206-210	2010	Colorimetric	synthesised dyes are immobilised on thin film, interrogated at appropriate peak wavelengths.		reversible, dye functional group may be selected to tune absorbance properties	typical pH range of 6-10, sensor stability not assessed after 5 hrs
W. Xu, S. Lu, Y. Chen, T. Zhao, Y. Jiang, Y. Wang & X. Chen, <i>Sens Actuat B</i> , 2015, 220, 326-330	2015	Colour Analysis	ratiometric colour analysis of fluorescent dye and pH-independent reference pigment.		stable over 30 days, compatible with common camera technologies	±0.2 pH units, not designed for online analysis, suffers from photobleaching
pH - Fluorescence						
M. Franke, S. Leubner, A. Dubavik, A. George, T. Savchenko, C. Pini, P. Frank, D. Melnikau, Y. Rakovich, N. Gaponik, A. Eychemuller & A. Richter, <i>Nanoscale Res Lett</i> , 2017, 12, 1-8	2017	Fluorometric	dye immobilised on polyacrylate hydrogel, excited at 485 nm to emit at 685 nm.		demonstrates integration of off-on pH-responsive hydrogel valve with indicating fluorescent dye	quantum dots unstable at pH below 7.0, no precision or sensitivity data available

Reference	Year	Method	Principle	Schematic	Strengths	Limitations
D-Y Kim & H.J. Kim, <i>Sens Actuat B</i> , 2015, 206, 508-515	2015	Fluorometric	dye immobilised on thin film is set inside flow cell and fluorescence peak (specific to dye variant) monitored.	dye immobilised onto polymer membrane on glass slide. Placed inside a flow cell within a spectrophotometer. Fluorescence spectroscopy.	precise (RSD 0.4%), no dye leaching over 25 days	specialised pH range of -1.0-2.0, some intensity decrease after 6 hrs continuous monitoring
D. Wencel, M. Barczak, P. Borowski & C. McDonagh, <i>J Mater Chem</i> , 2012, 22, 11720-11729	2012	Fluorometric	dye immobilised non-covalently within hybrid solgel/hydrogel structure. Dyes excited at 405 and 460 nm, emission at 515 nm	continuous wave spectrophotometer (fluor). Sensor film dip-coated onto substrate slide, secured in flow cell, fed by peristaltic.	response time 12 sec, precise (RSD 0.32%), no leaching after 48 hr	improper pH range of 5.0-8.0, no data given for photostability
pH - Chemo-mechanical						
K. Deng, C. Bellmann, Y. Fu, M. Rohn, M. Guenther & G. Gerlach, <i>Sens Actuat B</i> , 2018, 255, 3495-3504	2018	pH-responsive material	size change of pH-responsive hydrogel, monitored through the equilibrium pressure required from a temperature-sensitive hydrogel employed opposite the pH-responsive hydrogel		reduces response time of native pH-responsive gel by 27.4%, wide operating window of pH 4-10	needlessly complex and requiring 4 dependent stages, 60-120 minute response time
S.K. Mishra, B. Zou, K.S. Chiang, <i>IEEE J Sel Top Quantum Electron</i> , 2017, 23, 5601405	2017	Refractometric	size change of pH-responsive hydrogel on fibre optic core, changing resonance wavelength. Interrogated by spectrum analyser.		wide pH range of 2-12, response time of ~2 sec	uncertainty of 0.5 pH units due to wavelength measurement, temperature sensitive with $\pm 0.5$ °C causing $\pm 0.61$ pH units

Reference	Year	Method	Principle	Schematic	Strengths	Limitations
B.N. Shivananju, M.Kr. Priyadarshi, D.R. Mahapatra, G.M. Hedge & S. Asokan, <i>Proceeding of 1st International Symposium on Physics and Technology of Sensors</i> , 2012, Pune, India	2012	Refractometric	size change of pH-responsive hydrogel cladding on fibre optic core, changing Bragg wavelength conditions. Interrogated alongside unclad reference fibre.		wide operating window of pH 2-10, temperature independent	non-linear response from multi-layer clad fibre, single fibre sensitivity of only 3 pm/pHU
Anal. Methods, 2014, 6, 5191	2014	Refractometric	unclad optical fibre is coated in plasmonic material, then in hydrogel. Copolymer recognition element complexes with CrO <sub>2</sub> <sup>-</sup> to form temporary additional crosslinks, causing deswelling		Good sensitivity, selective for CrO <sub>4</sub> <sup>2-</sup> at sub- $\mu$ M ion concentrations	Results dependent on total salt concentration and pH of solution

## 1.6.1. Means of Sensing pH

The sensing of pH is a diverse field which gathers great interest and may be approached from a variety of scientific disciplines.<sup>22, 23, 26, 29, 102</sup> While a wide and growing range of sensors are available, pH transduction generally falls into three categories – visual, electrochemical and optical.<sup>40 2</sup>

Visual tests, such as test paper strips, are among the simplest possible forms of sensor readout,<sup>22</sup> lacking accuracy<sup>2</sup> despite their simplicity and heritage. There is however some interest in utilising visual pH reporting where a qualitative response is required, such as a yellow/pink binary colorimetric reporting system for a bacterial DNA detection array.<sup>34</sup>

Electrochemical pH sensors are a diverse group that includes ion-exchange, redox, potentiometric, resistometric and voltammetric sensing schemes.<sup>40</sup> Conventional glass electrodes are of the potentiometric type, originally developed by Beckman in 1934.<sup>38</sup> Although long-serving and still the most common pH sensor, they tend to be fragile, slightly slow in response (~30 seconds),<sup>122</sup> relatively costly (~£100 apiece) and require frequent calibration and maintenance.<sup>40</sup> The glass electrode nonetheless remains the most popular pH probe for common use,<sup>4</sup> and serves as the benchmark against which novel pH sensors are tested.<sup>40</sup>

Optical pH sensors, or optodes, have enjoyed a wide and sustained interest.<sup>2, 4</sup> A number of possible detection methods are available,<sup>4, 22, 26, 31, 52, 123</sup> as shown in **Table 1.3**, but optical pH sensors tend toward the colorimetric, incorporating and interrogating one or more immobilised pH-sensitive dyes.<sup>4</sup>

Optical sensors offer precision and sensitivity,<sup>4, 22, 123, 124</sup> alongside fast response times<sup>31, 123</sup> and low production cost.<sup>39</sup> One advantage of optical sensing, in the context of low-maintenance devices for wastewater control, is their suitability for continuous monitoring.<sup>4</sup> The primary challenge facing optical pH sensors is the need to achieve sufficient sensitivity, stability and utilising their response time advantage, in order to remain competitive with the more established glass electrodes.<sup>4</sup>

## 1.6.2. pH-Sensitive Dyes

pH-sensitive (also known as halochromic) dyes<sup>121</sup> are materials that alter their peak absorption wavelength and therefore their colour, in response to a shift in pH.<sup>2</sup> In colorimetric sensors the dye's capacity to undergo a colour change defines the operating range of the optical sensor<sup>3</sup> which may limit the sensor's linear range,<sup>40</sup> although by mixing two complimentary pH-sensitive dyes an extended working range may be reached.

pH-responsive dyes may display a bathochromic (shifted to longer wavelengths) or hypsochromic (shifted to shorter wavelengths) shift of absorption peak. Dyes such as phthaleins which feature bathochromic shift typically transition between a higher-wavelength neutral state and a lower-wavelength negatively charged state, and are referred to as negative halochromic dyes. The reverse is true for positive dyes, which often experience a hypsochromic shift upon protonation.<sup>121</sup>

Dyes typically fall into four structural categories, phthalides, triarylmethanes, fluorans and azo dyes, as illustrated in **Figure 1.3**.<sup>121</sup> The presence of functional groups on a dye enacts changes upon the dye's optical properties as the electron environments of the dye alter.<sup>23</sup> It is therefore possible to synthesise halochromic compounds with tailored properties.<sup>23, 125</sup> Likewise, chemically bonding a

pH-responsive dye to a substrate alters its halochromic properties, often broadening the dynamic range of the dye.<sup>126</sup>

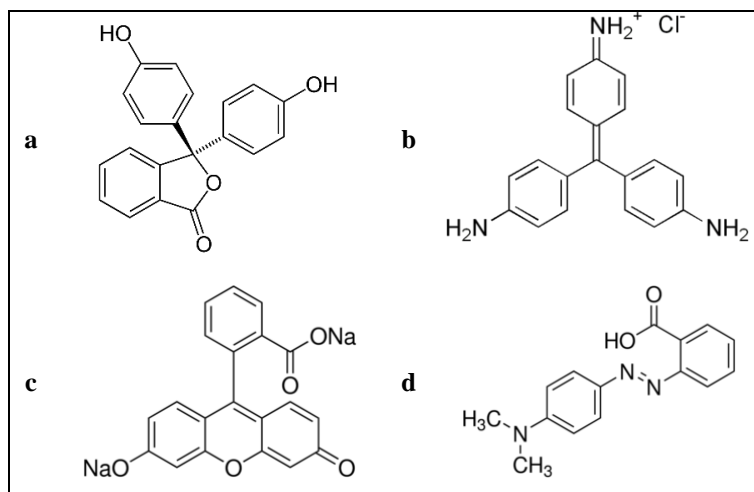


Figure 1.3 - Sample dye structures. a: phenolphthalein, a phthalide dye. b: pararosaniline, a triarylmethane dye. c: fluorescein, a fluoran dye. d: methyl red, an azo dye.

Permanent dye immobilisation is a common feature in the development of optical sensors which solved early issues with dye leaching, with effects on absorption wavelengths and in cases a broadening of the dye's dynamic range.<sup>121</sup> Encapsulating the dye in a solgel<sup>123</sup> or nanocapsule<sup>4</sup> is still practiced, in the former case owing to the limited choice of organosilicate monomers that may serve as binding sites.<sup>123</sup>

Immobilisation strategies may also consider the structure of the substrate. The substrate is largely defined by the sensor mechanism and geometry, but the most common forms are the simple and direct immobilisation on thin films<sup>2, 3, 23, 123, 127</sup> and hydrogels.<sup>26, 35, 124, 126</sup> Alternative substrate forms are utilised as required - cellulose particles may be securely immobilised within a soft material such as fabric while limiting cytotoxicity,<sup>22</sup> electrospun fibres feature a small pore size, high porosity but often the cost of susceptibility to temperature and pH,<sup>128</sup> and nanocapsules offer tuneable porosity

and almost no leaching potential in a substrate that can interface with a macroscopic structure such as a hydrogel.<sup>4</sup>

Waveguide optics may also be found in conjunction with pH sensitive materials, where numerous sensing parameters such as refractive index<sup>17, 30, 31, 52</sup> and the evanescent field<sup>13, 17</sup> become available. Refractometry especially provides a good sensitivity, effective range and response times, as shown in **Table 1.3**. However, the capabilities of waveguide transduction do depend on the sensitivity and especially selectivity of the receptor component.

### **1.6.3. Fluorescent pH Sensors**

Fluorescence typically involves optical excitation at one wavelength band, leading to emission at another wavelength band. This wavelength change is a function of the dye's electronic structure. pH-responsive fluorescent dyes alter the strength of emission in response to pH changes.<sup>123</sup> Fluorescence is an alternative to colorimetry, and it offers typically superior sensitivity at the cost of a narrower linear range.

Using multiple dyes to independently monitor multiple wavelength bands allows for ratiometric spectroscopy. Comparison with an internal reference dye minimises the effects of detector drift and changes in dye concentration, and in the case of fluorescent dyes also accounts for changes in fluctuation source. Wencel, Barczak *et al*<sup>123</sup> produced a fluorometric sensor employing ratiometric excitation at pH-dependent absorption bands, ultimately offering a response time of only 12 seconds and a relative standard deviation of 0.32%. However, little data was presented regarding photostability of the sensor after 48 hours.



Fluorescence may be achieved through the use of nanoparticles, including the optically active quantum dots (QDs). Historically, QDs suffer from leaching, instability,<sup>26</sup> and feature hazardous heavy metals which carry the risk of serious environmental damage.<sup>103</sup> Binding quantum dots to a substrate alleviates the leaching issues, and may be accomplished by binding the nanoparticle to the substrate polymer directly, or by capping the nanoparticle with the prepolymer.<sup>26</sup> Given these issues, especially the potential health effects of leaked nanoparticles in the water supply, the use of pH-sensitive QDs in wastewater sensor design may not be recommended.

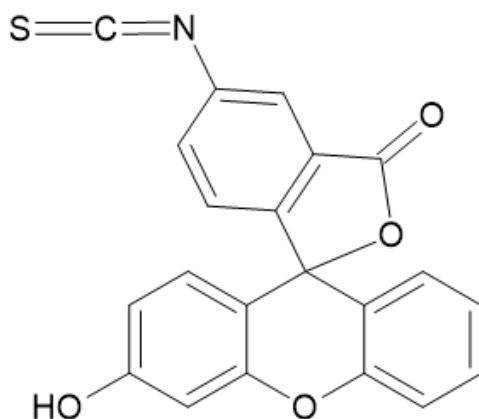


Figure 1.4 - Fluorescein isothiocyanate (FITC), a common pH-sensitive fluorescent dye.

Rather than interrogating the sensor at a known wavelength, it is possible to use image or colour analysis to detect changes in dye activity. Combining a differently coloured sensing and reference dyes, such as pH-sensitive yellow fluorescein isothiocyanate (**Figure 1.4**) and insensitive 4,40-bis(2-benzoxazolyl) stilbene, forms a ratiometric sensor that transitions from blue to pale green with increasing pH. The smartphone-compatible colour sensor demonstrated by Xu, Lu *et al*<sup>35</sup> offers stability and reversibility in the medium term, but suffers from poor resolution and photobleaching in the long term.

#### 1.6.4. Chemomechanical pH Sensors

It is worth noting that hydrogel-based chemical-mechanical pH sensors have also been developed, however it is thought that long response times and physically brittle structures may render them impractical as on-line sensors.<sup>40</sup> Stimulus-sensitive hydrogels (smart gels) feature networks of polymers which undergo large volume changes following a change in parameters such as pH, temperature, ion concentration, electric field, solvent composition or light.<sup>52</sup> In the case of pH, this change is due to ionic moieties within the hydrogel that dictate the degree of hydrophilicity. By inducing a pH change that neutralises these charges, the gel affinity for water reduces, which reduces the amount of water contained within the gel and so its shape.<sup>52</sup>

Water within a hydrogel can be thought of as three types, relating to the interactions between water and the polymer network.<sup>129, 130</sup> Free water fills pores and cavities within the gel's network may be exchanged or frozen without regard for the hydrogel's presence; Intermediate water is loosely bound to the polymer and responds to physical conditions in ways that depend on the polymer's characteristics; Bound water is considered to be wholly bound to the polymer by more than one hydrogen bond per water molecule, thereby unable to freeze at the conventional temperature. The majority of hydrogel-based sensors incorporating a change in the gel's swelling ratio operate by exchanging the free water fraction by inducing swelling or osmotic pressures in the presence of their analyte.<sup>131, 132</sup>

Chemomechanical sensors hold the advantage of wide operating ranges and can be made to be temperature independent<sup>52</sup>, for example through the use of a cantilever mount that counteracts strain upon a Bragg fibre sensor directly<sup>133</sup> or through partial etching of a sensor cladding to provide two independently tracked effective mode indices with a temperature-insensitive difference.<sup>134</sup> However, sensitivity and response times are a concern, with many sensors requiring multiple minutes to stabilise after a step change in conditions.<sup>31, 135</sup> As the response time of chemomechanical pH sensors is a major concern, there has been some interest in reducing the response

time, including using more porous or thinner hydrogels, however it has been found that increasing response time often degrades the signal-noise ratio.<sup>29,52</sup> By tuning parameters such as the waveguide size, selection of materials and swelling ratio, the rate of response of the waveguide has been reduced to the order of minutes.

Imparting a responsive force upon the gel is an exception – it allows a chemo-mechanical sensor to measure the swelling force of the gel rather than the eventual physical dimensions, allowing for a more immediate response. Pressure actuators are a bulky but effective means of accomplishing this, with an approximate response of 60 seconds comparable to certain optical devices. Smaller alternatives are nonetheless under investigation, such as a complex thermoresponsive hydrogel-peltier heating/cooling element, itself slower than an actuator by a factor of 60.<sup>29</sup>

Chemomechanical hydrogels can also impart secondary strain on optical components, warping the component to a measurable degree. Such a sensor requires only very thin hydrogel layers, in the range of 0.5  $\mu\text{m}$ , without sacrificing too much sensitivity. For example, a hydrogel may be inscribed upon an optical fibre to form a long-period fibre grating that leaks a specific peak wavelength in the microwave region,<sup>31</sup> or may be deposited upon an optical fibre bearing a Bragg grating that back-reflects a known peak wavelength dependent on the refractive index of the materials and the grating periodicity.<sup>52, 136</sup>

Bragg reflector based hydrogel sensors incorporating synthetic opals have seen considerable interest in recent years. Polymers may be created as colloidal crystals upon a swellable hydrogel substrate,<sup>137</sup> or as porous beads that themselves change in size or refractive index.<sup>138, 139</sup> The relative simplicity of manufacturing monodisperse micro- or mesoparticles for grating construction, as well

as their vibrant wavelength sensitivity,<sup>140</sup> allows for effective low-cost sensors capable of competing with immunosensors for specificity.<sup>139</sup>

Typically in hydrogel sensors, the hydrogel swells or contracts as the pH alters, changing its own refractive index or expanding/contracting the substrate.<sup>31, 52, 140</sup>

## **1.7. Project specification and objectives**

As mentioned in Section 1.1 and elucidated in Sections 1.3-1.4, the identified needs of an integrated sensor for water quality are expected to be environmental pH and disinfection-level chlorine. The sample matrix is therefore to be dilute aqueous media in all cases. The content of real samples should also be investigated for their effect on the final sensor, particularly components normally found in drinking water or involved in wastewater processing that may interfere with the analysis.

For the purposes of this research project, a free chlorine content of 0-4.0 mg/L and a pH addressing the typical environmental range of natural waters at 4 - 9 will be the expected analytes and their ranges.<sup>6</sup> As the conditions affecting water quality are changeable but not immediate, an immediate sensor response is preferable but not essential especially where resolving small pH changes is concerned. The objective of this project therefore is to develop a sensor for pH and chlorine, of sufficient sensitivity and range for municipal water quality, suitable for continuous data reporting.

Additional note – due to events outside of our control, the scope of the project was reduced in its final stages and much of the chlorine detection work was unfortunately deferred. As a result, chlorine detection experiments can not be adequately described.

## 1.8. Thesis Outline

This thesis as continues below consists of 7 chapters. Firstly, Chapter 2 presents the theory and operation behind the optical phenomena observed and their applications with both popular, established optical sensors and the scope of the ensuing project. Chapter 3 discusses the experiments performed to develop the following leaky waveguide methodology, particularly developing and demonstrating the ability detect and track pH changes in a copolymer ionogel. Chapter 4 then demonstrates a model system for an internally referenced pH sensor by stacking hydrogels, using the polysaccharides agarose and deacetylated chitosan as the respective reference and sensing materials. Returning to synthetic materials, Chapter 5 presents the optimisation process for a stacked copolymer system for pH sensitivity in which dimethylamino groups provide the sensing ability. The suitability of the stacked sensor for its intended use cases, including testing against known contaminants or chemicals present in potable water and wastewater, is examined in Chapter 6, as is a means of including free chlorine sensitivity by incorporating a third stacked layer. Finally, some concluding remarks as well as a discussion of future work (as well as the extent of the scope unfortunately reduced in the course of the thesis project) are provided in Chapter 7.

## **Chapter 2. THEORY OF WAVEGUIDE OPTICS**

### **2.1. Introduction**

In Chapter 1, an optical detection method for the selected analytes was chosen. However, it would be valuable to providing understanding on how optical sensors function and the means by which a change in the sensor state is introduced. This chapter will therefore provide an abbreviated summary of the theory behind optical sensors. Section 2.2 provides the basics of refraction, the critical angle and waveguides as the basis for future discussion of optical sensors and as a direct relation to topics taken forward later. Section 2.3 then describes more fully the nature of electromagnetic radiation in terms of waves. Section 2.4 provides a brief examination of specific phenomena, underlying both for the type of sensor discussed in later chapters and the current gold standard for label-free optical sensors.

### **2.2. Optical Waveguides**

#### **2.2.1. Refraction and Snell's Law**

In a transparent, dielectric medium, the speed achieved by the crests of the light waves (phase velocity of light) deviates from the speed of light in vacuum  $c$  as the medium becomes less able to permit transmission of the electric and magnetic fields. As indicated in **Figure 2.1**, with the

reduced phase velocity comes a contracted distance between wavefronts and in order to accommodate it, a change in transmission angle (the energy of each photon, and therefore wavelength, is unaffected). The refractive index  $n$  of the material can therefore be described as:

$$n = c/v$$

*Equation 2.1*

Where:

$c$  = the speed of light in vacuum;

$v$  = the phase velocity of light in a given medium;

This induced change in angle is known as refraction. The mathematics are best described in an environment where the change occurs across a flat plane, such as at a flat boundary at the surface of a liquid. The degree to which light is bent is governed by Snell's Law, as follows:

$$n_1 \sin(\theta_1) = n_2 \sin(\theta_2)$$

*Equation 2.2*

Where:

$n_1$  and  $n_2$  = the refractive indices of the respective materials 1 and 2;

$\theta_1$  and  $\theta_2$  = the incident and/or reflected angle of light relative to the normal (the perpendicular plane of the boundary), with respect to materials 1 and 2.



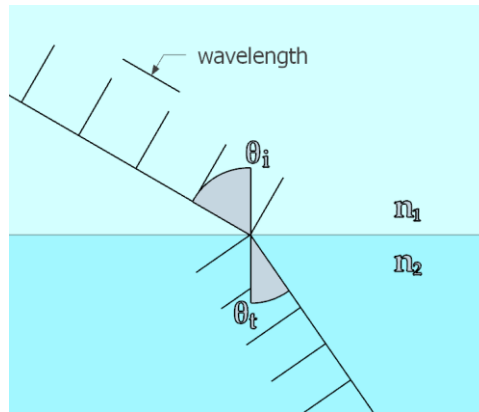


Figure 2.1 - refraction occurring where  $n_1 < n_2$ . Note the shortening of apparent wavelength as the ray enters the denser medium.

As can be noted from the equation above and from **Figure 2.1**, Snell's law applies both when light moves from a lower to higher refractive index material (for example, air to water) and from a higher to lower refractive index material. There are, therefore, circumstances where a solution of Snell's law would provide transmission at an angle of or exceeding  $90^\circ$ , or in other words where refraction would have sent light from a denser medium back into the denser medium, refraction is impossible and the incident light is losslessly reflected instead. This is total internal reflection (TIR), and the minimum angle required to create it is referred to as the critical angle or  $\theta_c$ .

$$n_1 \sin(\theta_c) = n_2 \sin(90^\circ)$$

$$\theta_c = \sin^{-1}(n_2/n_1)$$

Equation 2.3

Unlike with more conventional means of reflection, TIR conserves the energy of the incident light. Therefore, if a ray of light is propagated in a denser medium between two lower RI media,

and at an angle at or exceeding  $\theta_c$  for both boundaries, TIR will occur each time the ray strikes the boundary of the denser medium and therefore remains contained for as long as the boundaries continue in their current relation. This constitutes a waveguide, initially demonstrated by Colladon<sup>141</sup> and later presented by Tyndall<sup>142</sup> using water jets in air as a smooth, curved surface to show light following the contours of a narrow stream (**Figure 2.2**)

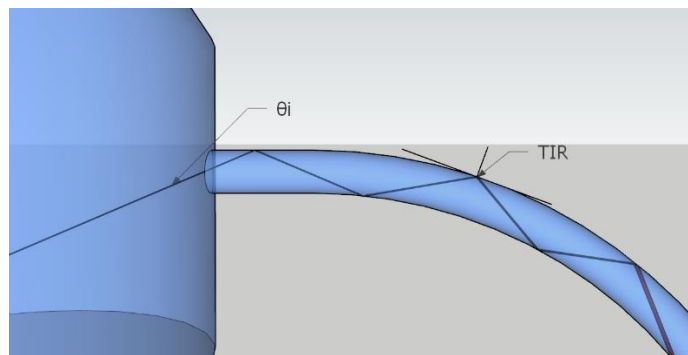


Figure 2.2 - model of Colladon and Tyndall's demonstrations of a waveguide. The light angle exceeds  $\theta_c$  at each boundary, resulting in reflection that guides the light ray down the waterspout.

## 2.2.2. The Guided Mode

For waveguide cores of diameter significantly greater than wavelength, the reflection behaviour remains geometric in nature, and the light path within may be considered through resolving Snell's law (**Equation 2.3**) on each reflection. However, at wavelength-scale waveguide diameters, other factors come into play. A wave reflected between multiple close interfaces will interfere with itself, requiring constructive interference to propagate usefully. The combination of path length between interfaces, thickness of the waveguide and incident angle are governed by the *transverse resonance condition*:

$$2kd \cos \theta + \varphi_{w,c}(\theta) + \varphi_{w,s}(\theta) = 2m\pi$$

Where:

$k$  = the distance travelled between each mutual internal reflection;

$d$  = diameter of waveguide core;

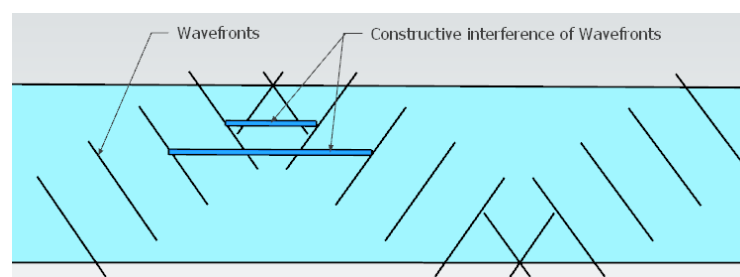
$\theta$  = Incident, and by extension reflection, angle;

$\varphi_{w,c}$  = phase shift encountered at the interface of waveguide and cover (cladding) materials;

$\varphi_{w,s}$  = phase shift at the interface of waveguide and substrate materials;

$m$  = any suitable integer.

It is worth noting that for waveguides where the same material interfaces are encountered both on the ‘upper’ and ‘lower’ reflections,  $\varphi_{w,s}$  will equal  $\varphi_{w,c}$ . The terms are differentiated for asymmetric waveguides where  $n_c$  and  $n_s$  differ, for example a thin film deposited onto glass and immersed in water. Varying  $\theta$  will give certain valid solutions of  $m$  for given values of  $\lambda$  and  $d$  – these solutions indicate angles at which the terms are otherwise balanced and constructive interference becomes replicable from one reflection to another, known as a guided mode, as illustrated in **Figure 2.3**. By keeping input wavelength and geometry of waveguide fixed, finding the number of guided modes a waveguide can support becomes experimentally and conceptually simpler.



*Figure 2.3 - Constructive interference of a guided mode, with emphasis on wavefronts. For purposes of illustration, the effects of  $\varphi$  have been disregarded for this cartoon.*

The phase shifts  $\varphi$  encountered in **Equation 2.4** are polarisation-dependent to some degree, supporting TE and TM modes at slightly different incident angles as  $\varphi_{w,s}$  and  $\varphi_{w,c}$  are polarisation dependent with TM modes typically requiring more space,<sup>143</sup> although the mode that couples in more effectively may vary with a range of factors.<sup>144</sup>

The integer  $m$  also represents the opportunity for multiple solutions of the transverse resonance conditions within the same waveguide – where  $k$ ,  $d$  and  $\lambda$  permit it, multiple guided modes may be found within the same waveguide. the guided mode where  $m = 0$  is known as the fundamental mode, while additional modes (where  $m > 0$ ) are referred to as higher-order modes. As multiple modes within the same waveguide travel different distances and interact with different conditions at the waveguide boundaries, the light may encounter interferences or influencing factors differently.

## **2.3. Maxwell's Equations**

In order to properly understand a number of properties of waveguides, it is useful to define something of the nature of light. Typically for optical sensors, the classical field equations collated by Maxwell provide the basis for understanding the electromagnetic waves that make up light, and although this classical model does not account for the existence of photons it does describe the relationship between the electric and magnetic component of light. Maxwell's

equations suppose the existence of electric and magnetic fields which permeate all space, and through which charges or changes in electric or magnetic forces can be measured.

### 2.3.1. Underpinning Equations

The first of the necessary equations is **Gauss's Law** for the electric, relating to changes (flux) in electric field and its relationship with charge. This may be best explained by taking an arbitrary area and examining the electrical field through its boundaries – if no change occurs, then the electrical field flowing in will be equal to the field flowing out and the net electric flux will equal zero. However if some inlet (source) or outlet (sink) affects the total charge inside that area, a nonzero rate of discharge will be identifiable. The changing net rate of discharge, or the electric flux  $\Phi_E$ , can then be described in terms of the closed surface S around an arbitrary space A:

$$\frac{1}{\epsilon_0} \sum q. = \Phi_E = \oiint_A \vec{E} \cdot d\vec{S}$$

*Equation 2.5*

Where:

$\epsilon_0$  is the electric permittivity of free space (vacuum);

$q.$  is a single point charge upon the exterior area;

$\Phi_E$  is the electric flux;

$\vec{E}$  is the electric field;

$d\vec{S}$  is the outgoing electric field crossing the surface.

Since  $\sum q$ . equals the sum of point charges across the surface of the area, this indicates that the electric field is produced by that charge. Of note is the permittivity in free space  $\epsilon_0$ . Permittivity relates to the degree to which a material is permeated by an electric field. Where a dielectric medium is used, as is the case for optical waveguides, the permittivity  $\epsilon$  is related to the phase velocity of light in the medium via the dielectric constant  $K_E$  and from there to the refractive index.

**Gauss's Law** for the magnetic is somewhat simpler as unlike the electrical field, the magnetic field is incapable of forming monopoles and so cannot exist as a charge. With no sources or sinks to add or remove charge from a given enclosed area, in the absence of other fields in consideration, a magnetic flux must on balance equal zero. This simplifies the corresponding equation:

$$\oiint_A \vec{B} \cdot d\vec{S} = \Phi_M = 0$$

*Equation 2.6*

Where:

$\vec{B}$  is the magnetic field;

$d\vec{S}$  is the outgoing electric field crossing the surface;

$\Phi_M$  is the magnetic flux (as a counterpart to the electric flux).

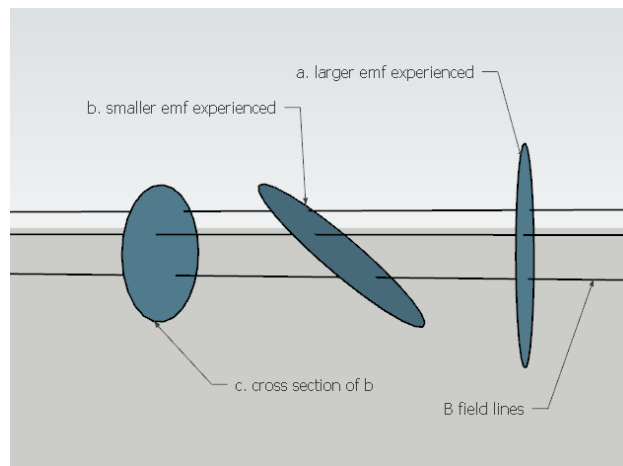
When considering in further detail the relationship between electric and magnetic fields, **Faraday's Induction Law** may prove useful. Discovered in part by monitoring the current

briefly induced during a change in magnetic field, it was found that an induced electromotive force (emf, more accurately a voltage) relates to the size of an area  $A$  lying perpendicular to the magnetic force, and therefore governed by the area of the loop that is penetrated by this field as the magnetic change is experienced (**Figure 2.4**). In other words, where  $\Delta B/\Delta t \neq 0$ , emf is proportional to the perpendicular portion of the area ( $A_{\perp}$ ), and where  $A_{\perp}$  is constant emf must be proportional to  $A_{\perp}\Delta B/\Delta t$ .

Together this provides another possible phrasing for the magnetic flux, in terms of the proportional effect upon area  $A$ :

$$\Phi_M = B_{\perp}A = BA_{\perp} = BA \cos \theta$$

*Equation 2.7*



*Figure 2.4 – Demonstrations of the dependence of the cross-section of an area intersecting an magnetic field undergoing flux, upon the emf experienced upon that area.*

As the comparison with Gauss's equation for magnetic flux shows, a magnetic flux must on balance equal zero – therefore the magnetic flux experienced upon area  $A$  can be said to generate an electrical potential difference (emf) that in turn generates an opposing magnetic flux which balances the forces experienced. If taken in terms of an area  $A$  bounded by a closed curve  $C$  (**Figure 2.5**Figure 2.5 - Visualisation of spatial terms used in Equation 2.8Equation 2.9, specifically closed loop  $C$ , open area  $A$  and the vector from the surface  $d\vec{S}$ ), we find the following:

$$\text{emf} = \oint_C \vec{E} \cdot d\vec{l} = -\frac{d}{dt} \iint_A \vec{B} \cdot d\vec{S}$$

Equation 2.8

The negative magnetic force experienced in the magnetic expression demonstrates that the induced magnetic field is a force proportional to and opposing the emf, as described above. In the absence of any electrical charge sources, the field  $\vec{E}$  parallel to the closed area  $C$  cannot flow anywhere and so must close around itself – in other words, a loop of electrical charge occurs around and always perpendicular to the lines of magnetic field experiencing flux, and the magnetic flux changes because the magnetic field changes.

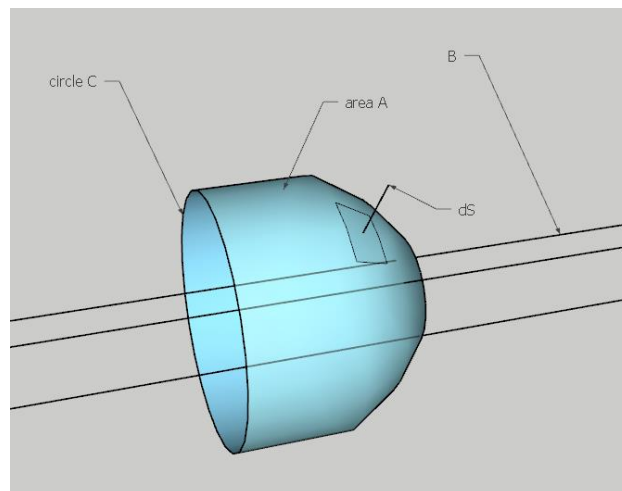




Figure 2.5 - Visualisation of spatial terms used in Equation 2.8 Equation 2.9, specifically closed loop  $C$ , open area  $A$  and the vector from the surface  $d\vec{S}$

The Induction Law can therefore be rewritten as a partial derivative with respect to time (due to the factor of changing spatial conditions altering  $\vec{B}$ ), as follows:

$$\oint_C \vec{E} \cdot d\vec{l} = - \iint_A \frac{\partial \vec{B}}{\partial t} \cdot d\vec{S}$$

Equation 2.9

**Ampere's Circuital Law** may be described by first considering a closed magnetic field surrounding a current-carrying wire, just as Faraday's Law considers emf induced by an area penetrated by a magnetic field. The magnetic field can be calculated by  $B = \mu_0 i / 2\pi r$ , derived from experimentation. The work done by this field (a way of describing the force parallel to the line of its travel, in this case around the circle described by the magnetic field around the current-carrying wire) can be found by summing components of the line, and simplifies to:

$$\sum B_{\parallel} \Delta l = \mu_0 i$$

Or:

$$\oint_C \vec{B} \cdot d\vec{l} = \mu_0 \sum i$$

Equation 2.10

Where:

$\mu_0$  is the permeability of free space, or  $4\pi \times 10^{-7} \text{ N} \cdot \text{s}^2/\text{C}^2$ ;

$i$  is the current of one or more current-carrying wires encapsulated by  $C$ .

As this description of Ampere's Law does not account for nonuniform cross section of current density, it is also written once again in terms of an open area  $A$  (**Figure 2.6**, left):

$$\oint_C \vec{B} \cdot d\vec{l} = \mu_0 \iint_A \vec{J} \cdot d\vec{S}$$

Equation 2.11

Where:

$\vec{J}$  is the current per unit area, here the area over the specified area  $A$ .

Where the current is transferred in a medium other than vacuum,  $\mu_0$  may be substituted for the appropriate value of  $\mu$ , which is proportional to its relative permittivity.

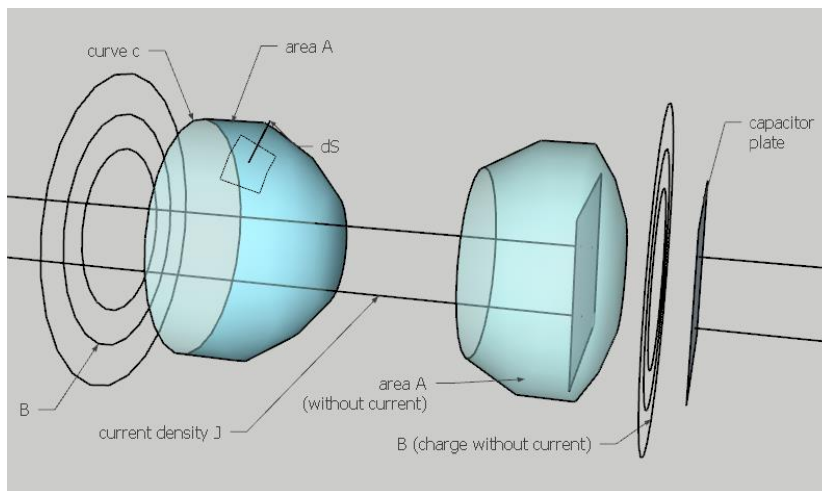


Figure 2.6 - Left: Visualisation of spatial terms used in Equation 2.12Equation 2.8Equation 2.9, specifically closed loop  $C$ , open area  $A$  and the vector from the surface  $d\vec{S}$ . Right: The same conditions when applied to one half of a charging capacitor. Note the presence of a  $B$  field between the capacitor.

Another restatement of Ampere's Law was proposed by Maxwell in response to an issue with calculating magnetic fields around capacitors, and regarding magnetic fields experienced in the

gap between capacitor plates. As **Figure 2.6** (right) illustrates, while Ampere’s Law is indifferent to the geometry of area  $A$  and its disposition, should one plate of a capacitor be included the equation will describe a null electrical current even when the closed area  $C$  has not moved and nothing physically has changed. This apparent contradiction may be solved by considering the magnetic field within a charging or discharging capacitor – even when no current appears to flow, a magnetic field is detectable between the plates indistinguishable from the field found along the wires.

If the electric field over a capacitor is governed by the area of each plate and the charge on the plate in the form  $E = \frac{Q}{\epsilon A}$ , then the derivative as the charge varies may be described in terms of current density  $\vec{J}_D$ :

$$\vec{J}_D = \epsilon \frac{\delta \vec{E}}{\delta t} = \frac{i}{A}$$

*Equation 2.12*

Maxwell restated Ampere’s Law in order to include a time-varying electric field even when the current density is 0:

$$\oint_C \vec{B} \cdot d\vec{l} = \mu \iint_A \left( \vec{J} + \epsilon \frac{\delta \vec{E}}{\delta t} \right) \cdot d\vec{S}$$

*Equation 2.13*

## 2.3.2. Arrangements of Maxwell’s Equations

With the four underlying laws described, it becomes possible to describe **Maxwell’s Equations**. By examining equations Equation 2.5, Equation 2.6, Equation 2.9 and Equation

2.13, given no currents and no charges in free space, a remarkable symmetry can be found in the relationship between electric and magnetic fields:

$$\oiint_A \vec{E} \cdot d\vec{S} = 0$$

*Equation 2.14*

$$\oiint_A \vec{B} \cdot d\vec{S} = 0$$

*Equation 2.15*

$$\oint_C \vec{E} \cdot d\vec{l} = - \iint_A \frac{\partial \vec{B}}{\partial t} \cdot d\vec{S}$$

*Equation 2.16*

$$\oint_C \vec{B} \cdot d\vec{l} = \mu_0 \epsilon_0 \iint_A \frac{\partial \vec{E}}{\partial t} \cdot d\vec{S}$$

*Equation 2.17*

As the electric field effects the magnetic field, so the magnetic field will affect the electric field. Provided no other external influences are accounted for, these interactions suitably balance one another.

While so far vectors such as  $\vec{E}$  and  $\vec{B}$  have sufficed to describe the electric and magnetic fields around defined areas, especially closed circles and the surfaces of closed or open areas encapsulating flux along linear paths, it is possible to recontextualise the equations by considering fields from a specific point in space. The differential operator Del ( $\vec{\nabla}$ ) contains the sum of the Cartesian coordinates for the associated vector field, for example:

$$\vec{\nabla} \cdot \vec{E} = \frac{\delta E_x}{\delta x} + \frac{\delta E_y}{\delta y} + \frac{\delta E_z}{\delta z}$$

Here Del (or the divergence) of  $\vec{E}$  is the sum of the changes along the x, y and z axes, and indicates the presence of a charge at the point described. This is in contrast to flux  $\Phi$ , which describes a change in the field across the defined surface.

We understand from Equation 2.5 that the net electric flux is equal to the net charge enclosed, and by dividing by volume describes the charge density at the given point. Therefore the divergence of Gauss's Law for electric fields is as follows:

$$\vec{\nabla} \cdot \vec{E} = \frac{\rho}{\epsilon_0}$$

*Equation 2.18*

The differential version of Gauss's Law for magnetic fields is simpler due to the absence of magnetic point charges, meaning the divergence must always be zero:

$$\vec{\nabla} \cdot \vec{B} = 0$$

*Equation 2.19*

To take the corresponding differential versions of Faraday's and Ampere's laws, which consider the closed loop of induced field around the flux at the point described, the corresponding operator curl ( $\vec{\nabla} \times$ ) is required in place of Del. Loosely, if  $\vec{V}$  is the flux across the surface of an infinitesimally small volume, then  $\vec{\nabla} \times$  can be considered the induced charge encountered in a closed loop around an infinitesimally small closed circle. This allows the differential of Equation 2.9 and Equation 2.13 as follows:

$$\vec{\nabla} \times \vec{E} = -\frac{\partial \vec{B}}{\partial t}$$

Equation 2.20

$$\vec{\nabla} \times \vec{B} = \mu_0 \epsilon_0 \frac{\partial \vec{E}}{\partial t}$$

Equation 2.21

A third way to describe Maxwell's equations, and a useful way to describe electromagnetic radiation, is to rephrase Equations 2.17-2.20 as eight differential equations in terms of cartesian coordinates, as follows:

Faraday's Law

$$\frac{\delta E_z}{\delta y} - \frac{\delta E_y}{\delta z} = -\frac{\delta B_x}{\delta t}$$

$$\frac{\delta E_x}{\delta z} - \frac{\delta E_z}{\delta x} = -\frac{\delta B_y}{\delta t}$$

$$\frac{\delta E_y}{\delta x} - \frac{\delta E_x}{\delta y} = -\frac{\delta B_z}{\delta t}$$

Ampere's Law

$$\frac{\delta B_z}{\delta y} - \frac{\delta B_y}{\delta z} = \mu_0 \epsilon_0 \frac{\partial E_x}{\partial t}$$

$$\frac{\delta B_x}{\delta z} - \frac{\delta B_z}{\delta x} = \mu_0 \epsilon_0 \frac{\partial E_y}{\partial t}$$

$$\frac{\delta B_y}{\delta x} - \frac{\delta B_x}{\delta y} = \mu_0 \epsilon_0 \frac{\partial E_z}{\partial t}$$

Gauss's Law Magnetic

$$\frac{\delta B_x}{\delta x} + \frac{\delta B_y}{\delta y} + \frac{\delta B_z}{\delta z} = 0$$

Gauss's Law Electric

$$\frac{\delta E_x}{\delta x} + \frac{\delta E_y}{\delta y} + \frac{\delta E_z}{\delta z} = 0$$

*Equation 2.22*

From this point, electromagnetic waves can be described.

### 2.3.3. Electromagnetic Waves

The electric field produced by a magnetic disturbance, and correspondingly the magnetic field created by an electric disturbance, are vector cross products, or in other words will be perpendicularly oriented to one another. In this way it is possible to consider a time-varying  $\vec{E}$  field that generates a  $\vec{B}$  field oriented perpendicularly, which in turn generates a similarly perpendicular  $\vec{E}$  field, and so on. A chain of disturbances so described will result in a pulse that propagates as mutually transverse electric and magnetic fields. This pulse is effectively self-sustaining in vacuum, and constitutes an electromagnetic wave. In this way, light is described.

The perpendicularity of an electromagnetic wave can be described by considering a plane wave propagating in direction x (**Figure 2.7**). The electric field will have no component in the direction of propagation, or  $\frac{\delta E_x}{\delta x} = 0$ , therefore the  $\vec{E}$  field can be said to be transverse to the

direction of travel. We can instead fit the moment-to-moment direction of  $\vec{E}$  to the y axis, at which point it can be described by:

$$\vec{E} = \hat{j}E_y(x, t)$$

Equation 2.23

Returning to Faraday's Law as described in Equation 2.22,  $B_x$  and  $B_y$  remain constant, and the time-dependent  $\vec{B}$  field is left with the z axis in which to have a component. Therefore:

$$\frac{\delta E_y}{\delta x} = \frac{\delta B_z}{\delta t}$$

Equation 2.24

The  $\vec{B}$  field is therefore also transverse, and mutually perpendicular with the  $\vec{E}$  field. This provides the understanding of a light ray as an electromagnetic wave, with an orthogonal electric and magnetic component in phase with one another.

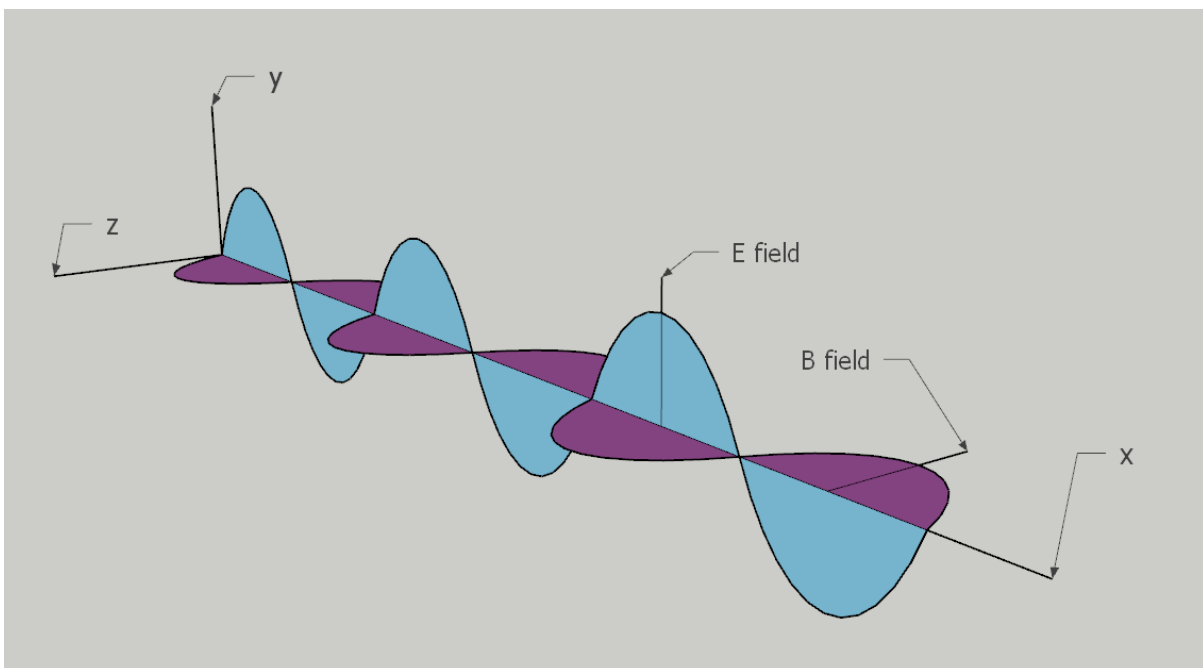


Figure 2.7 – Visualisation of electromagnetic wave, travelling in direction x, with transverse  $\vec{E}$  and  $\vec{B}$ .



## 2.4. Optical Waveguides and Related Phenomena

Popular in telecommunications contexts such as optical fibres, waveguides use ongoing TIR to deliver light waves through channels with minimal loss of power or coherence. The waveguide may also be used as a sensor, whether in configurations such as a 2d microfluidic chip<sup>145, 146</sup> or a 1d optical fibre.<sup>147, 148</sup> The following sections cover some of the phenomena surrounding waveguides, however in the interests of brevity only a small selection is presented.

### 2.4.1. The Goos-Hänchen Effect

Discovered in 1947,<sup>149</sup> the Goos-Hänchen shift is a phenomenon in which internally reflected light undergoes a small lateral shift from the position where incident light strikes the interface. This is sometimes described as the effect of the bulk cladding material, rather than the interface stopping all propagation with the first plane of atoms,<sup>150</sup> but is a form of optical vortex.<sup>151</sup> The shift encountered is often on the order of the wavelength tested, and can be calculated by finding a virtual reflective plane of distance  $\delta$  behind the true interface:

$$\Delta x = 2\delta \tan \theta_i$$

*Equation 2.25*

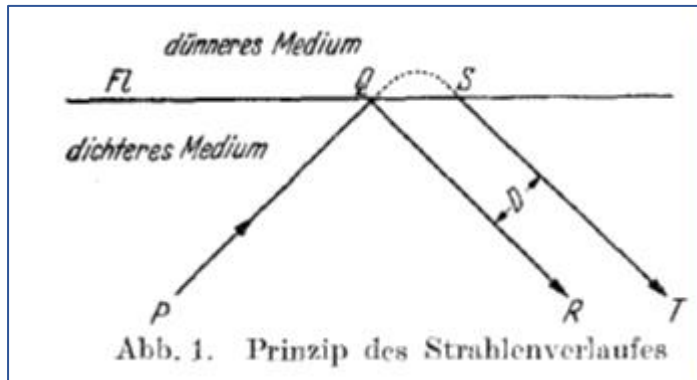


Figure 2.8 - excerpt from the original paper,<sup>149</sup> showing displacement of the reflected light (T). In the above equation,  $\Delta x$  represents distance of displacement QS.

## 2.4.2. The Evanescent Field

While all energy is contained within the boundary of the core by TIR, that does not mean necessarily mean nothing propagates into the cladding. The optical vortex formed during internal reflection and described by Goos-Hänchen shift may be interacted with. The power of any transmitted component is governed by resolving the boundary conditions:

$$r_{\perp} = \frac{\cos \theta_i - (n_{ti}^2 - \sin^2 \theta_i)^{1/2}}{\cos \theta_i + (n_{ti}^2 - \sin^2 \theta_i)^{1/2}}$$

$$r_{\parallel} = \frac{n_{ti}^2 \cos \theta_i - (n_{ti}^2 - \sin^2 \theta_i)^{1/2}}{n_{ti}^2 \cos \theta_i + (n_{ti}^2 - \sin^2 \theta_i)^{1/2}}$$

Equation 2.26

Where:

$r_{\perp}$  and  $r_{\parallel}$  are the amplitude of transverse electric and transverse magnetic polarisations, respectively.

During total internal reflection, this resolves to  $r_{\perp} r_{\perp}^* = r_{\parallel} r_{\parallel}^* = 1$  and therefore in terms of energy contained,  $I_i = I_r$  while  $I_t = 0$ . In other words, while there is a transmitted wave, it contains no energy whatsoever. This is known as a standing wave, or due to its exponentially attenuating field, the evanescent wave. Interruption of this evanescent wave with another core material has an adverse effect on the quality of total internal reflection, permitting partial transmission of light across the cladding gap – this is known as frustrated total internal reflection (FTIR).

### 2.4.3. Surface Plasmon Resonance

Unlike dielectric materials, metals do not easily permit the passage of light. This is attributed to the presence of free electrons which may absorb the photons, resulting in electron excitation but rapid attenuation of transmitted light. As most light cannot be transmitted, metals appear reflective across the visible spectrum. This contributes to the silvery appearance of most metals. However at a certain  $\theta_i$ , light may couple with the contained electrons and create a charge density wave or plasmon, propagating parallel to the metal's surface. The resonant angle  $\beta$  at which SPR occurs is dependent on the permittivity of the metal, and is governed by the equation:<sup>152</sup>

$$\beta = \sin^{-1} \sqrt{\frac{\epsilon_m}{(\epsilon_m + \epsilon_c)\epsilon_s}}$$

*Equation 2.27*

Where:

$\epsilon_m$ ,  $\epsilon_c$  and  $\epsilon_s$  are the relative permittivity of the metal film, cover and substrate respectively.

Not unlike the evanescent wave of TIR (above), the surface plasmon wave generates its own electric field which extends beyond the metal surface and may propagate around 300 nm into the cover layer beyond.<sup>153</sup> Any interruption or a change in  $n_c$  for the standing wave will alter  $\epsilon_c$ , changing in turn the resonant angle. By this measure,  $n_c$  may be monitored as a typically very sensitive means of label-free sensor, provided a suitable detection scheme to provide the change in refractive index is used.<sup>154</sup>

#### 2.4.4. Fresnel Reflections and the Leaky Waveguide

A variant of the conventional slab waveguide. An optical leaky waveguide uses Fresnel reflection, the partial reflection encountered as light interacted with the interface of transparent media at a grazing angle (**Figure 2.9**), rather than total internal reflection on one or both interfaces. Recalling **Equation 2.4**, where there are three components to the phase of the guided mode required to ensure constructive interference - the phase shift at core-cover interface  $\varphi_{w,c}$ , and the phase shift at core-substrate interface  $\varphi_{w,s}$ . For ease of illustration, Fresnel reflection shall occur at the  $\varphi_{w,s}$  interface only.

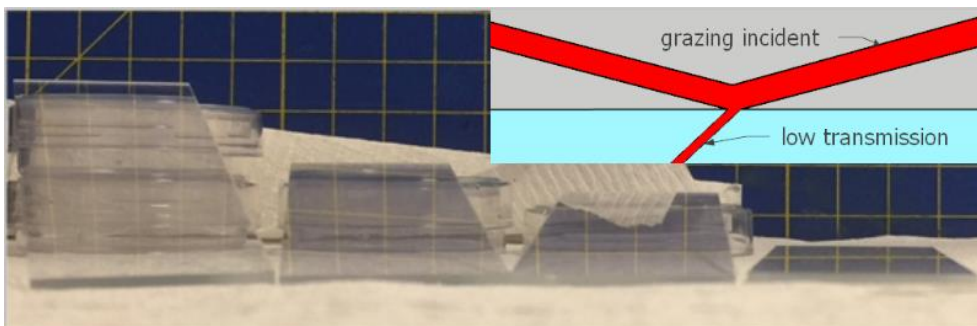


Figure 2.9 - Demonstration of Fresnel reflection. As incident angle increases, a greater proportion of light is reflected, and the blue/yellow chequered pattern becomes more clearly visible. Inset: a cartoon of Fresnel reflection. A broader line indicates a greater relative proportion of the incident light.

Fresnel reflection is polarisation-dependent to some degree. For the transverse electric (TE) component of light,  $\varphi_{w,s} = \pi$ . For the transverse magnetic (TM) component, only for incident light greater than Brewster's angle does  $\varphi_{w,s} = \pi$  remain true. Brewster's angle is a solution of Fresnel's equations in which the transmission and reflection angles of a TM ray equal  $90^\circ$  (after reflection). This can be calculated using the following:

$$\theta_B = \tan^{-1}\left(\frac{n_w}{n_c}\right)$$

Equation 2.28

By incorporating Fresnel's equations into the transverse resonance condition (**Equation 2.4**) and substituting the guided mode for the total phase or  $\varphi_{total}$ , we can calculate the phase that may constructively interfere and so operate as a guided leaky mode:

$$\varphi_{total} = 2kd \cos \theta + 2 \left( \frac{2\pi h}{\lambda} \sqrt{n_w^2 - N^2} \right) + \pi - 2 \tan^{-1} \left( \frac{n_w^{2p}}{n_c^{2p}} \sqrt{\frac{N^2 - n_c^2}{n_w^2 - N^2}} \right) = 2m\pi$$

$$\varphi_{total} = 2kd \cos \theta + \left( \frac{4\pi h}{\lambda} \sqrt{n_w^2 - N^2} \right) - 2 \tan^{-1} \left( \frac{n_w^{2p}}{n_c^{2p}} \sqrt{\frac{N^2 - n_c^2}{n_w^2 - N^2}} \right) = (2m - 1)\pi$$

Equation 2.29

Where:

$N$  (alternatively written as  $N_{eff}$ ) is the effective mode index, an expression of the refractive index of the waveguide core after accounting for phase shift on each boundary.

$h$  is the waveguide diameter

This is the mode equation for leaky waveguides. In order to prevent introducing an unintentional imaginary component,  $N$  must be greater than  $n_c$  (to satisfy the second phrase) but less than  $n_w$  (to satisfy the first phrase). Therefore, the leaky waveguide must have a slightly smaller refractive index than the substrate and not function as a conventional waveguide.

In such conditions, light is internally reflected at the waveguide-substrate interface but not wholly as per TIR. The relative strength of light reflected is thus governed by Fresnel's equations. For dielectric substances and following Snell's law (**Equation 2.2**), this can be simplified to its perpendicular and parallel components (respectively):

$$r_{\perp} = \frac{\sin(\theta_w - \theta_s)}{\sin(\theta_w + \theta_s)}$$

$$r_{\parallel} = \frac{\tan(\theta_w - \theta_s)}{\tan(\theta_w + \theta_s)}$$

*Equation 2.30, Equation 2.31*

For a leaky waveguide, light will be decoupled from the structure into the substrate on a piecemeal basis, as a  $1 - r$  fraction of amplitude is transmitted with each reflection. Combined with the more lossless TIR on the other waveguide boundary, any transmitted amplitude will necessarily emerge at a value of  $\theta$  suiting an integer of  $m$  in **Equation 2.29**, or in other words a guided mode. Quantitative analysis with an optical leaky waveguide is therefore a matter of ensuring the analyte alters a term within the mode equation, then monitoring the loss or recovery of transmitted light from the mode.<sup>20, 155</sup>

What is more, additional modes may be introduced into the leaky waveguide for each solution of  $m$  that the modified transverse resonance equation (**Equation 2.29**) may support, as related in Section 2.2.2 above. It may also be possible to entrap a leaky waveguide mode between a waveguide-surface interface and an additional waveguide-waveguide interface – this would permit the operation of a *stacked leaky waveguide* in which depending on incident angle, light may be partially contained in one waveguide layer only or may cross both waveguide layers and sample both waveguides.

## 2.5. Summary

In this chapter, the core relationships and formulae surrounding waveguides was introduced. Additionally, the theory underlying certain sensing parameters (evanescent field, surface plasmon resonance, and leaky mode) were described. Of these primarily the leaky waveguide will be relevant in future chapters, however SPR remains a popular sensing method for detecting small shifts in refractive index, and so may be used as a point of comparison during the project's development.

# **Chapter 3. PRELIMINARY STUDIES FOR THE SYNTHESIS OF PH-SENSITIVE REFERENCE HYDROGEL WAVEGUIDES**

## **3.1. Introduction**

To facilitate easier reference, the majority of this chapter will be split into three subdivided sections to simplify multiple experimental stages and will contain the respective experimental procedure internally. Section 3.2 discusses the fabrication and assessment of polyacrylamide waveguides produced by casting, using both positive photoresist and microsphere deposition to form cast spacers. Section 3.3 explores the production, characterisation and gel formation characteristics of linear polyacrylamide and selected copolymers, using a small shortlist of chemical crosslinkers. Section 3.4 assesses the pH sensitivity of the polyacrylamide leaky waveguides tested in previous sections, and briefly interrogates certain means by which pH sensitivity may be provided in the form of a swellable hydrogel.

## **3.2. Casting Methodology and Assay**

As the most direct means of producing polyacrylamide gel, the prepolymer solution was selected and a means of physical casting developed. In this section, two types of spacer are tested – a commercially available positive photoresist and later spot-deposition of monodisperse latex microspheres. The replicability and suitability of each casting method is then assessed by



determination of the gel porosity and the refractive index sensitivity of the LW. In order to maintain comparability, the crosslinker *N,N*-methylenebisacrylamide (Bis) was fixed at 1/30 molar fraction of total monomer.

### **3.2.1. Chemicals and Materials**

Acrylamide/bisacrylamide blends for gel electrophoresis (40% w/v), *N,N,N',N'*-tetramethyl ethylenediamine (TEMED), ammonium persulphate (APS), (3-Aminopropyl) triethoxysilane (APTES), allyltrichlorosilane (ATCS), poly(ethylene glycol) (PEG) of selected molecular weights, toluene and reactive blue 4 (RB4) was procured from Sigma Aldrich (UK).

Decon 90 was procured from Fisher Scientific (UK)

Chloro(dimethyl)vinylsilane (CDVMS) was purchased from TCI Chemicals (UK)

Glass microscope slides of thickness 1 mm (to standard ISO 8037/1) was purchased from VWR (UK)

MEGAPOSIT SPR220-7.0 and SPR220-3.0 photoresists and MF-24A developer were procured from the manufacturer.

All chemicals were used without further purification.

### **3.2.2. Experimental Procedure**

### **3.2.2.1. The Leaky Waveguide Testing Apparatus**

The leaky waveguide apparatus generally follows the Kretschmann configuration used in Surface Plasmon Resonance sensors (see Chapter 2) and is described in more detail in prior publications by its pioneers.<sup>156</sup> Briefly, a hydrogel waveguide deposited on a glass microscope slide is placed atop a glass prism, with refractive index matched oil between the glass surfaces to ensure incident light is not affected by surface imperfections or imperfect seal. A superluminescent diode of wavelength 660 nm is used as the light source. Collimated input light is focused by cylindrical lens into a wedge-shaped beam and directed into the prism, with the hydrogel waveguide at the focal point. Reflected light leaves the prism, is collimated by a second cylindrical lens and is detected by charge-coupled device (CCD) camera. The CCD output is therefore 2D, with a small variation in incident angle and a narrow interrogated area of the chip on the respective axes.

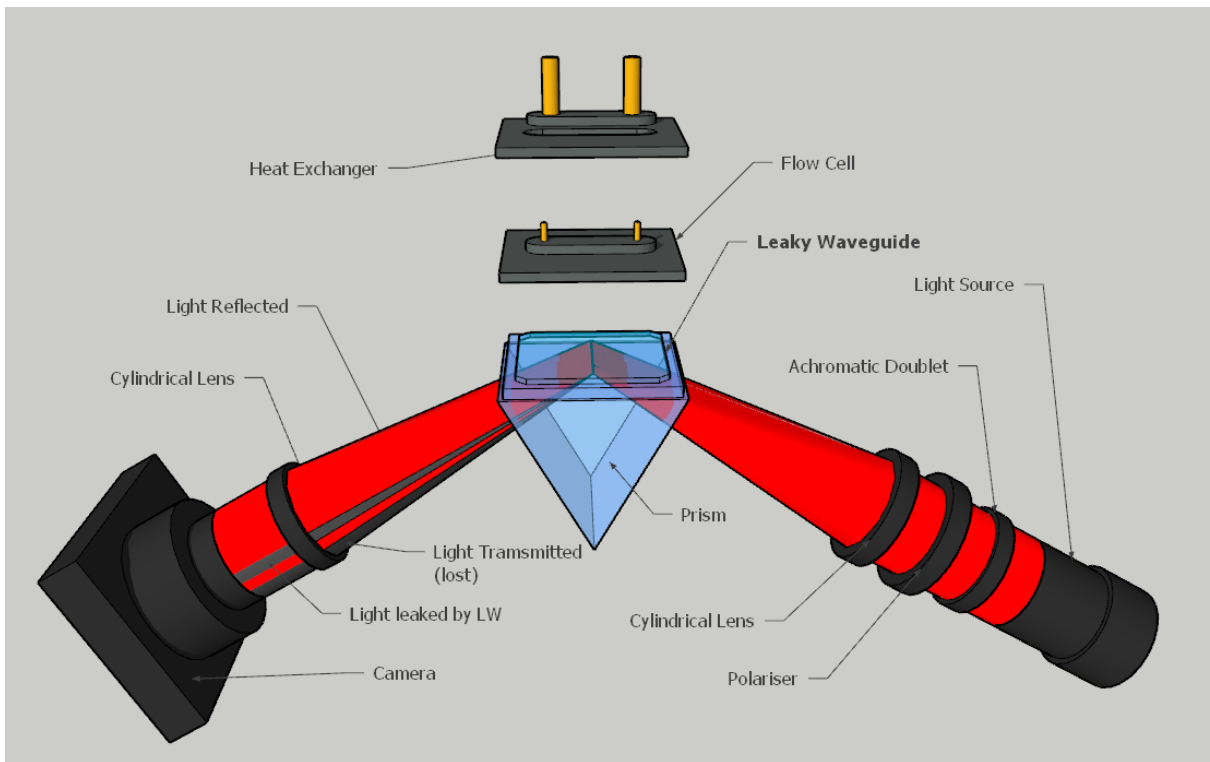


Figure 3.1 - Diagram of leaky waveguide (LW) apparatus.

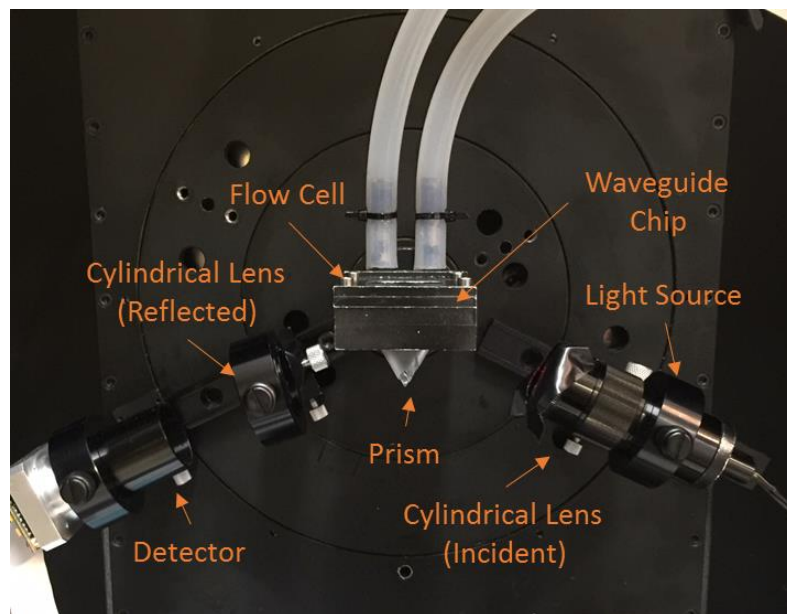
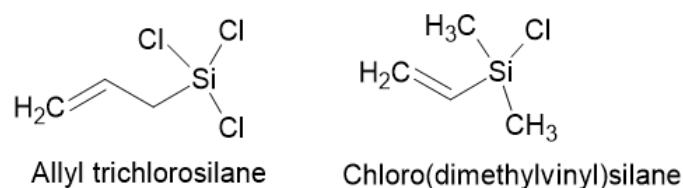


Figure 3.2 - Photograph of leaky waveguide apparatus interior while in use.

Resonance line positions were determined by real-time image analysis, locating the centre of a dip in light intensity (corresponding to the resonance angle, where reflected light is lost to absorption or scattering). In order to eliminate the effects of small aberrations or imperfections in the glass or waveguide surface, multiple independent measurements were taken at numerous positions along the chip and were subsequently combined during data analysis. Solutions are introduced to the chip by a temperature-regulated flow cell and are delivered by peristaltic pump at 1.50 ml/min. In the case of specific incident angle scans (such as those shown in **Figure 3.16**), a photodiode was used in place of the CCD and the cylindrical lens arrangement was removed entirely to ensure interrogation of the entire waveguide area at single wavelengths. This was performed to quickly assess a broader range of wavelengths than the cylindrical lens alone could permit.

### **3.2.2.2.Cast Production**

Before use in any application, 25 x 25 mm glass slides were sonicated for 30 minutes each in Decon 90 detergent solution, deionised water and ethanol, before drying in air. Photolithographed casts were prepared by spin-coating the selected photoresist solution directly onto the glass as per the manufacturer's instructions, utilising UV exposure at 220 nm. Spin parameters are described in Table 1, below. Substrate slides were cleaned as described above, then were immersed in a 1% (later 0.2%) v:v solution of allyltrimethylchlorosilane (ATCS) or chloro(dimethylvinyl)silane (CDMVS) (**Figure 3.3**) in toluene. Slides were then transferred to clean toluene for 5 minutes before drying on soft tissue paper.



*Figure 3.3 - Glass functionalisation agents. Allyltrichlorosilane (ATCS) may bond readily with silanol groups but can polymerise or form multiple layers if an oxygen source is introduced. Chloro(dimethylvinyl)silane (CDMVS) may less efficiently coat a silica surface due to steric hindrance but suffers no risk of multilayers or 3d structures forming.*

*Table 3.1 - Photolithographic spin conditions for cast film fabrication*

Target Thickness	Photoresist Formulation	Spin Speed (rpm)	Exposure Time (s)
10 μm	SPR 220 7.0	1700	120
5.5 μm	SPR 220 7.0	6000	120
4.5 μm	SPR 220 3.0	1500	60
2.0 μm	SPR 220 3.0	7000	60

Microsphere casting slides were produced by spotting clean glass slides in each corner with 1 μl of a 1% suspension of microspheres in water (the microsphere selection occurring at the procurement stage) and dried at 60° overnight. The integrity of the microsphere deposition on sample slides was examined by microscope before use. The microspheres were found to collect mainly at the rim of the deposited spot rather than distribute evenly through the area, and so microscopy was primarily used to verify that the spheres formed a single layer at the perimeter of their deposition site rather than a multilayer. Where a multilayer was detected, the slide was

discarded. Unfortunately, a camera-equipped microscope was not available for this stage and so no suitable image of microsphere deposition is available

Polyacrylamide was manufactured by polymerisation of acrylamide and N,N'-methylenebisacrylamide (**Figure 3.4**), using ammonium persulphate (APS) and Tetramethylethylene diamine (TEMED) (**Figure 3.5**) as initiator regime, using a common Free Radical Polymerisation protocol.<sup>157-159</sup>

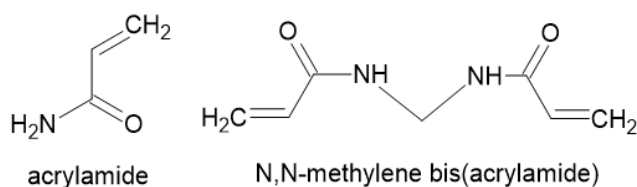


Figure 3.4 - The favoured backbone polymer for waveguide production acrylamide, alongside its compatible short-chain crosslinker equivalent methylenebis(acrylamide) (bis).

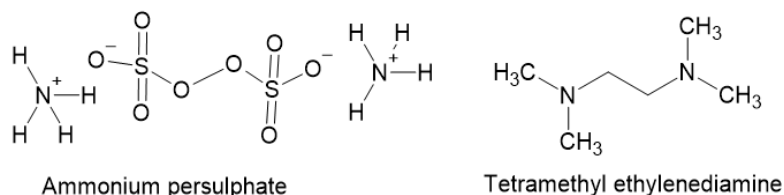
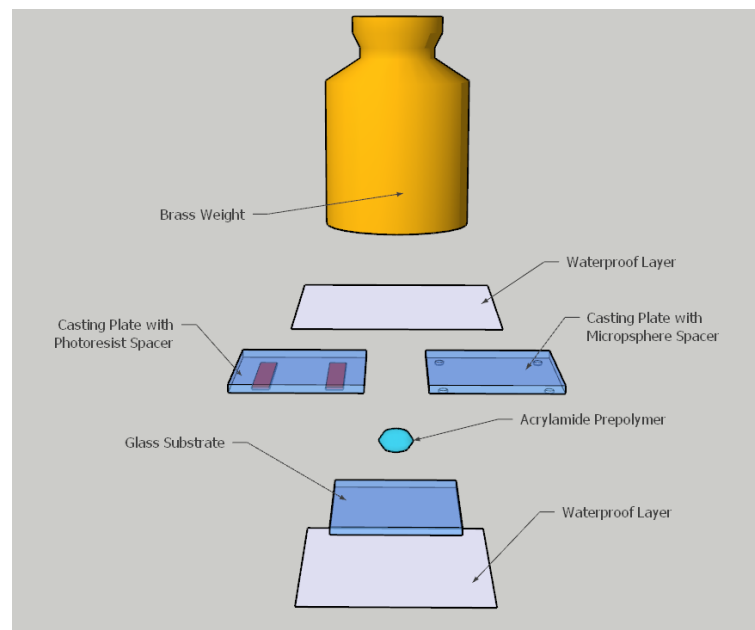


Figure 3.5 - Ammonium persulphate (APS) and N,N,N',N-tetramethyl ethylenediamine (TEMED), a common pair of activation reagents for free radical polymerisation of acryl-bearing monomers. Upon combination, the persulphate ion cracks the TEMED over the C-C central bond to provide an available free radical

Briefly, to 1.75 ml water is added 250 ml of acrylamide/bis(acrylamide) 29:1 solution. 40% w/v. 2.5  $\mu$ l of TEMED is also added, and finally 25  $\mu$ l of APS, 10%, w/v. The solution is immediately mixed thoroughly and a 100  $\mu$ l aliquot is deposited on a suitably treated glass slide (see above). A clean glass slide with appropriate spacer plus a 500 g brass weight is placed on top. Following the formation of an invertible gel (as can be found by monitoring the solution not aliquoted), the cast is immersed in deionised water for at least 2 hours before gently prying apart and storing under deionised water. Thicknesses provided by the tested photoresist formulations were 10-5.5  $\mu$ m and 4.5-2.0  $\mu$ m. The minimum and maximum bounds of each were taken forward in order to assay for best available conditions. This layout is described visually in **Figure 3.6**. The intended configuration of the slide is shown in **Figure 3.7**.



*Figure 3.6 - Casting arrangement for polyacrylamide LW production.*

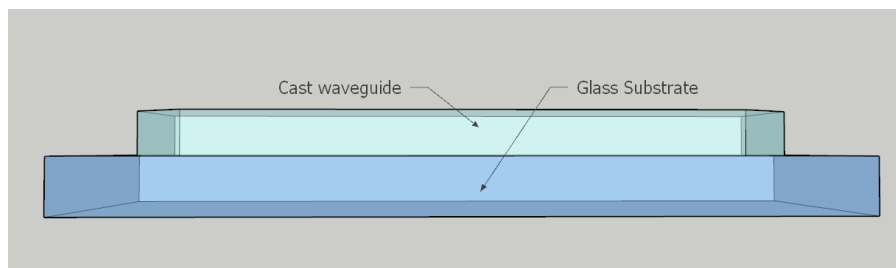


Figure 3.7 - Cartoon of single-layer cast leaky waveguide layout

### 3.2.2.3. Metal-Clad Leaky Waveguides (MCLW)

In order to rapidly assay waveguides for leaky modes that may not be visible without excessive dye-doping or other measures, metal cladding on the waveguide substrate may be employed. Metal cladding of the substrate causes light not at resonance angle to be absorbed as heat, while providing a sharp peak in reflectivity at the waveguide's mode resonance angle – see section 2.4.3 for an analogous description. Formulations for spincoating were trialled using glass substrates coated with 9 nm titanium, as has been described elsewhere.<sup>156, 160, 161</sup> The MCLW is explicitly neither the action nor part of the final configuration of the planned sensor, and so is not described in detail here, but it does effectively demonstrate the presence or absence of the leaky mode.

### 3.2.2.4. Waveguide Operation and Testing

In order to determine the sensitivity of the waveguide to changes in the waveguide bulk, of which the pH-induced expansion/contraction of the hydrogel is a part, small refractive index shifts were simulated. Glycerol solutions were introduced to the waveguide bulk by flow cell,



and the position of the resonance line tracked using bespoke software. Drift correction was performed by repeating one known measurement as an internal standard. RI shift measurements were converted from change in resonance line position (measured by image-processing the camera output per second, and reported in pixels) to change in resonance line angle. The pixel/angle relationship was calculated using half-degree step changes in camera angle position.

In order to determine in-situ pore sizes of the waveguide structure and analyte permeability, inert polymers of known hydrodynamic radius were introduced and their relative detection was determined. PEG solutions of 1% (w/v) were produced using commercially procured polymers, of average molecular weight 6, 10, 35, 100 and 300 kDa. Hydrodynamic radii of the polymers (**Table 3.2**) was found by photon correlation spectroscopy.

*Table 3.2 - Hydrodynamic radii of polymers used to probe for waveguide porosity and protein compatibility.*

M.W. of PEG	Hydrodynamic radius (nm) $\pm$ S.D.
6000	4.05 $\pm$ 0.037
10000	5.012 $\pm$ 0.700
35000	7.935 $\pm$ 0.111
100000	11.15 $\pm$ 0.010
300000	11.79 $\pm$ 0.319
BSA (see Section 3.3.3.3)	6.848 $\pm$ 1.172

### **3.2.3. Results and Discussion (Casting)**

#### **3.2.3.1. Leaky Waveguide Production**

Initial conditions were chosen to demonstrate viability of the photoresist method to manufacture thin films. Film thicknesses were compared, and in addition a brief comparison of the relative viabilities of casting weights employed. The presence or absence of total internal reflection and leaky modes were primarily assessed by the device described above. All interrogation of the waveguides occurred with a 633 nm, collimated superluminescent diode, and detection was by CCD or photodiode as fit the application. Initially, the viability of achieving total internal reflection with these thin films was assessed. As can be seen in **Figure 3.8**, a total internal reflection (TIR) line occurs, marking the boundary between transmission and reflection of incident light by the waveguide. Fresnel reflection, partial internal reflection approaching but weaker than the TIR line, is also visible as a fading intensity towards the top of the image.

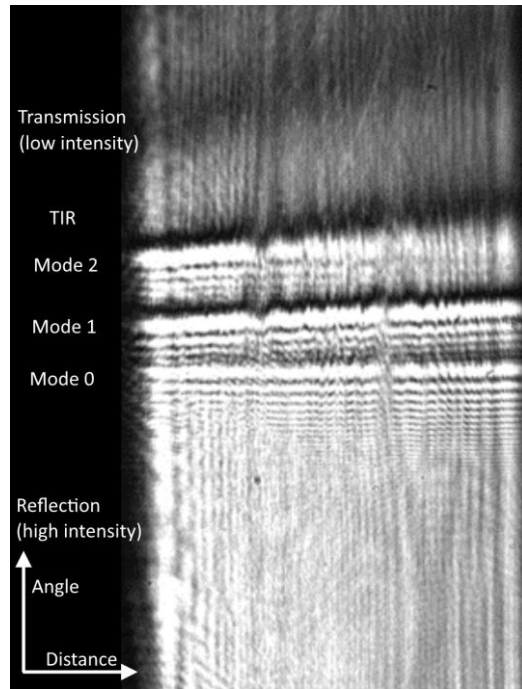


Figure 3.8 - annotated image of a leaky waveguide, taken by attached CCD.

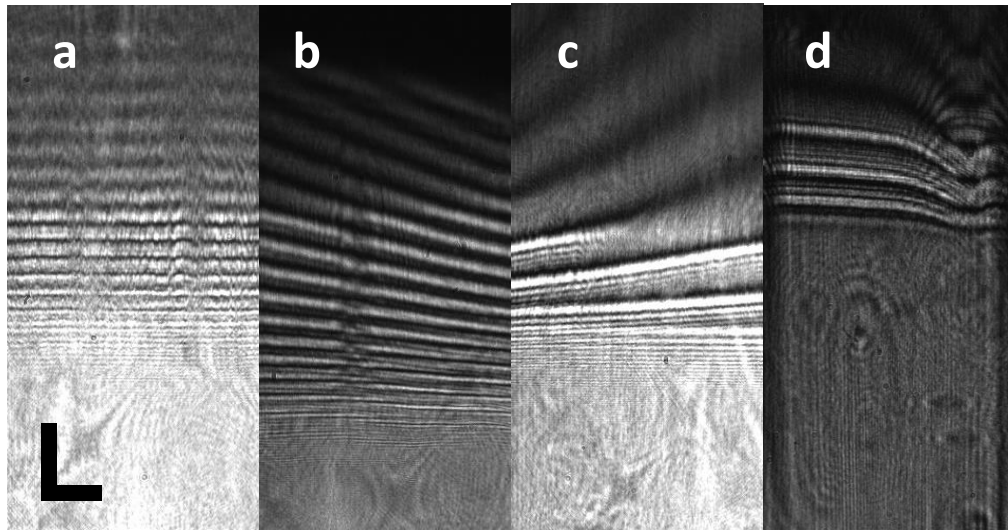


Figure 3.9 - Cast polyacrylamide waveguides by photoresist spacer of size (a)  $5.5 \mu\text{m}$ , (b)  $4.5 \mu\text{m}$ , (c)  $2.0 \mu\text{m}$ . (d) cast polyacrylamide waveguide by microspheres of median size  $1.1 \mu\text{m}$ . Scale bars are  $2^\circ$  (vertical) and  $2\text{cm}$  (horizontal).

**Figure 3.9a-c** shows the waveguides produced by the tested photoresist spacers. While 10  $\mu\text{m}$  provided no visible evidence of leaky modes, 5.5 and 4.5  $\mu\text{m}$  spacers provided only extended interference patterns. By reducing the spacer thickness to 2.0  $\mu\text{m}$ , a leaky waveguide with 2-3 modes was achieved. A single, clean mode was considered preferable, but by measuring only the first leaky mode (furthest from the TIR) suitable data could be collected. Fringes may be seen developing beneath the leaky modes in **Figure 3.9c-d**. Originally these were considered to be the result of interference thrown up by an additional layer of polymerised ATCS between the glass and waveguide, but are likely to have been evidence of diffraction waveguides being formed. As this was not known at the time and was later identified by the principal investigator independently,<sup>99</sup> substitution of ATCS for CDMVS was instead performed to prevent the formation of these fringes.

Modelling of leaky mode expression was hampered by the unanticipated presence of fringes, however it was found that with the selected substrate and cover of glass and water respectively, a multimode waveguide could not be achieved at 1.1  $\mu\text{m}$  film thickness no matter the gel refractive index selected. An approximate match for the appearance of **Figure 3.9d** was found after increasing the gel thickness to 2.7  $\mu\text{m}$  before other optimisation (**Figure 3.10**). Some degree of expansion may be expected due to the cast hydrogel swelling to its full capacity in the running solution, which likely accounts for this change.

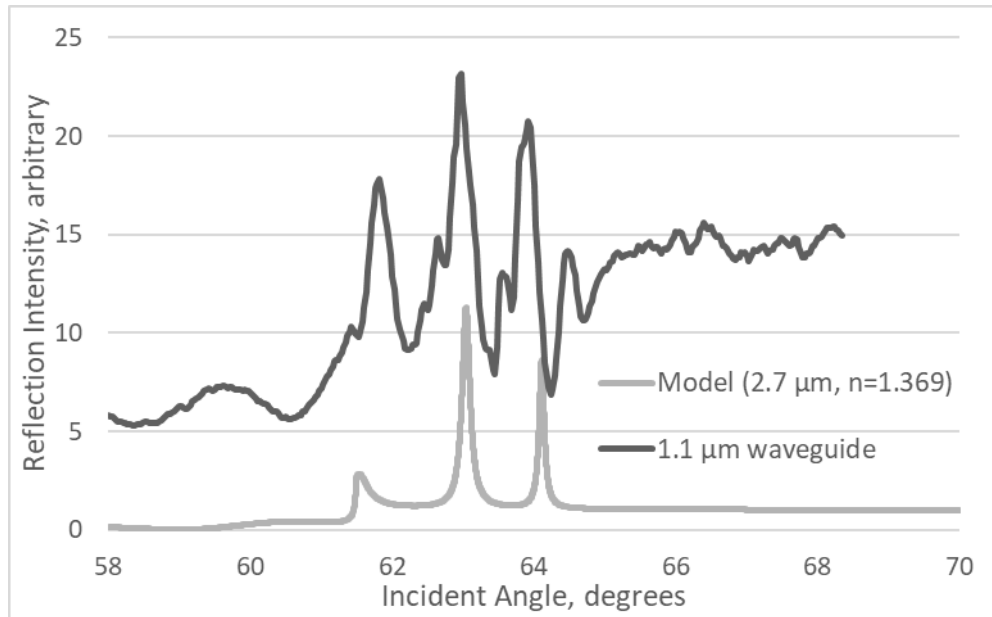


Figure 3.10 - Predicted reflection characteristics of waveguide, following data recovered from Figure 3.9d as model. Note the waveguide thickness required to replicate a waveguide fabricated at 1.1  $\mu\text{m}$  thickness.

With significant variability in both waveguide appearance and leaky mode count from waveguide to waveguide, an alternative casting method was sought to ensure better reliability. Trading the multi-step process to generate photoresist spacers for a single step would eliminate a number of possible sources for operator error or malfunction, particularly at the post-bake development stage where a percentage of casts consistently failed. Latex beads or microspheres were therefore assessed as discrete objects of a known and replicable median diameter.

With adoption of microspheres, replicability between slides becomes dependent purely on particle size distribution, and the use of 1.1  $\mu\text{m}$  beads provided a thinner gel than that of the photolithographic resins available at the time. However, by adopting microspheres the potential capacity for fine control of cast thickness (by adjusting resin spin speed) is entirely lost. Therefore, varying the waveguide's properties would need to be performed using other

parameters. The microsphere casting process is comparable to that of photoresist casting, and besides the change in spacer no other changes in process were adopted. Optical microscopy of deposited microspheres revealed that the microspheres dispersed away from the interior of their spotting location but had accumulated around the exterior, forming a ring stain due to the capillary action of suspended microspheres during evaporation.<sup>52</sup>

### **3.2.3.2. Refractive Index Sensitivities of Cast Films**

**Figure 3.11** demonstrates the mean sensitivities achieved by the cast polyacrylamide leaky waveguides, presented above. For photoresist-based casting, passable intra-batch repeatability was demonstrated, with a typical relative standard deviation (RSD) of 4.27%. Experimental sensitivities of around 130 degrees/RIU are comparable to that achieved experimentally by Mizutani et al<sup>161</sup>, who used a more complex and expensive resonant grating waveguide assembled on a gold thin film. Achieving a good degree of refractive index sensitivity with a low-cost and relatively simple to construct sensor, is a promising indication of its viability for further applications. Switching from photoresist to microsphere casts a small benefit to sensitivity, with a mean sensitivity of 148.7 degrees/RIU and a relative standard deviation of 7.31%. A similar sensitivity value indicates that the waveguides respond similarly to changes in refractive index regardless of cast spacer. The modest change in waveguide sensitivity however is not currently understood, and may form the basis for interesting future research – this may simply be due to a thinner gel providing more opportunity for responsive swelling and deswelling action.

In the above cases, RSD was found by taking the sample standard deviation of at least 3 measurements, performed upon different waveguides in order to provide a more practical comparison, represented as a fraction of the sensitivity. The resolution of these waveguides is dependent on the quality and resolution of the CCD used to capture, but with the camera used 300 px/degree was readily achievable. With signal noise generally sub-pixel in character, a resolution of 39000 and 44610 px/degree (respectively) could be not just reported but acted upon. A typical per-waveguide limit of detection of 5 px was found, however this varied from waveguide to waveguide and largely depended on the quality of the resonance line and its visualisation.

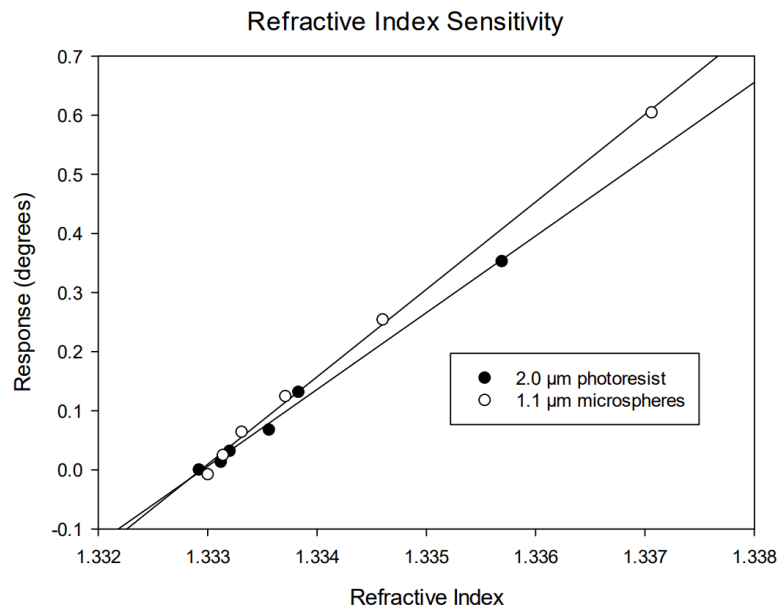


Figure 3.11 - Refractive index sensitivities of polyacrylamide cast gels produced with photolithographic or microsphere spacers

### 3.2.3.3. Porosities of Cast Films

To assess waveguide porosity, the more common method (scanning electron microscopy, SEM) faces some challenges. While techniques such as cryo-SEM can provide data on the pore sizes of hydrogels as well as their topology,<sup>162</sup> micro- or nanopores may be lost due to damage caused by the freezing process. Instead, the porosity of hydrogels was determined by direct interrogation by an inert material of known hydrodynamic radius, in this case poly(ethylene glycol) (PEG). As the waveguide is sensitive to the refractive index change only within the hydrogel bulk, PEG response is expected to be proportional to the fraction of PEG that can infiltrate the waveguide. Use of microspheres provided a typically greater permeability than photoresist-based spacers, although it is unclear at present why this occurred.

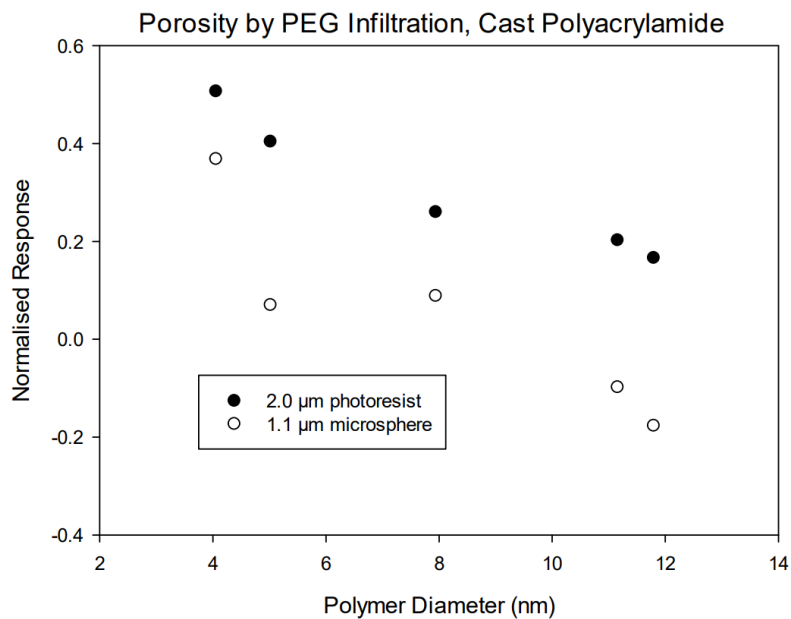
This method was settled on after considering potential issues with the more traditional and popular mercury intrusion porosimetry<sup>163, 164</sup> due to the thin nature of the cast (and especially later spun) films upon their glass substrate. While alternatives exist, such as ellipsometric monitoring of adsorption of organic solvent vapours,<sup>165</sup> these are typically restricted to xerogels, less polar hydrogels than acrylamide which do not collapse upon pore water evacuation. PEG intrusion is not a traditional measure, however due to cost and availability it was suggested for adoption.

For the purposes of comparing datasets, PEG response data was converted to a normalised response to account for inconsistencies in both specific waveguide sensitivity and variance in PEG refractive index. Normalised response was found by dividing the waveguide response by the glycerol sensitivity curve found concurrently. A normalised response of 1 therefore would mean the response of PEG relative to RI is equal to that of glycerol, and in turn that no exclusion



from the waveguide pores is occurring. A response of 0.5 would be expected to indicate 50% of the hydrogel is accessible to the PEG solution, with the inaccessible fraction of the gel providing no increase in overall response. A negative response, as encountered below, was not originally anticipated.

It was found that when the radius of PEG exceeded the polymer pore size, the waveguide reported a negative response (**Figure 3.12**). This may be due to polymer interactions between polyacrylamide and PEG, in which PEG coats polyacrylamide strands by formation of hydrogen bonds. However this binding is quite weak, and PEG is removed through a buffer wash.<sup>166</sup> Where PEG could infiltrate the polymer without hindrance, only a small reduction in response is seen and the response subsequently scales with the refractive index of the PEG solution, indicating a fraction of PEG retains its spherical conformation until interrupted by the polymer network. The use of buffer in place of deionised water was found to mitigate this phenomenon.



*Figure 3.12 - PEG permeation capacity, for polyacrylamide cast gels produced with photolithographic or microsphere spacers. "Normalised response" here means the waveguide response for the indicated polymer as a function of its expected sensitivity by refractive index alone.*

### **3.3. Linear Polymer Production and Characterisation**

An alternative to thin film casting, the topic of spin coating was investigated. However, the high toxicity of polyacrylamide monomer makes reusing the same methodology impractical. By synthesising a linear polymer that may later be crosslinked, a means of polymerising polyacrylamide may be reached that permits a swellable, chemically inert gel while also proving safe to spin coat in pre-gelled form. The epoxide ring opening reaction by amine, central to many epoxy resins and similar thermosetting materials,<sup>167-171</sup> was initially selected as the crosslinking mechanism with a view to its later use in the immobilisation of sensing moieties. Although these reactions often require elevated temperatures,<sup>168</sup> catalysis<sup>171</sup> or irradiation,<sup>169</sup> the reaction may still occur at room temperature.<sup>170</sup>

#### **3.3.1. Chemicals and Materials**

Acrylamide (40% w/v), N,N,N',N'-tetramethyl ethylenediamine (TEMED), ammonium persulphate (APS), N-aminopropyl methacrylamide (APMA), glutaraldehyde 25% (v/v), poly(ethylene glycol) (PEG) of selected molecular weights, (3-Aminopropyl) triethoxysilane (APTES), allylamine, toluene, bovine serum albumin (BSA), hydrochloric acid 1N, and reactive blue 4 (RB4) was procured from Sigma Aldrich (UK).

Decon 90 was procured from Fisher Scientific (UK)

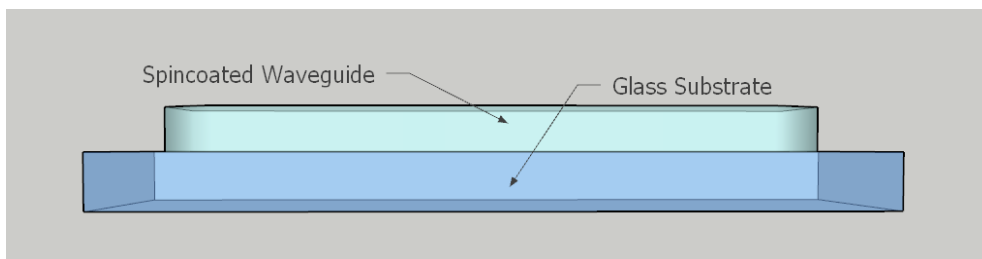
(N-dimethylamino)ethyl methacrylate (DMAEMA) was procured from Acros Organics (UK).

Chlorodimethyl vinyl silane (CDVMS) was purchased from TCI Chemicals (UK)

Glass microscope slides of thickness 1 mm (to standard ISO 8037/1) was purchased from VWR (UK)

### **3.3.2. Experimental Procedure**

Linear polymers were manufactured using free radical polymerisation in the absence of a chain transfer agent. Typical batch sizes used were 21.1 mmol acrylamide and 0.7 mmol copolymer, approximating 1.50 g by weight. Typically 1.2 g were recovered following lyophilisation. In all cases, the method was as follows. 24.5 ml deionised water was purged under nitrogen for 30 minutes, to which was added 3.75 ml of acrylamide (40% solution) and 0.7 mmol of the selected copolymer. To this solution 37.5  $\mu$ l of the initiators N,N,N',N'-tetramethyl ethylenediamine (TEMED) and 37.5 mg ammonium persulphate (APS) were rapidly added and the reaction vessel covered. The reaction was stirred for 2 hours. At this stage a noticeable increase in viscosity typically occurred after approx. 15 minutes of stirring. Following reaction, the polymer was precipitated in methanol and the diluent centrifuged and washed in methanol. The precipitate was then dried under vacuum, redissolved in approx. 20 ml deionised water and dried by lyophilisation.



*Figure 3.13 - Cartoon of spun single-layer waveguide layout*

To deposit the thin film, 50 mg of the chosen acrylamide copolymer was dissolved in 1 ml, 1 N hydrochloric acid to provide a 5% solution. To a 200  $\mu$ l aliquot was added 1  $\mu$ l of 5% GA solution (in the case of the 250 ppm gel) to provide the intended crosslinker concentration. The solution was then mixed thoroughly and immediately pipetted directly onto an APTES-functionalised slide. The slide was then spun to the conditions indicated. After recovery, the thin films were allowed 18 hours (overnight) to cure. The intended configuration of the slide is shown in **Figure 3.13**.

As can be seen in **Table 3.3**, synthetic linear polymers are named according to their manufacture and batch. Assuming an acrylamide backbone, the name consists of a two-letter summary of the copolymer tested (for example, AA for allylamine), then a number indicating the copolymer fraction (for example, AA15 for a 15:1 acrylamide-allylamine copolymer), then a numerical batch identifier. The exception to this is polyacrylamide homopolymer, which is given the abbreviation PAAm followed by a batch number, and non-synthetic polymers such as the polysaccharides found in Chapter 4. For the purpose of this chapter, the batch number may be omitted if not relevant to the test such as if only one batch was manufactured.

Table 3.3 – Materials and proportions used in initial linear polymer manufacture, along with

<b>Polymer</b>	<b>Copolymer</b>	<b>Acrylamide Content (mmol)</b>	<b>Copolymer Content (mmol)</b>	<b>Notes</b>
PAAm-1	--			--
AA10-1	Allylamine	4.22	0.42	--
AA15-1	Allylamine	21.10	1.40	--
AA30-1	Allylamine	21.10	0.70	--
AA60-IPA	Allylamine	4.22	0.07	Isopropyl alcohol chain transfer agent
NP30-1	N-aminopropyl methacrylamide	17.59	0.58	High degree of physical crosslinking
NP20-1	N-aminopropyl methacrylamide	4.00	0.26	High degree of physical crosslinking

Gelling tests were performed as follows. A coin-shaped core of bulk gel of mass approximately 0.1 g was immersed in deionised water for 1 day to fully swell and its weight recorded in the absence of excess water. The gel was then transferred to the selected buffer for 72 hours, after which the gel was reweighed and the swelling ratio determined from the relative difference.

IR spectra were produced using a Cary 660 FTIR-ATR benchtop instrument. All polymer samples were analysed as dried powders.

<sup>1</sup>H NMR analysis was performed using a Bruker 300 MHz NMR spectrometer. Due to the strong hydrophilicity of polyacrylamide and the used copolymers, which were found to precipitate out in 50% (v/v) methanol in water and did not dissolve in any aprotic solvent, all NMR data collections used deuterium oxide solvent.

### 3.3.3. Results and Discussion

Before production of thin films by spincoating, the successful crosslinking and gelation of polymers was investigated. A number of crosslinking mechanisms were assessed, namely amine-epoxide, isothiocyanate-epoxide, amine-N-Hydroxysuccinimide, amine-aldehyde and amide-aldehyde, using solutions of 5% polymer and 1 molar equivalent crosslinker per polymer functional group. Of these, invertible gels were produced using amine-epoxide (polyallylamine with ethylene glycol diglycidyl ether) and amide-aldehyde (using polyacrylamide and glutaraldehyde (GA)).

Amine-epoxide gels were produced with a maximum molar ratio of 200 allylamine units per epoxide. However substituting polyallylamine with a copolymer of acrylamide and N-aminopropyl methacrylamide ceased to provide invertible gels with epoxide crosslinkers at the same or any concentration, thereby ruling out epoxide crosslinkers for the time being. Amide-aldehyde gels were produced with a maximum molar ratio of 282 acrylamide units per glutaraldehyde. Substitution of linear polyacrylamide for copolymers of acrylamide (described in section 3.4.3) also produced invertible gels in similar conditions. The IR spectra of crosslinked gels (**Figure 3.15**) found a small loss of shape in the doublet at 1650 and 1605 cm<sup>-1</sup>

<sup>1</sup> characteristic of amide, due to interference from the Schiff base imide bond formed by the crosslinker.<sup>172</sup> Presence of this bond was confirmed by further <sup>1</sup>H NMR (**Figure 3.14**).

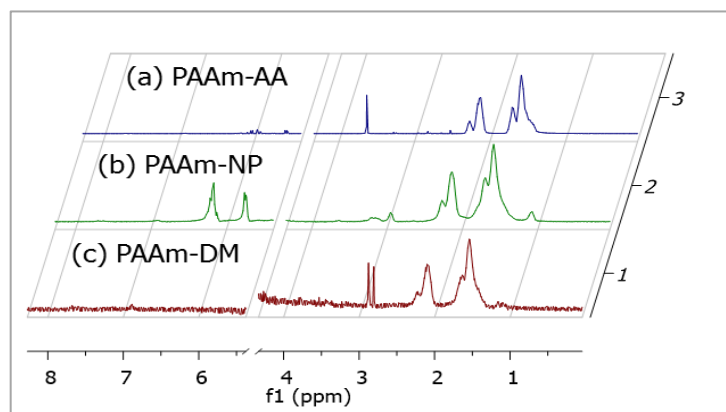


Figure 3.14 - <sup>1</sup>H NMR spectra of acrylamide copolymers. Solvent peak at 4.7 ppm removed for clarity. (a) Polyacrylamide co-allylamine polymer. (b) Polyacrylamide co-N-aminopropyl methacrylamide polymer. (c) polyacrylamide-(N,N-dimethylamino)ethyl methacrylate copolymer. Presence of broad asymmetric doublets at 1.5 ppm (polymer backbone CH<sub>2</sub>) and 2.1 (acrylamide CH) indicate acrylamide units; presence of indistinct peak at 1.2 (methyl CH) indicates methacrylate or methacrylamide units.

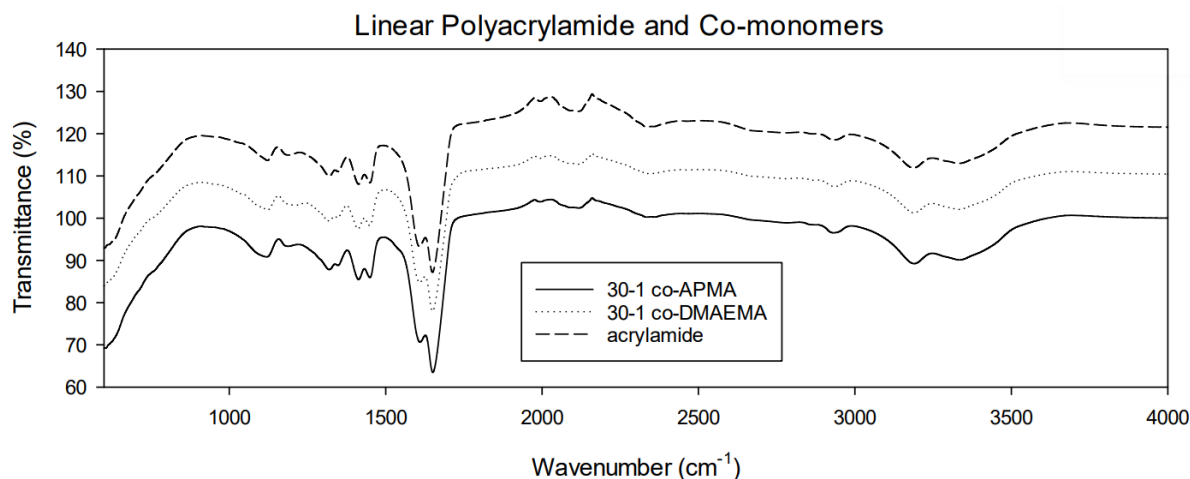


Figure 3.15 - FTIR spectra of acrylamide homopolymer, plus 30:1 statistical copolymers of, Polyacrylamide co-N-aminopropyl methacrylamide and polyacrylamide-(N,N-dimethylamino)ethyl methacrylate. Spectra are offset to provide legibility.

NMR traces for the linear polymers tested show significant broadening of otherwise relatively defined peaks at 1.5 and 2.1 ppm marking the acrylamide (and comonomer) polymer backbone – broadening occurs due to a wide range of subtly different proton environments across the polymer chain creating a spectrum of outcomes rather than clearly defined peaks. Due to the exclusively water-soluble nature of the copolymers and therefore proton exchange between amine groups and the deuterium oxide solvent, no N-H amine peaks were visible. Nonetheless, evidence of copolymers remained – for example the NC-H peak at 3.5 ppm for allylamine (**Figure 3.14a**) and (much broader) at 3.2 ppm for N-aminopropyl methacrylamide (**Figure 3.14b**). Integration of these peaks relative to the polymer backbone peaks confirmed a ratio of approximately 29-1 for all three copolymers, in line with the relative comonomer concentration used at the time and discussed further in Section 3.4.3. As also shown by **Figure 3.15** FTIR data does not significantly differentiate between acrylamide homopolymer and the copolymers tested – while not initially useful this comparison does demonstrate the high degree of similarity between 29-1 acrylamide-comonomer blends, and that their characteristic behaviour remains governed by the acrylamide backbone. It is likely that the acrylamide is overpowering any results of the comonomer. Should different copolymer concentrations be used, FTIR may be comparatively more useful in their characterisation.

### **3.3.3.1. Production and Testing of Spincoated Waveguides**

Given fixed glutaraldehyde content (0.2%, v/v) and spin conditions, the concentration of polymer was varied. Viable waveguides were found at 10 and 7.5% (w/v) polymer, the latter being single-moded (**Figure 3.16**). Of note is the rather high incident angle of the mode, over



7 degrees beyond the critical angle, indicating a dense hydrogel that can be improved upon. As reduction of hydrogel density improves both sensitivity and permeability to analytes, the polymer content and the quantity of glutaraldehyde crosslinker were reduced to 5% (w/v) and 250 ppm (0.025% v/v), respectively.

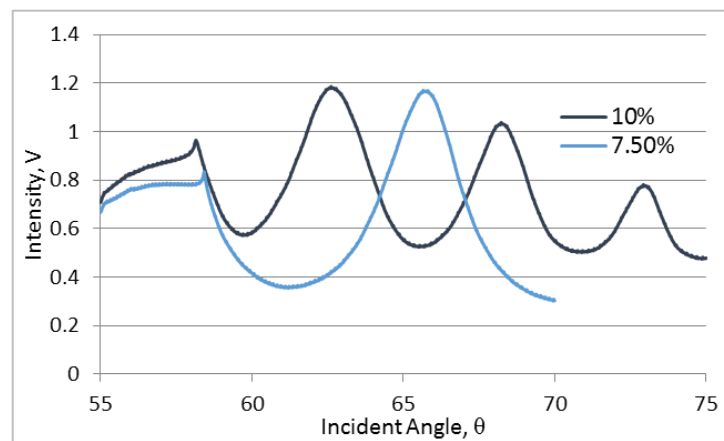


Figure 3.16 – Photodiode-detection scan of metal-clad leaky waveguides. Enhanced intensity indicates a resonance angle.

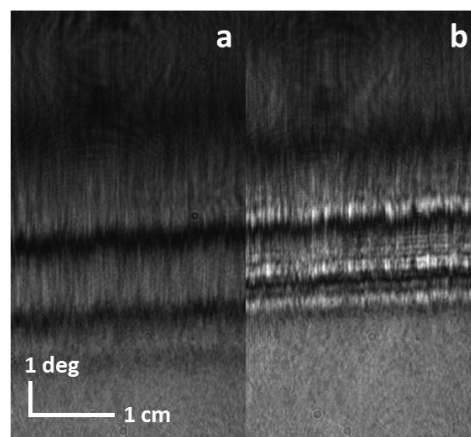


Figure 3.17 – waveguide appearance with (a) and without (b) dye addition.

Initially, a dye-doped waveguide system was employed, in which the amine-reactive dye reactive blue 4 (RB4) was immobilised upon the waveguide or added to cover solutions in order to visualise the mode. However as the density of the waveguide was reduced, a small degree of light scattering was observed within the waveguide and allowed for mode visualisation under colourless buffer or deionised water (**Figure 3.17**). While a non-transparent waveguide layer is potentially detrimental to optical clarity, eliminating the need for dye addition was deemed an advantage. Dye addition to running solutions hinders the determination of their refractive index (RI), limiting the precision with which RI sensitivity could be determined. In addition, dye immobilised in the waveguide is vulnerable to bleaching agents in the solution bulk, and may alter the pH response of the waveguide when present.

As CDVMS was ineffective as a glass functionalisation agent for linear polymers, owing to no opportunity to form covalent bonds between the vinyl group and the polymer during the crosslinking stage, (3-Aminopropyl)-triethoxysilane (APTES) was chosen instead. APTES provides a surface of consistent hydrophilicity and known surface chemistry, mitigating certain issues encountered while using untreated cleaned glass. Hydrophilic hydrogels (such as linear polyacrylamide and copolymers, or polysaccharides as discussed in Chapter 4) were found to adsorb onto an APTES-coated surface without requiring provision of additional polymer functional groups for covalent binding.

### **3.3.3.2. RI Sensitivity of Spincoated Waveguides**

The summarised results of sensitivity tests are found in **Table 3.4**. Sensitivity testing initially occurred using a 0.1% (v/v) or 1000 ppm glutaraldehyde content. Reducing the crosslinker was expected to reduce the gel density while permitting a larger gel volume, providing a larger waveguide bulk for interaction with analytes. Correspondingly, the sensitivity to glycerol increased as the glutaraldehyde content was reduced to 250 ppm. An alternative polymer batch tested in the same conditions provided a dissimilar response. This is likely due to the free radical polymerisation method used to create linear polymers, which offers poor control over overall polymer size.

*Table 3.4 – Sensitivities of selected polyacrylamide co-allylamine leaky waveguides. All errors represent 1 standard deviation.*

Waveguide Conditions	Sensitivity (degrees/RIU) $\pm$ S.D.
1000 ppm GA	110 $\pm$ 6.8
250 ppm GA	134.5 $\pm$ 5.6
250 ppm GA, alternative polymer batch	116.6 $\pm$ 7.3
250 ppm GA, FITC doped polymer	133.4 $\pm$ 0.55
250 ppm GA, 20% glycerol humectant	164.8 $\pm$ 0.54
Cast polyacrylamide, 2.0 $\mu$ m photoresist	129.9 $\pm$ 5.8

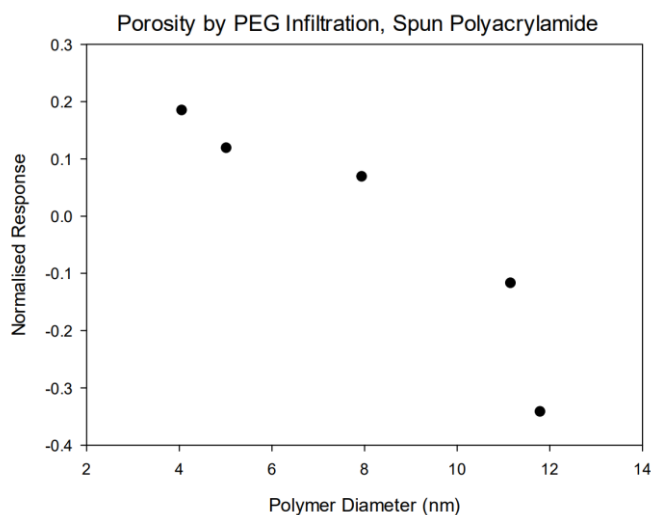
Waveguides formed from FITC-fixed poly(acrylamide-allylamine) were produced and their sensitivity assessed, with comparable results to that of the unlabelled polymer. As a xanthene dye FITC is rather bulky, however its inclusion in the absence of a pendant linking moiety appears not to have affected the ability of glutaraldehyde to crosslink the gel. The resulting sensitivity is not remarkable compared with other optical sensors, especially the popular surface plasmon resonance (SPR) type, which is capable of reaching sensitivities of up to 250 degrees/RIU.<sup>173</sup> However SPR sensors are considerably more expensive and difficult to produce, often requiring gold nanolayers on the sensor surface, and generally are not designed to interrogate the entirety of the sample area efficiently.

### **3.3.3.3. Porosity and Other Tests for Spincoated Waveguides**

The porosity achieved by the 5% hydrogel was poor, largely unable to accept PEG with a hydrodynamic radius of 4 nm and performing worse with larger molecules. Considerable variance in the PEG response was also seen. Reducing the polymer fraction was not effective in improving pore size, while further reducing the glutaraldehyde content did not produce viable waveguides at all. A reduction in spin speed allowed for some improvement to PEG response at the cost of overall sensitivity and so was avoided as a solution.

Addition of 20% glycerol to the spincoated polymer solution (**Figure 3.18**) provided much greater porosity, responding similarly to 6 and 10 kDa PEG and retaining 50% of expected

response for 35 kDa PEG. Introduction of glycerol also significantly improved the RI sensitivity of the polymer (**Table 3.4**). It is likely that as the waveguide is curing, water loss causes the porous structure to collapse, and the polymer partially condenses around the more hydrophobic polymer backbone. These interactions, though weak, occur while the gel is being crosslinked and may lead to more restrictive crosslinking regimes. Addition of glycerol, which does not evaporate during the curing process, simply holds these pores open while crosslinking occurs.



*Figure 3.18 - PEG sensitivity of spun polyacrylamide co-allylamine, 250 ppm GA, 4000 rpm spin speed. Values are calculated by sensitivity relative to glycerol, calculated by response/RI.*

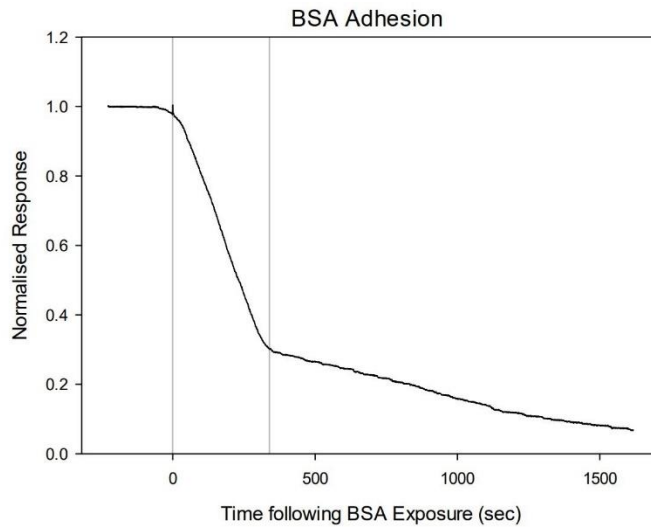


Figure 3.19 - retention of bovine serum albumin on spun polyacrylamide gel. Vertical lines represent initiation of buffer wash and the point where all free BSA is evacuated. Subsequent tailing of response represents gradual loss of bound BSA.

Some interference studies were also briefly performed. A temperature change was administered by heating of the water bath attached to the flow cell, and a small temperature-dependent resonance angle shift  $8.61 \times 10^{-3} \text{ deg}/^{\circ}\text{K}$  was determined. Additionally, albumin from bovine serum (BSA) was introduced to the polymer as a model protein. BSA is known to adsorb onto polymers leading to fouling, and interacts readily with the acrylamide monomer unit.<sup>174</sup> Under a flow of albumin solution followed by buffer, the response peak of albumin experienced considerable tailing, around 30% of the peak intensity remaining after the BSA not adsorbed had been extracted (**Figure 3.19**). This tailing presents a potential problem should the sensor be adapted for biosensing or clinical roles, and indicates the need for building some antifouling protection into the sensing waveguide if possible.

### 3.4. pH Sensitivity of Waveguides

### **3.4.1. Chemicals and Materials**

Linear polymer manufacture was performed as per Section 3.3, and used chemicals and materials described therein.

sodium phosphate monobasic monohydrate, polyacrylamide co-acrylic acid 10% (mol) sodium nitrite, hydrochloric acid (1N) and sodium phosphate dibasic dodecahydrate was procured from Sigma Aldrich (UK).

Decon 90 was procured from Fisher Scientific (UK)

(N-dimethylamino)ethyl methacrylate (DMAEMA) was procured from Acros Organics (UK).

Chlorodimethyl vinyl silane (CDVMS) was purchased from TCI Chemicals (UK)

Glass microscope slides of thickness 1 mm (to standard ISO 8037/1) was purchased from VWR (UK)

### **3.4.2. Experimental Procedure**

Running solutions were produced using a phosphate salt system (phosphoric acid, sodium dihydrogen phosphate, disodium hydrogen phosphate, sodium phosphate). Stock solutions were made to a target concentration of 100 mM, then running solutions made from a 10 mM solution of each. As the ionic strength of a buffer is proportional to its refractive index, the RI of the running solutions was measured and then adjusted to 1.33314 before use.

Acid treatment of waveguides followed a reported method.<sup>175</sup> A waveguide was tested to ensure a trackable waveguide, and then was transferred to deionised water and cooled by ice bath. The waveguide was then treated with 7  $\mu\text{mol}$  (later increased to 14  $\mu\text{mol}$ , 35  $\mu\text{mol}$ , 70  $\mu\text{mol}$ ) each of hydrochloric acid and sodium nitrite. Increase of value was performed as insufficient pH response was found through polymer treatment, with an excess of nitrous acid production tried with a final testbed waveguide treated with 2.89 mol of hydrochloric acid and sodium nitrite. After 24 hours, the waveguide was returned to room temperature and excess nitrous acid was removed by sequential deionised water washes. To ensure the viability of this method with the linear polymer generated, a 300 mg sample of linear polyacrylamide was used as the testbed, and was dissolved and treated with 0.42 mmol ice-cold nitrous acid as described above. Following recovery by lyophilisation, a brittle, glassy polymer was retrieved that did not fully dissolve in deionised water or hot phosphate buffer but did swell as expected for a hydrogel once in aqueous media.

### **3.4.3. Results and Discussion**

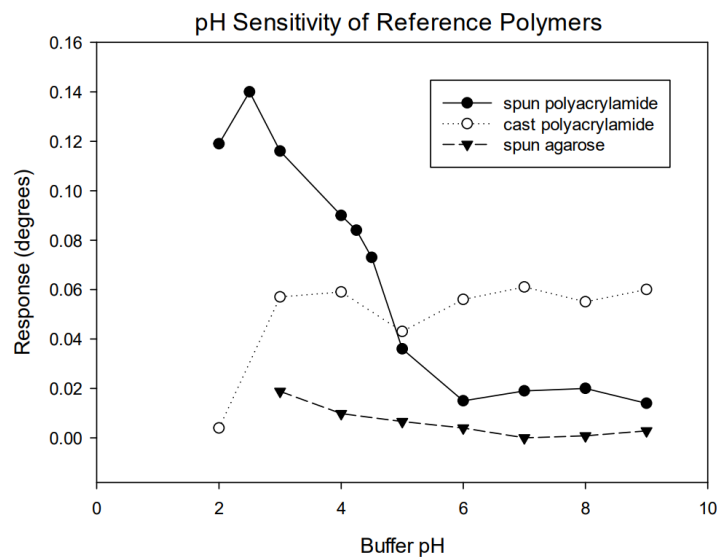
#### **3.4.3.1.pH Sensitivity of Reference Polymer**

Initially, the pH sensitivity of waveguides optimised for responsivity and porosity was assessed over the pH range 4.0-9.0. This range was subsequently expanded to include pH 3 and in cases pH 2, as points of interest were found at lower pH values. The best-result reference polymers as per RI sensitivity was brought forward for pH testing. To meet the requirements of an



environmental monitoring sensor, a pH range of 6.0 – 9.0 was considered the initial region of interest.

The pH response of spun polyacrylamide gel is shown in **Figure 3.20**. Little significant pH shift over neutral and alkaline pH ranges was detected, however a sigmoidal curve was detected in the acidic region, indicating a moiety with a  $pK_a$  of approximately 4. As polyacrylamide is ordinarily non-ionic and does not readily accept protons, this was considered abnormal. Removal of the basic groups considered responsible for this, in the form of allylamine copolymer, was performed by synthesis of polyacrylamide homopolymer and provided a reduced intensity of response but not a significantly different  $pK_a$  or dynamic pH range. As can be seen in **Figure 3.20**, removal of the glycerol humectant further reduced the intensity of the sigmoidal curve but had no significant effect on its range or placement.



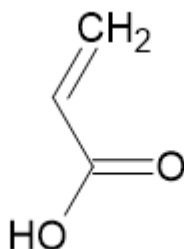
*Figure 3.20 - pH response profiles of cast and spun polyacrylamide leaky waveguides. Agarose (from Chapter 4) included for reference.*

The pH sensitivity in the 3-5 region found in all spincoated waveguides below may be attributed to the Schiff base formed by glutaraldehyde crosslinking. The presence of the nearby amide carbonyl both provides an electron-withdrawing effect on the nitrogen and may conjugate with the imine bond formed by glutaraldehyde addition. The detected pKaH of around 4, an achievable value for a weak base<sup>176, 177</sup> especially where multiple bases may be present in relative proximity and electrostatic repulsion may discourage subsequent ionisations.<sup>175</sup> While the glycerol-doped allylamine copolymer gel had proven suitable as a sensing material for RI changes, the pH response it displays is less than ideal for the intended application. This, coupled with the effect of glycerol upon poly(acrylamide co-acrylic acid) discussed below, led to the decision to remove glycerol doping from the spincoating process.

### **3.4.3.2. Provision of Acidic Functional Groups**

In order to produce a waveguide with ionisable groups for inducing pH responsivity, without incurring redundant optimisation time, an initial attempt was made to partially convert amide groups within the waveguide to carboxyl groups by treatment with nitrous acid<sup>178</sup> (**Figure 3.21**). A method demonstrated by Biçak was selected and adapted for gel-phase polymers.<sup>175</sup> A sample of acrylamide was selected to assay the nitrous acid content, and a treatment calculated for 10% conversion provided a  $13.3 \pm 0.45$  mol % acrylic acid groups on the linear polymer. As the acid content was not dissimilar to the theoretical value to be attained, the acidification process was performed on functional waveguides. However, little change in pH response was detected except with a considerable (potentially waveguide-damaging) increase in nitrous acid content

(**Figure 3.22**), and the treated linear polymer also too proved resistant to dissolution in water or buffer to be useful for waveguide formation.



*Figure 3.21 - Acrylic acid, a pH-responsive acidic monomer very similar in structure to the acrylamide backbone.*

It was thought that as the local environment of an anionic polymer alters the likelihood of acid dissociation, particularly the presence and quantity of adjacent charged monomer units, tuning the proportion of acrylic acid groups will in turn tune the  $pK_a$  of the waveguide and with it the dynamic pH range. However given the lack of success in this area, a commercially available stock of poly(acrylamide co-acrylic acid) was acquired to ensure pH sensitivity was in fact achievable, and focus in later experiments pivoted from modifying an extant waveguide to incorporating pH-sensitive monomer units into the polymer.

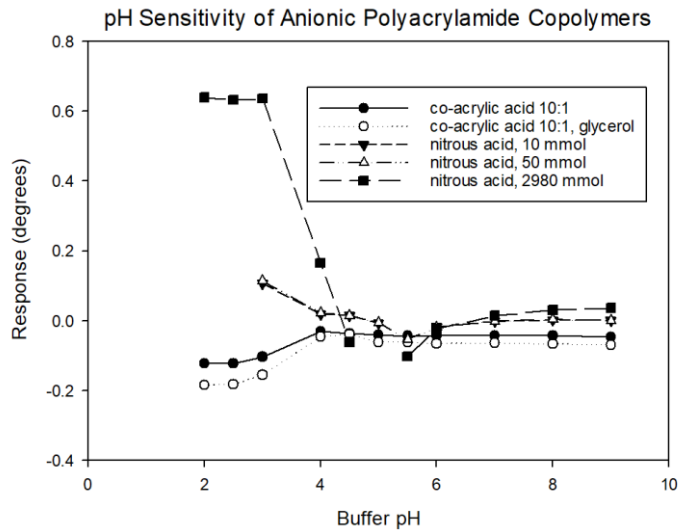


Figure 3.22 - Effects of nitrous acid treatment on the pH sensitivity curves of spun polyacrylamide waveguides. Spun polyacrylamide co-acrylic acid included for comparison. Note strength of nitrous acid treatment, given in the legend.

An 80:20 blend of poly(acrylamide co-acrylic acid) (PAAm-Ac) was procured and waveguides were spun with and without addition of 5% glycerol humectant (**Figure 3.22**). Alone, the acrylic acid copolymer waveguide provided an anionic response from pH 2.5-4.5, around the range expected of carboxylic moieties. This weakly acidic property can quite confidently be ascribed to the acrylic acid co-monomer. With glycerol included, the inverse is seen - a strong cationic response similar in both shape and intensity to that of glycerol-doped PAAm or PAAm-AA was encountered. As mentioned above, glycerol addition appears to provide a similar magnitude and pattern of response irrespective of the copolymer used, and so it was decided that clearer pH sensitivity is preferable to porosity for pH-sensitive hydrogels.

### 3.4.3.3.N-Aminopropyl Methacrylamide Copolymer

One alternative to using acidic polymers is to utilise other ionisable groups. Amine-bearing poly(acrylamide co-N-aminopropyl methacrylamide) (PAAm-NP, **Figure 3.24**) formulations trialled in Section 3.3.3.1 were tested for pH sensitivity (**Figure 3.23**). Initial testing provided a response pattern amphoteric in nature, with an increased response both above and below an approximate pH. After subtracting the effects of spun polyacrylamide, a positive pH response in the range 5-7 remains. It is highly likely that this dynamic range is due to pendant primary amines. As N-aminopropyl methacrylamide monomer has a pKaH of 8.3, proximity within the waveguide structure may be responsible for weakening the basicity of the aminopropyl unit.

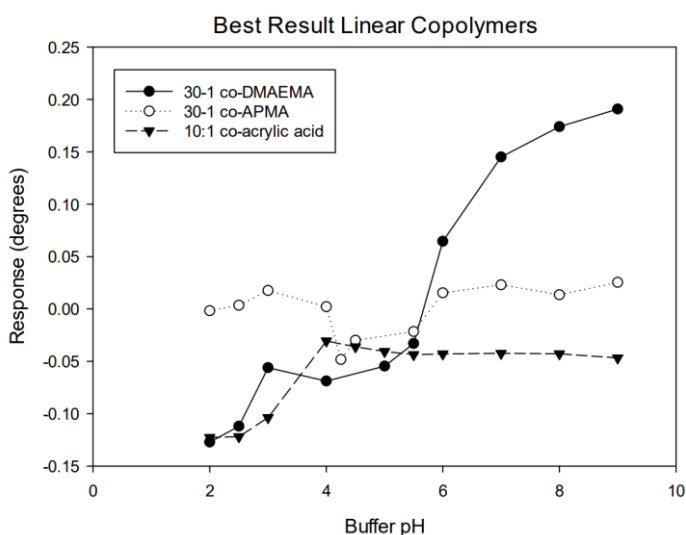


Figure 3.23 - pH sensitivity curves of spun acrylamide copolymers containing molar ratios of 1/10 acrylic acid, 1/30 N-aminopropyl methacrylamide and 1/30 N,N-(dimethylamino)ethyl methacrylate.

It is also of note that the response seen in PAAm-NP waveguides increases with increasing pH, implying the polymer is anionic over this region. However according to  $^1\text{H}$  NMR (**Figure 3.14**, above) the amino group is unmodified (although NH peaks themselves are absent due to proton exchange with the solvent). Washing of waveguides with a basic solution of an electrophilic dye

such as RB4 resulted in covalent binding and permanent staining of the waveguide, indicating free amine remain. The cause of this response inversion is likely not chemical in origin.

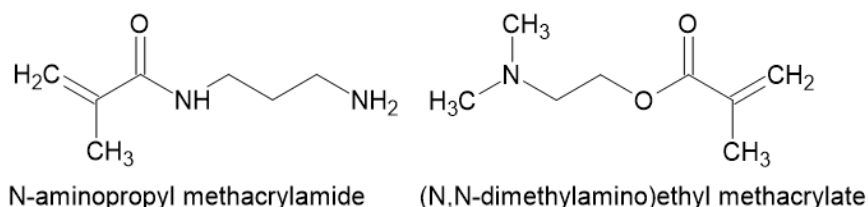


Figure 3.24 - pH-sensitive copolymers *N*-aminopropyl methacrylamide (NAPMAAm) and (*N,N*-dimethylamino)ethyl methacrylate (DMAEMA). Note the presence of the ester linkage in the latter, rather than a secondary amide.

### 3.4.3.4. *N,N*-(Dimethylamino)ethyl Methacrylate Copolymer

(dimethylamino)ethyl methacrylate (DMAEMA, **Figure 3.24**) waveguides were produced at a similar monomer-backbone molar ratio and their pH sensitivity assessed (**Figure 3.23**). After correcting for the effects of spun polyacrylamide homopolymer, a relatively gradual response from pH 5-8 can be identified. The intensity of this response, while still small, is greater than that of polyacrylamide or PAAm-NP (above) by a factor of 2-3. As with the PAAm-NP hydrogel, the response shift of polyacrylamide co-DMAEMA (PAAm-DM) appears anionic in nature (increasing optical density with proton scarcity) despite the (dimethylamino)ethyl functional group being a proton acceptor, and despite no evidence of reaction with glutaraldehyde. The linear polymer dissolved directly into deionised water retained a pH of

8.02, not dissimilar to that of the monomer, and cast waveguides of a similar makeup (adapting the methodology of Section 3.2.2) gave a similar response.

### 3.4.3.5. Response Intensity of pH-Sensitive Polymers

Unfortunately, as may be gathered from **Figure 3.23** above, responses found by inducing pH shifts are in the region of 0.2-0.6 degrees in total. Despite the trends already described, this small magnitude in shift is troubling especially given the polymers used – for example, Turan and Çaykara<sup>179</sup> reported a polyacrylamide-acrylate copolymer gel of similar molar ratio that swelled from 6 to approx. 20 times its dry mass over the same pH range, while the thin film displayed little change in density. In comparison with reported swelling capabilities of pH-responsive polymers, it was also noted that the majority of otherwise comparable polymers used a crosslinker incorporated into the polymer backbone (such as methylene bis(acrylamide)<sup>180</sup> or oligo-ethylene glycol dimethacrylate<sup>181-183</sup> rather than a post-hoc crosslinking scheme.

Much higher relative concentrations of polymer have been used by others, for example DMAEMA copolymers are often seen at 30%, 1:3 or as the majority comonomer in order to provide pH sensitivity.<sup>180-183</sup> In order to evaluate the effects of the crosslinking reactions and copolymer content upon the pH profile, PAAm-NP and PAAm-DM hydrogels were produced by microsphere casting with methylene bis(acrylamide). In addition, a PAAm-DM cast hydrogel of 10:1 ratio was tested. Increasing the DMAEMA concentration did not alter the pH response in the range 5-9, which remained at only 0.06 degrees, however lower pH behaviour was affected.

Swelling tests of the bulk gels given above revealed that while aminopropyl content increased both overall swelling capacity and induced greater swelling at pH 5 (where a response minimum is seen in waveguide response), PAAm-DM gels did not significantly alter their pH response even at a 20% DMAEMA concentration. This may be due to the relatively hydrophobic nature of DMAEMA<sup>184</sup> – should non-protonated dimethylamino units congregate into hydrophobic centres while highly hydrophilic acrylamide units are already fully swollen, such groups would resist swelling.<sup>182</sup> The apparently cationic response of the hydrogel may therefore be a function of the refractometric sensing scheme, rather than the swelling ratio of the gel.

### **3.5. Summary**

In this chapter, methods of casting for polyacrylamide gel were assessed and suitable conditions found for production of hydrogel leaky waveguides, with a refractive index sensitivity of 148.7 degrees/RIU. A method was also developed for the spincoating of leaky waveguides of tuneable properties, using linear polyacrylamide crosslinked with glutaraldehyde, providing a refractive index sensitivity of 134.5 degrees/RIU. Tests for pore sizes and pH sensitivity were also performed. Finally, the possibility of developing pH sensitivity by inclusion of ionisable copolymers into linear acrylamide was assessed.

Compared with the cast hydrogels initially attempted, spincoating of linear polymers has shown promise as a means of manufacturing leaky waveguides, especially with regards replicability. The RI sensitivity achieved by the spincoated waveguide is not remarkable given the scope of



what is possible with optical sensing devices, however is acceptable given the low cost of materials and simple construction the waveguides described above. The porosity, however, is less than ideal and may present a barrier for adaptation of this sensor to biosensing or immunosensing applications in its current form.

As treatment of polyacrylamide thin films with nitrous acid did not prove an effective means of imparting pH sensitivity to the waveguide, tuning of linear copolymers of acrylamide was adopted in its place. Incorporation of acrylic acid, (N-aminopropyl)methacrylamide and (dimethylamino)ethyl methacrylate have all permitted the construction of potentially effective pH sensitive waveguides, albeit waveguides with very low responses due to their low copolymer content. It was therefore suggested that more effective means of imparting pH sensitivity, as well as prototyping of suitable common-path measurements with pH, be found.

# Chapter 4. PH SENSITIVITY OF POLYSACCHARIDE AND INTERNALLY REFERENCED POLYSACCHARIDE LEAKY WAVEGUIDES

## 4.1. Introduction

In Chapter 3, a leaky waveguide constructed using synthetic polymers such as polyacrylamide was demonstrated, and some possible routes to ensuring pH sensitivity were assessed. With limited success in terms of ensuring pH sensitivity, an alternative was suggested based on both prior and current work by the research unit.<sup>18, 19, 21, 99, 155</sup> Polysaccharides are naturally formed polymers based on repeating a sugar unit, and have good gelling ability. The inert polymer agarose (often used as a medium for electrophoresis) and chitosan (a polysaccharide with an available amine moiety, known mesoporous character and a  $pK_aH$  of around 6.5)<sup>185</sup> were selected, shown in **Figure 4.1**.

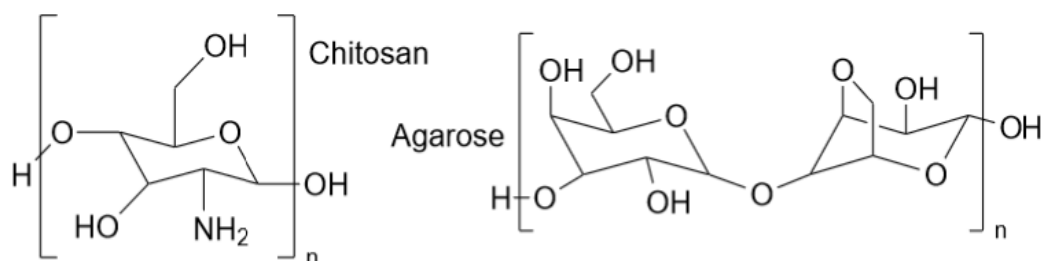


Figure 4.1 - Chemical structures of the repeating units of agarose and chitosan. Note the presence of primary amine group in the structure of chitosan.

This chapter is arranged as follows. Section 4.2 contains the materials and instrumentation used herein, except where the instrumental function would be replicated from Chapter 4. Section 4.3 then describes the procedures and methodologies followed in the rest of this chapter. Sections 4.4.1 and 4.4.2 discuss the characterisation of agarose and chitosan hydrogels, respectively, as well as their suitability for waveguide manufacture. The production of an internally referenced sensor by stacking the two polysaccharides together is explored in Section 4.4.3, and the suitability of the sensor for pH sensing is assessed in Section 4.4.4. Finally, in Section 4.4.5 the agarose material was substituted for a polyacrylamide blend previously optimised for, and the suitability of a synthetic-organic hybrid stacked leaky waveguide for pH sensing is briefly discussed.

## **4.2. Materials**

### **4.2.1. Chemicals and Materials**

Acrylamide 40% (w/v), mono- and dibasic sodium phosphate, 4-(2-hydroxyethyl)-1-piperazineethanesulfonic acid (HEPES), glutaraldehyde, ethanol, (3-Aminopropyl) triethoxysilane (APTES), 0.1 M acetic acid and reactive blue 4 (RB4) were procured from Sigma Aldrich (UK).

Decon 90 detergent, sodium chloride and chitosan ( $M_w$ : 100 000–300 000, 90% deacetylated) was procured from Fisher Scientific (UK).

Phosphoric acid and trisodium phosphate were procured from Acros Organics (UK).

Agarose (low melting point, ultrapure) was purchased from Life Technologies (UK).

Chlorodimethyl vinyl silane (CDVMS) was purchased from TCI Chemicals (UK).

Glass microscope slides of thickness 1 mm (to standard ISO 8037/1) were purchased from VWR (UK).

## **4.2.2. Instrumentation**

The majority of analysis occurred using a waveguide apparatus, described in Chapter 3. A flow rate of 1.50 ml/min was used throughout. Solution refractive indices were found using a Bellingham Stanley RFM970-T refractometer, the specifications of which are given in Chapter 4, and used as per manufacturer's instructions. Likewise, the pH of running buffers and other test solutions was found using a Hanna HI 2210 benchtop electrochemical pH meter previously discussed.

## **4.3. Experimental Procedure**

### **4.3.1. Polymer Deposition**

Glass substrates were prepared using a variation on the method described in Chapter 3. Briefly, 25 mm square glass plates were cut from microscope slides and cleaned by sonication with detergent solution, deionised water and ethanol. Slides were stored dry and covered until use. Immediately before deposition of polysaccharide, slides were functionalised by immersion in 1% (aminopropyl)triethoxysilane (APTES) in toluene for 30 minutes, and then transferred to a fresh toluene solution for 5 minutes. APTES was selected in place of vinyl-bearing surface

functionalisation used previously, due to the lack of suitable groups on the polymer to interface with. Polyacrylamide films were prepared as was discussed in Chapter 3.

Agarose films were prepared by hot spin-coating. 100 mg of agarose powder was dissolved in 5 ml deionised water through microwave heating, using a minimum total exposure of 50 seconds. heating was performed in 3-5 second stages in a closed container interspersed with stirring by vortex mixer. Care was taken to avoid boiling the solution. Following complete dissolution, 6.25  $\mu$ l of 25% glutaraldehyde solution is added and the solution is held at 50 °C by stirrer-hotplate to prevent premature setting. A clean aminopropyl-bearing slide is brought to 50 °C on a cleaned, covered hotplate. 150  $\mu$ L of the glutaraldehyde-doped agarose solution was spin coated at a spin speed of 3000 rpm for 60 seconds, with acceleration of 100 rpm/s, inside a laminar flow cabinet air-conditioned to 20 °C. The intended configuration of both agarose and chitosan single-layer slides is shown in **Figure 4.2**.

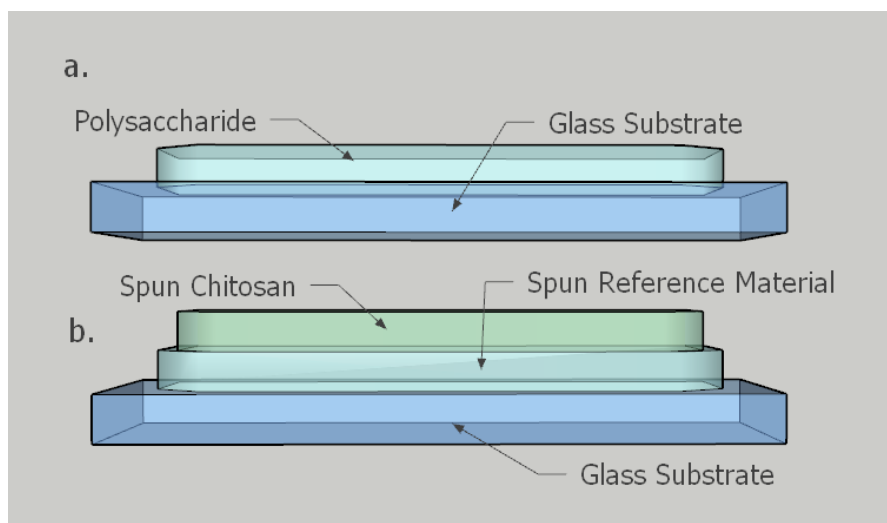


Figure 4.2 - Cartoon of polysaccharide-based leaky waveguide layouts in this chapter. Single-layer waveguides (a) followed the configuration of spun waveguides in the above chapter. Stacked leaky waveguides (b) use the reference material below – this may be agarose or (later) polyacrylamide.

Chitosan films were prepared by a similar spin-coating process. 20 mg of purified chitosan was dissolved in 2 ml of 0.1 M acetic acid over a period of 18 hrs, to produce a 1% w/v polymer solution. This solution was then filtered to 5  $\mu\text{m}$  by syringe and kept stirring until needed. A 150  $\mu\text{l}$  aliquot of chitosan solution was then deposited onto a clean aminopropyl-bearing slide and spin coated over at a spin speed of 900 rpm for 30 seconds, with acceleration of 100 rpm/s, inside a laminar flow cabinet. The spin coated substrates were placed inside an incubator maintained at 25  $^{\circ}\text{C}$  and humidity of 75–80% for 3 min, then immersed in a crosslinking solution of 0.03% (v/v) glutaraldehyde in 100 mM HEPES buffer for 5 minutes. The chitosan slide is then washed and subsequently stored in 100 mM HEPES buffer, pH 7.4, until needed.

To deposit the chitosan layer onto an inert film a broadly similar method was followed. However, in place of a fresh APTES-coated slide, an agarose or polyacrylamide leaky waveguide was immersed in deionised water for  $\sim$ 1 minute, and then the slide underside dried

and excess water wicked away. A 150  $\mu$ l aliquot of chitosan solution was then deposited onto the hydrated waveguide and both spincoated and crosslinked as described above.

### **4.3.2. Sample Preparation**

Running solutions were produced using a phosphate salt system (phosphoric acid, sodium dihydrogen phosphate, disodium hydrogen phosphate, sodium phosphate). Stock solutions were made to a target concentration of 100 mM, then running solutions made from a 10 mM solution of each. As the ionic strength of a buffer is proportional to its refractive index, the RI of the running solutions was measured and then adjusted to 1.33314 before use. Alternative buffers made from HEPES were manufactured by preparing a 10 mM HEPES stock solution in deionised water, then pH adjusting with 1 M sodium hydroxide or hydrochloric acid as appropriate. Buffers were then RI adjusted to 1.33314 before use.

Waveguides are stored dry by default, following experiences with polysaccharide slides, and were kept in the dark unless the immediate batch was in use. Likewise, running solutions and buffers were stored in a cool dark place unless expected to be used. Buffers around neutral pH were examined monthly for microbial growth and were disposed of and replaced if any evidence of contamination was found. For some experiments regarding leaching-out of material, a number of waveguides were stored under deionised water. These samples were maintained safely in a cupboard, as above, and were gently air-dried prior to use.

Refractive index sensitivity testing used the method described in Chapter 3, without modifications.

## **4.4. Results and Discussion**

Following the findings of Chapter 3, a proposal was made to find an alternative polymer regime in order to better assess pH sensitivity. As mentioned above, chitosan was selected to test. In addition, agarose was selected as a pH-impervious polysaccharide to act as a compatible reference material. In the following segment, Sections 4.4.1 and 4.4.2 demonstrate testing and assess suitability of agarose and chitosan leaky waveguides (respectively). Section 4.4.3 then discusses the production of an internally referenced leaky waveguide sensor for pH. Section 4.4.5 finally assesses the possibility of using a synthetic reference material in place of agarose.

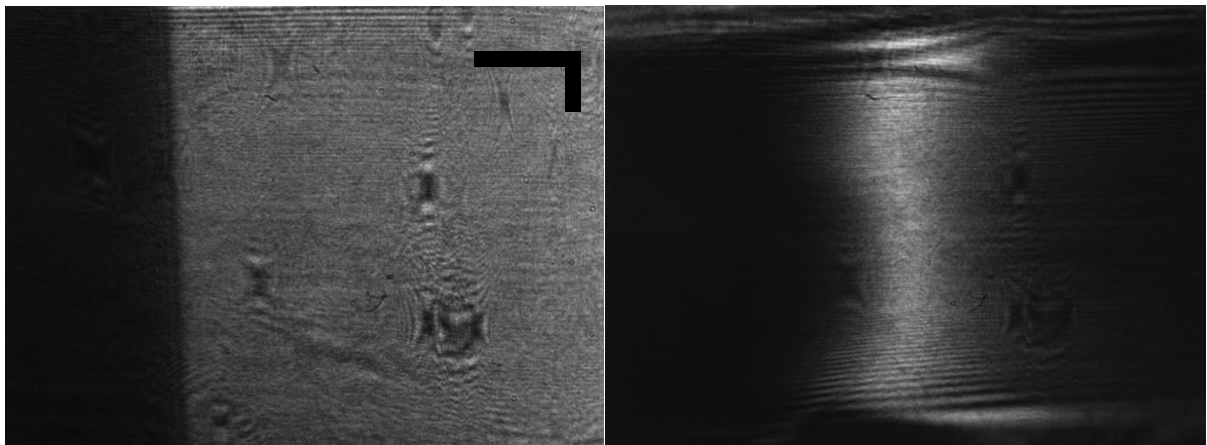
### **4.4.1. Single-Layer Agarose Waveguides**

Following the decision to adopt polysaccharides as part of gel production, there was found a need to manufacture new pH-insensitive reference waveguides. Agarose was selected for its pH insensitivity and good chemical inertness,<sup>186</sup> owing to the nonionic polysaccharide structure<sup>187</sup> not decorated by functional groups. The ability of agarose to reversibly form a mechanically stable gel due to cooling is also useful, however glutaraldehyde has been introduced in order to provide additional stability.<sup>188</sup> After selection, agarose waveguides were manufactured as per a method previously used for similar experiments,<sup>155, 189</sup> with some modifications described in Section 4.3.1. In particular, a spin speed of 3000 rpm was adopted following initial failures.



Following manufacture, the agarose waveguides were exposed to a range of phosphate buffers in the pH 3-9 region in order to measure the overall pH sensitivity response.

Initially, the waveguides generated from spun agarose did not provide any visible evidence of a leaky mode. As **Figure 4.3** shows, while agarose provides a clean output image free of significant blemishes, it does not provide a visible leaky mode. Dye-doping revealed the presence of a single, relatively broad leaky mode, however dye-doping of the gel itself was not considered valuable given its intended role as an inert reference waveguide. Therefore, a metal-clad leaky waveguide (MCLW, see Chapter 3) was manufactured by replacing the clean glass slide with an equivalent slide bearing a 3  $\mu\text{m}$  titanium layer. One mode is visible using the MCLW, which indicates a viable leaky waveguide.



*Figure 4.3 –Leaky waveguide on glass (left) and metal-clad leaky waveguide (right) for selected agarose reference material. Scale bars are 2° (horizontal) and 2cm (vertical).*

The issues with detecting agarose have been deemed due to its fair degree of optical transparency. With no absorbing component or light scattering occurring, light that couples into

the leaky waveguide at the resonance angle is not depleted in any significant manner, meaning it is visually indistinguishable from light that does not travel within the waveguide. While a non-visible leaky mode is not useful for this experiment, it was found by parallel testing that chitosan (Section 4.4.2) is less problematic. For analysing agarose alone, it was decided to use the MCLW as a proxy for the otherwise identical agarose optical leaky waveguide as the alternative (dye-doping running buffers and test solutions) would not be compatible with chitosan.

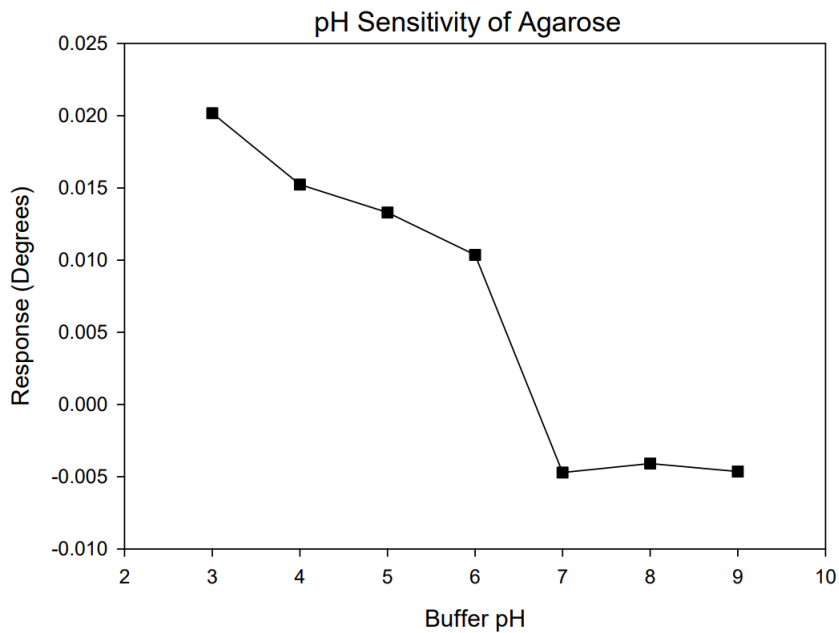
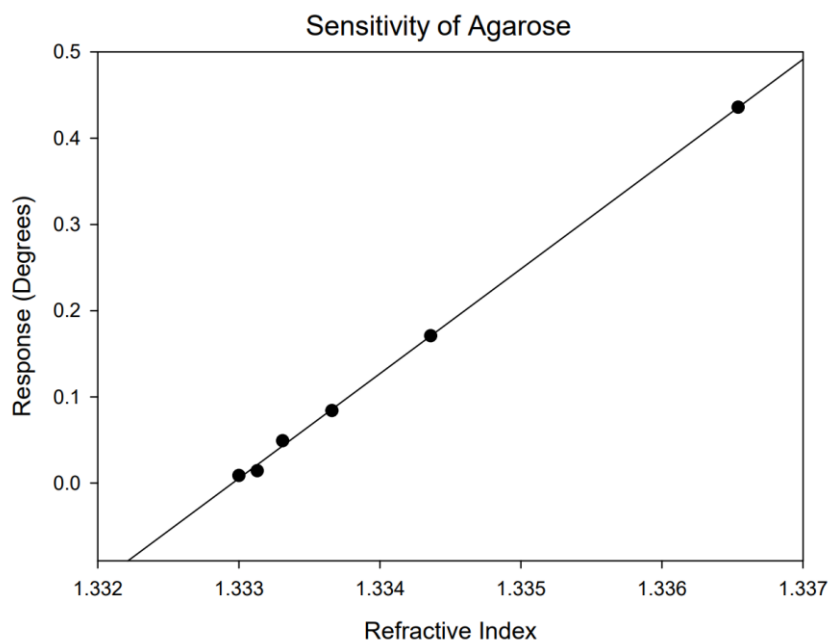


Figure 4.4 - pH sensitivity of agarose reference gel, using MCLW in place of LW.



*Figure 4.5 - RI sensitivity of agarose single-layer gel, as determined with glycerol solutions.*

Following tests with a range of phosphate buffers, the pH sensitivity of agarose films may be seen from **Figure 4.4**. Overall a very small degree of response is found, over a range of 0.03 degrees and with a sensitivity slope of  $4.68 \times 10^{-3}$  degrees/pHU. This equates to a total RI range of around 25 degrees or 0.20 mRIU across the indicated range, slightly greater than the difference between the buffers used and the refractive index of deionised water.

While smaller variations may be due to small degrees of user or measurement error in buffer production, this shift (especially over the pH 6-7 region) is stronger than the total RI difference between deionised water and the buffers used. As for causes, there are few known possibilities. As a linker, glutaraldehyde favours the use of amino groups as supports, although thiols, phenols and imidazoles may also suffice.<sup>190</sup> Glutaraldehyde has been considered to form acetal or hemiacetal linkages while reacting with hydroxyl-bearing polymers,<sup>191</sup> and in the absence of

other available functional groups there is not expected to be any ionisable groups. The presence of a slight negative shift as pH increases indicates a cationic character, and indeed the pH response curve in the 3-5 region bears some small resemblance to that of chitosan in the 2-4 region (**Figure 4.7**), albeit much smaller in intensity. It is possible that the agarose sample provided, although considered of high purity, contains traces of heterofunctional agaropectin<sup>188</sup> which introduces very small quantities of ionisable functional groups.

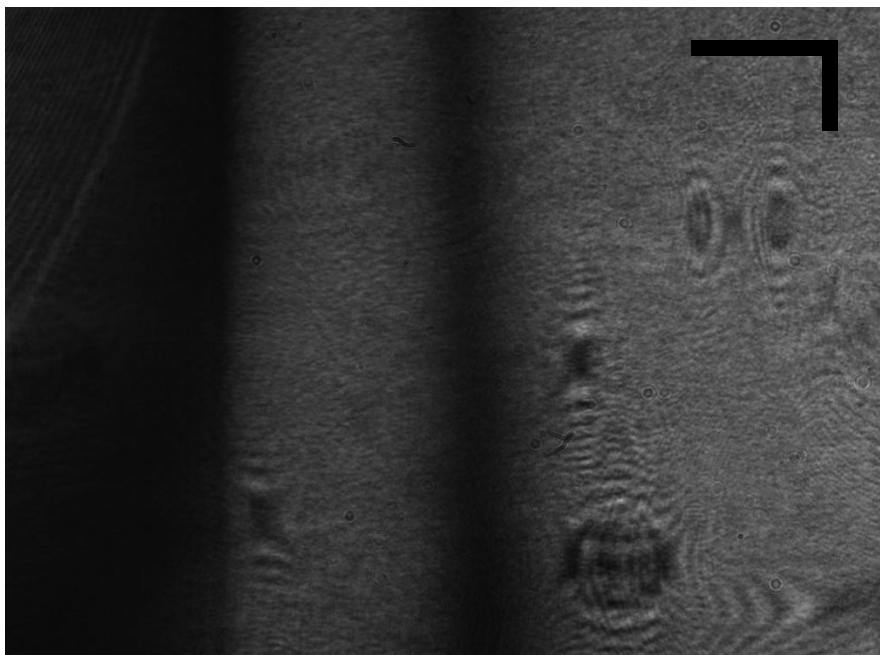
Relative to variations seen in cast and spun polyacrylamide gels (Chapter 3), agarose gels behave broadly similarly to the cast gel (**Figure 3.20**, above) in terms of total variance. The spun gel also exhibits a cationic character due to the stable Schiff bases, in this case formed by glutaraldehyde-amine links, however agarose gel exhibits only a small fraction of the extent of shift exhibited by the synthetic polymer.

#### **4.4.2. Single-Layer Chitosan Waveguides**

With agarose available as a reference waveguide material, chitosan was chosen as a compatible pH-sensitive waveguide material. Chitosan is a highly water-soluble polysaccharide characterised by a primary amine incorporated into the repeating unit, often used for facile reactions with crosslinkers or immobilisation of sensor recognition elements.<sup>192, 193</sup> The conditions used to manufacture chitosan waveguides were drawn largely from typical experimental practices used in the laboratory,<sup>99</sup> and after some assessment were found to be applicable without modification. However, as the mode detected was initially quite faint, a small amount of 100  $\mu$ M Reactive Blue 4 dye was added to the slide for 15-20 seconds to ensure

visibility. This accounts for the lack of a light-dark fringe seen in diffractive polyacrylamide gels (Chapters 4 and 6), instead providing the dark band seen in **Figure 4.6**.

In order to verify the pH sensitivity of chitosan, phosphate buffers of the formulations used with agarose gels (Section 4.4.1, above) were flower over the waveguides and the relative position of the resonance line monitored. **Figure 4.7** indicates the response pattern received. Chitosan waveguides were found to be pH sensitive, with a linear portion in the pH 5-8 range. A response magnitude of 1.08 degrees therefore provides a slope of 0.365 degrees/pHU over this range. The  $pK_{aH}$  of the waveguide was found experimentally to be around 6.3.



*Figure 4.6 - sample image of chitosan waveguide output. Scale bars are 2° (horizontal) and 2 cm (vertical).*

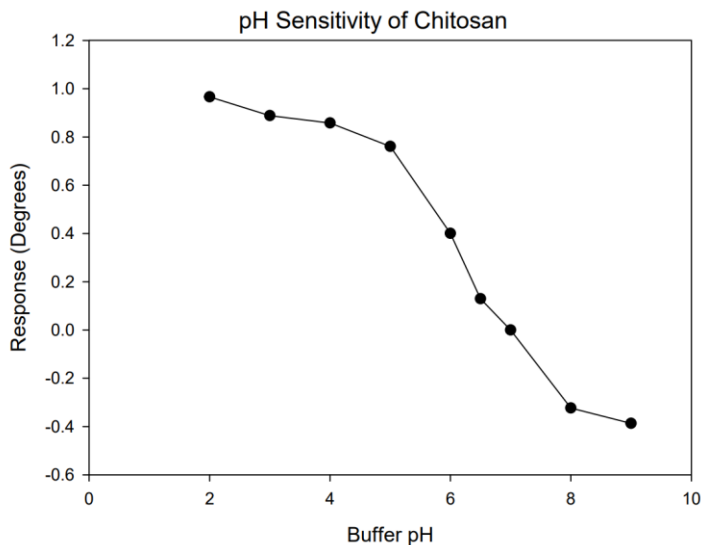
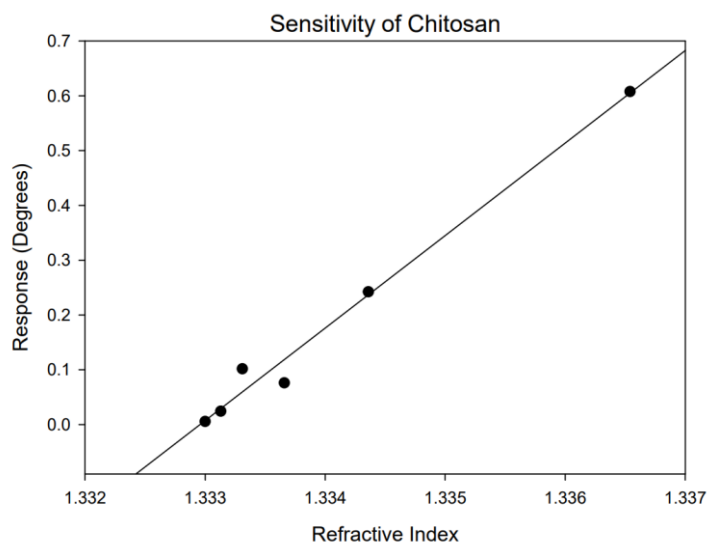


Figure 4.7 - pH sensitivity of chitosan waveguide

The  $pK_aH$  here detected demonstrates little overall change compared with that of linear deacetylated chitosan, around 6.5,<sup>185</sup> owing to the relatively minor chemical transformation between linear polymer and crosslinked polymer network. The response provided by chitosan is cationic in character, with the waveguide response falling as the pH increases. This is due to the primary amine charge collected as the pH falls. While the pH is acidic, the amino groups protonate, and so electrostatic repulsion causes the polymer strands to separate and so overcomes any tendency of chitosan to agglomerate. In the same way, as the pH rises a scarcity of available  $H^+$  causes the amino groups to deprotonate, reducing electrostatic repulsion and so allowing the gel to deswell. The linear portion of the pH response range covers the neutral range, from pH slightly acidic 5 to slightly basic 8. The sensitivity achieved over this linear portion is equivalent to 109.6 pixels per pH unit, with the camera used at the time. With the RI sensitivity data given in Section 4.4.3 (below) this offers a limit of quantitation of 0.08 pH units, however finer measurements may shed additional light on the best possible resolution.

Some consideration was also paid to RI sensitivity itself, measured by dosing with glycerol solutions as per similar experiments in Chapter 4. At a measured sensitivity of 169.76 degrees/RIU (**Figure 4.8**), the chitosan sensor appears superior to the 121.69 degrees/RIU achieved with compatible agarose gels (**Figure 4.5**), itself almost identical to the sensitivities of cast polyacrylamide films. Polysaccharide RI sensitivities also achieved an RSD of 6.89% and 4.00% for agarose and chitosan, respectively.



*Figure 4.8- RI sensitivity of chitosan single-layer gel, as determined with glycerol solutions.*

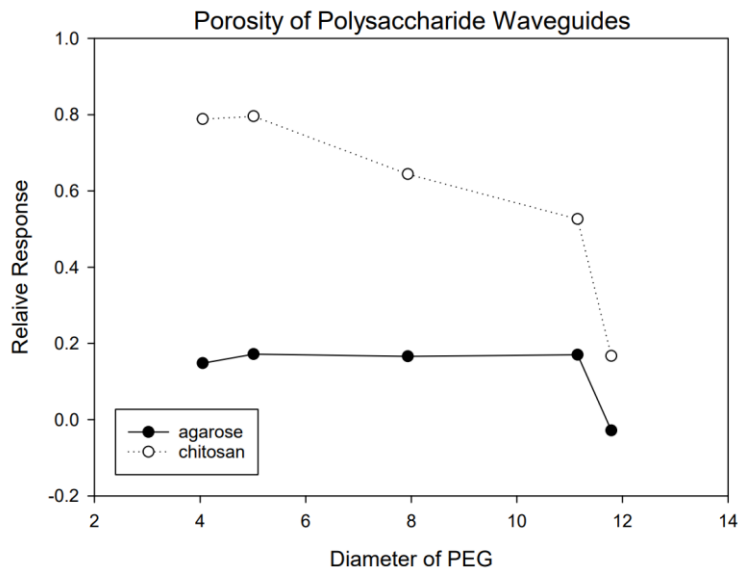


Figure 4.9 – Porosity assay, normalised with relative RI sensitivity of single-layer polysaccharide gels to PEG standards as described in Section 3.2.3.3. No negative responses were found, unlike polyacrylamide gels in the previous chapter, indicating a lack of nonspecific absorption between PEG and polysaccharides.

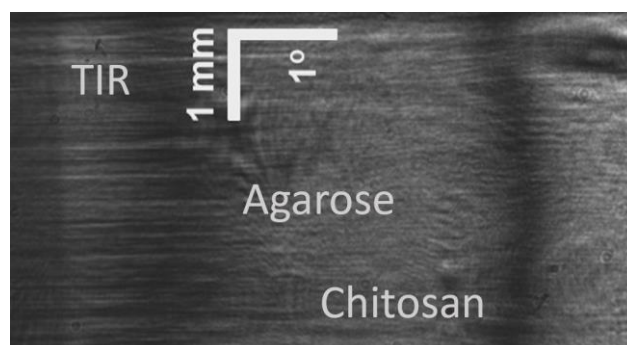
The greater sensitivity of chitosan is likely due to the different polymer sizes and manufacturing conditions. The glutaraldehyde content should be similar (312.5 ppm for agarose and approximately 300 ppm for chitosan), and the similar optical qualities of the leaky waveguides (**Figure 4.3 & Figure 4.6**) indicate a similar refractive index and thickness. However, agarose is a 2% polymer with a primarily self-assembled polymer network, while chitosan is a 1% polymer crosslinked by bathing the gel in glutaraldehyde rather than incorporating the crosslinker into the pregel solution. This is amply reflected in the porosities of the gels (**Figure 4.9**), with agarose unable to accept a PEG standard of any size in more than  $17\% \pm 0.072\%$  of the bulk hydrogel and wholly unable to accept the highest PEG standard of 300,000 MW, or 11.8 nm (by hydrodynamic radius).



### 4.4.3. Stacked Polysaccharide Leaky Waveguide

Following the assessment of the suitability of agarose and chitosan, a stacked leaky waveguide was assembled as per previous experiments by the laboratory.<sup>194</sup> The initial methodology, to layer chitosan onto a pre-existing agarose waveguide, was effective and generated waveguides similar to that shown in **Figure 4.10**. After some tests with metal-clad leaky waveguides, it was found that deposition of chitosan onto a hydrated agarose waveguide was effective while deposition onto dry agarose film was inconsistent and led to failed leaky waveguides. It is likely that the dry hydrophilic agarose leached water from the chitosan solution during deposition, reducing the volume of the layer while increasing its effective concentration and so deviating from the known waveguide conditions.

In the visual appearance of the two modes visible on the internally referenced sensor, the buried agarose mode remains close to the TIR line, commensurate with its position in MCLW, while the chitosan mode is shifted to a higher index contrast further from the TIR.



*Figure 4.10 - Output image for agarose-chitosan stacked waveguide. Due to larger area covered by the two modes, the TIR is visible as a straight line at the far left of the image.*

The RI sensitivity responses are provided in **Figure 4.11**. A refractive index sensitivity of  $150.6 \pm 19.25$  degrees/RIU was found for the buried agarose mode, and a sensitivity of  $136.7 \pm 7.51$  degrees/RIU was attained for the overhead chitosan mode. Of note is that the RI sensitivity of agarose both layers have changed relative to the single-layer variants, with agarose increasing in response and chitosan significantly decreasing. While more similar sensitivities simplify the task of filtering out RI interference from the pH response of the chitosan layer (described below), the loss of overall sensitivity indicates an unanticipated issue may have occurred with the layering of polymers together.

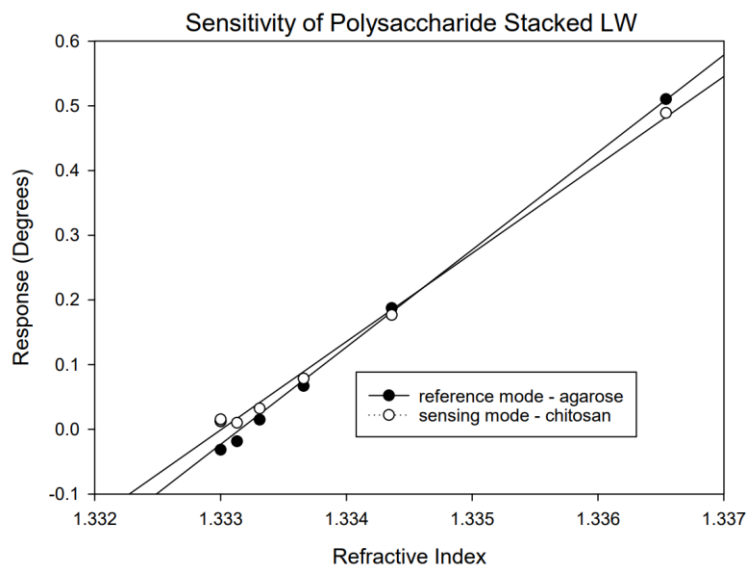


Figure 4.11 – Refractive index sensitivity of the stacked polysaccharide waveguide

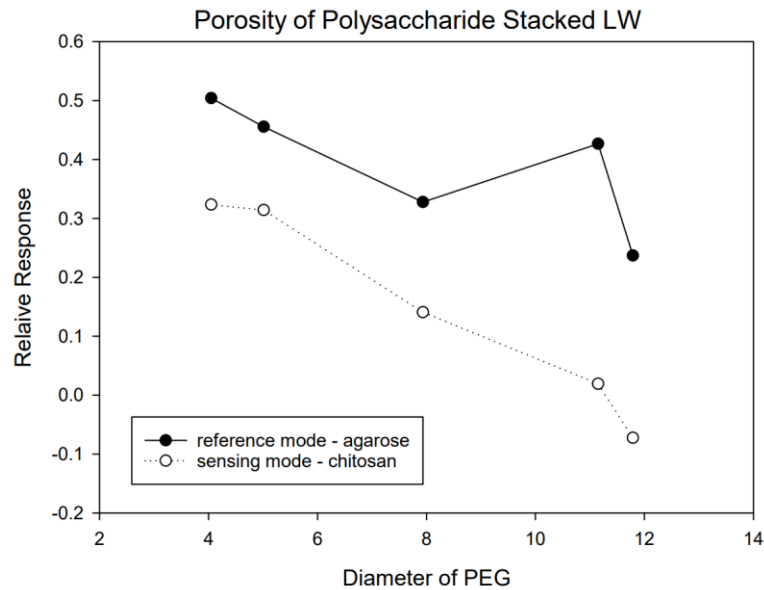


Figure 4.12 - Porosity assay, with relative RI sensitivity of stacked polysaccharide waveguides to PEG standards

As well as refractive index measurements, the porosity of the stacked leaky waveguide was measured by the same means as previously discussed (**Figure 4.12**). What can immediately be seen by contrast with **Figure 4.9** is that the available data is less consistent especially with agarose data, with less consistent measurements by a mean factor of 2.29 (calculated by comparing standard deviations). While the agarose mode behaves similarly to the single-layer agarose gels at or above 35,000 MW, indicating a similar distribution of pore sizes of size 7.94 nm or greater, the buried agarose appears superior to both the chitosan layer and the same gel without treatment. In other words, the buried agarose can admit more PEG into a greater proportion of its pores than the chitosan layer above it. However, agarose's capacity to admit larger molecules is unaffected.

Chitosan, in the stacked waveguide, suffers from poor porosity in general and does not match the pore size or distribution of pore sizes achieved by the single-layer chitosan waveguide.

Combined with the change in reduction in RI sensitivity, it may be said that the chitosan layer is less swellable or otherwise more closely crosslinked as a result of the sequential polymer deposition method. Overall, poor uptake limits the ability of this sensor from taking up proteins, limiting alternative applications in biosensing, but also may be an issue in wastewater or biologically contaminated water where an inconsistent degree of protein infiltration would make sensor calibration difficult to pre-empt.

The polymer may also have diffused into the agarose layer to some degree before crosslinking, which would create a dense and less clearly differentiable interface between the polymers. Unfortunately, the experimental tools necessary to interrogate this interface could not be procured for the majority of this project. As a result, the possibility of polysaccharide gels interpenetrating into one another will not be interrogated in this chapter.

#### **4.4.4. Internally Referenced pH Sensitivity and Buffer Selection**

With a functioning stacked leaky waveguide that responds suitably to refractive index, the next stage in development was ensuring a suitable pH response curve in both of the identified modes. To this end, it was found that a reference-adjusted by the expedient of subtracting the agarose output from that of chitosan – this is interrogated more directly in Chapter 7, however. The pH sensitivity of the stacked agarose-chitosan waveguide was analysed as per the method used for single-layer waveguides (above).

The data provided can be seen in **Figure 4.13**. A linear range of pH 3-7 is achieved by the chitosan mode, and 4-7 after subtracting the agarose reference mode. As measured, the reference-adjusted measurement has a  $pK_{aH}$  of 5.1 and a sensitivity curve of 0.168 degrees/pHU. A slightly more acidic  $pK_{aH}$  relative to that of single-layer chitosan (6.2) or the listed sensitivity of chitosan polymer (approx. 6.5) is unanticipated. Measured pH sensitivity has therefore decreased to less than half of that achieved by chitosan single-layer waveguides, with a corresponding impact on both limit of detection and pH resolution. The major feature of the agarose-chitosan waveguide is that, as was described by the group in previous experiments,<sup>194</sup> the reference and sensing modes appear to be contained within their respective layers of the waveguide. Had the mode contained within the buried agarose layer leaked significantly into the chitosan layer, this would have manifested as the reference mode displaying a small degree of pH sensitivity as well.

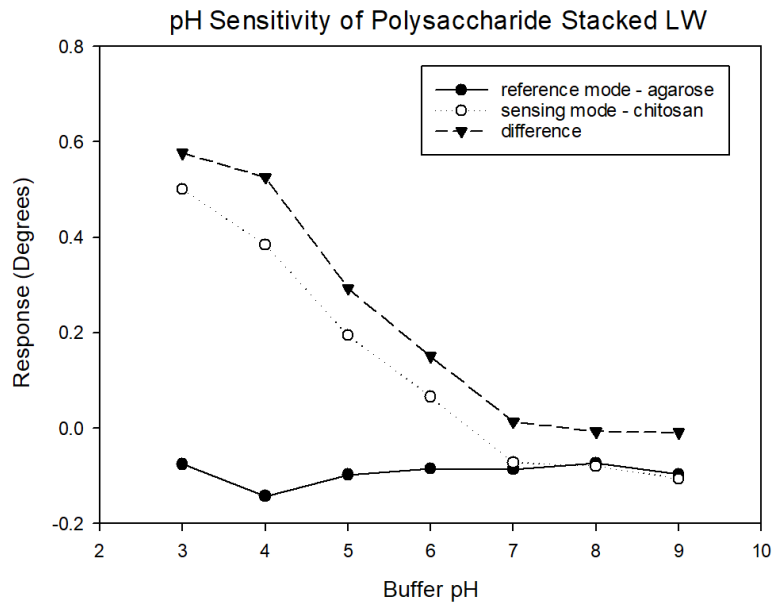


Figure 4.13 - pH sensitivity of stacked agarose-chitosan stacked waveguide

While performing these pH measurements, however, concern was raised over the choice of buffer used. While sodium phosphate salts exhibit a broad range of  $pK_a$  values at 2.2, 7.2 and 12.4,<sup>195</sup> making it an excellent buffer system for long pH ranges, there remains a risk of trivalent phosphate anions forming temporary binding sites among multiple protonated amino groups. If such transient binding occurs, a chitosan gel immersed in phosphate buffer would be slightly shrunk as binding holds together separate strands of polymer as temporary crosslinks. Substituting phosphate buffers with the zwitterionic, monovalent 4-(2-hydroxyethyl)-1-piperazineethanesulfonic acid (HEPES) is expected to provide information on the effect of buffer anion choice.

A comparison using the stacked agarose-chitosan waveguides was therefore performed (**Figure 4.14**). Measurements using HEPES found a range of 4-8, a sensitivity of 0.280 degrees/pHU, and a measured  $pK_aH$  of 5.6. While there is less clear linearity with HEPES buffers, a dramatic increase in the magnitude of response relative to phosphate buffer data indicates the possibility that (as mentioned above) phosphate buffers are posing a negative effect of binding capability. A change in  $pK_aH$  is also shown, now occurring closer to that of chitosan single-layer waveguides, which may also be due to reversible crosslinking effects by the phosphate ion. Bringing the ionisable amino groups into closer proximity may also hinder further ionisation by virtue of proximity, requiring more acidic conditions to apply additional (and indeed full) ionisation to chitosan, resulting in turn in a lower  $pK_aH$ .

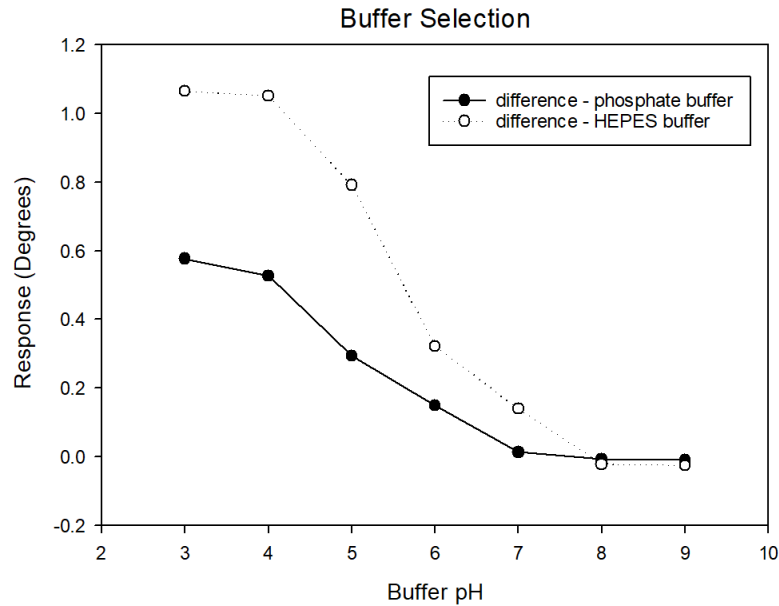


Figure 4.14 - pH sensitivity of stacked agarose-chitosan stacked waveguide with comparative running buffers. Internally referenced 'difference' data shown for clarity.

#### 4.4.5. Synthetic Reference Material

Following concerns from the principal investigator regarding the lifespan of agarose gel, particularly a concern in bacteriologically active media or in biosensing,<sup>196</sup> the possibility of transferring to another suitable reference material was considered. After some less successful tests of other materials, polyacrylamide was selected due to its known suitability as a leaky waveguide (Chapter 4). Spun polyacrylamide of the same batch was retrieved and waveguides fabricated as per previous methodologies. From there, chitosan was spun onto the polyacrylamide as per the above experiments. **Figure 4.15** demonstrates the stacked waveguide achieved with chitosan layered onto polyacrylamide. Of note is the relatively poor resolution of each mode – the resonance line nearer the TIR is visually similar to a diffraction pattern, especially in the shapes beyond the TIR, while the mode further from the TIR is typically

uneven in its distribution. In other waveguides, the latter mode was also relatively broad and faint.

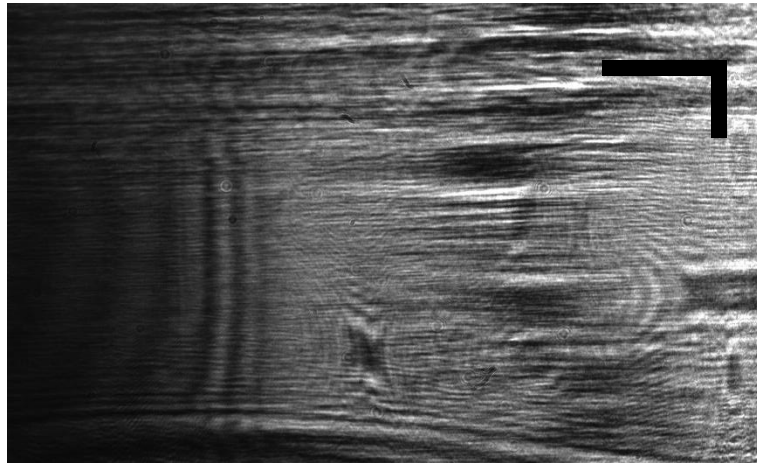


Figure 4.15 - Sample image of spun polyacrylamide-chitosan waveguide. Scale bars are 2° (horizontal) and 2cm (vertical).

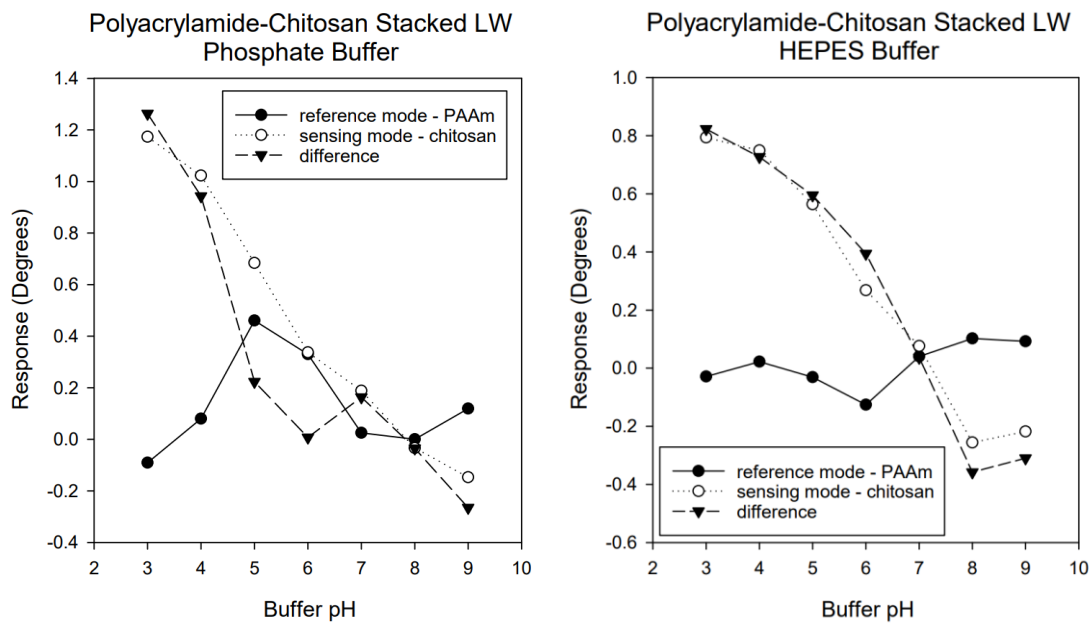


Figure 4.16 - pH sensitivity of stacked polyacrylamide-chitosan stacked waveguide with comparative running buffers., comparing phosphate buffer (left) and pH-adjusted HEPES buffer (right) solutions.



The stacked polyacrylamide-chitosan waveguides were tested with both phosphate and HEPES buffers (**Figure 4.16**). Buffer testing revealed the mode(s) nearer the TIR to be that of chitosan while the faint and broad mode further from the TIR was that of polyacrylamide, providing clarification for **Figure 4.15**. When tested with phosphate buffers, the chitosan layer provided a stable linear pattern with a good sensitivity slope at 0.235 degrees/pHU, and a linear portion that exceeds the pH 3-9 testing range. The latter is welcome, however it does prevent any calculation of the  $pK_aH$ . Unfortunately, abnormal behaviour was encountered with the polyacrylamide layer. This abnormal pattern was replicated on every polyacrylamide-chitosan sensor tested in this manner and was independent of the buffer batch, and appears to indicate either multiple pH-induced swelling actions or possibly an amphoteric pattern of response. The same internally referenced sensors did not report this response pattern with HEPES buffer, however.

Use of HEPES buffer for polyacrylamide-chitosan sensor was then performed. An asymmetric curve is present in chitosan response, causing some imprecision in finding the  $pK_aH$ , but it can be estimated to around 6.5. The internal referencing regime provided a sensitivity slope of 0.273 degrees/pHU in the 4-8 region, superior to other chitosan waveguides or testing regimes for pH sensing capacity. In addition, a small unanticipated dip in response was detected in both the sensing and reference modes, and by their subtraction the reference-corrected response eliminated much of its effect. This serves as a potential demonstration of the effectiveness of the internal referencing regime; however a more in-depth test will be required once the sensor technology is more mature.

#### **4.4.6. Summary**

In this chapter, leaky waveguides manufactured from pH-sensitive and -impervious polysaccharide gels were fabricated and their properties as RI sensors briefly assessed. An internally referenced leaky waveguide was fabricated by combination of the polysaccharide layers and the viability of pH sensing by an internally referenced sensor demonstrated. The effect of buffer selection on waveguide properties was briefly explored. Finally, a combination synthetic/polysaccharide internally referenced pH sensor was demonstrated.

The primary objective of this chapter, demonstrating the viability of an internally referenced sensor for pH, appears to have been met. However, further work remains and some limitations have not been addressed. The indicated sensitivity to buffer selection is a considerable barrier to the further adoption of chitosan, especially as it indicates a considerable sensitivity to polyvalent anions that may cause further issues with real samples. There are additional questions with the longevity of polysaccharide-based sensor components, however further opportunities will be needed to test this once a suitable pH sensor has been selected. In either case, one option to avoid these issues would be to return to synthetic pH-sensitive polymers. The following chapter will address this course of action.

## **Chapter 5. DEVELOPING SYNTHETIC LEAKY WAVEGUIDES FOR PH SENSING**

### **5.1. Introduction**

While in Chapter 4 (above) the viability of a stacked-construction leaky waveguide sensor was demonstrated, work must be performed to advance this design into a polymer of appropriate and tuneable characteristics. In Chapter 4, it was indicated that dimethylamino groups are a viable tool for providing pH sensitivity to an acrylamide copolymer. This chapter will address the development of a suitable synthetic pH-sensitive polymer for further application in a stacked polymer. As per previous chapters, Sections 5.2 and 5.3 provide the methods, materials, and procedures used in this chapter. Section 5.4.1 then describes the optimisation process used with (N-dimethylamino)ethyl methacrylate copolymer, the evaluation of a single-layer polymer produced by such methods, and flaws encountered with its use. Section 5.4.3 discusses (N-dimethylamino)propyl methacrylamide as an alternative, its optimisation and preparation as a copolymer for pH sensing. Section 5.4.4 describes some tests performed with interferants likely to be encountered in a water and wastewater quality environment.

### **5.2. Materials and Methods**

#### **5.2.1. Chemicals and Materials**

Acrylamide 40% (w/v), N,N-methylene bisacrylamide (bisacrylamide) 2% (w/v) and premixed acrylamide/bisacrylamide blends for gel electrophoresis (40% w/v) were procured from Sigma Aldrich (UK). Also from the same supplier were mono- and dibasic sodium phosphate and ethanol.

Decon 90 and sodium chloride was procured from Fisher Scientific (UK)

(N-dimethylamino)ethyl methacrylate (DMAEMA), phosphoric acid, trisodium phosphate, aluminium sulphate and humic acid were procured from Acros Organics (UK).

(N-dimethylamino)propyl methacrylamide (DMAPMAm) was procured from ABCR (Germany).

Chloro(dimethylvinyl)silane (CDVMS) was purchased from TCI Chemicals (UK)

Glass microscope slides (to standard ISO 8037/1) and sodium hypochlorite ~14% were purchased from VWR (UK)

All chemicals were used without further purification.

## **5.2.2. Instrumentation**

The majority of analysis occurred using a waveguide apparatus, described in Chapter 3. A flow rate of 1.50 ml/min was used throughout. Solution refractive indices were found using a Bellingham Stanley RFM970-T refractometer, the specifications of which are given in Chapter 3. Likewise, the pH of running buffers and other test solutions was found using a Hanna HI 2210 benchtop electrochemical pH meter previously discussed.

## **5.3. Experimental Procedure**

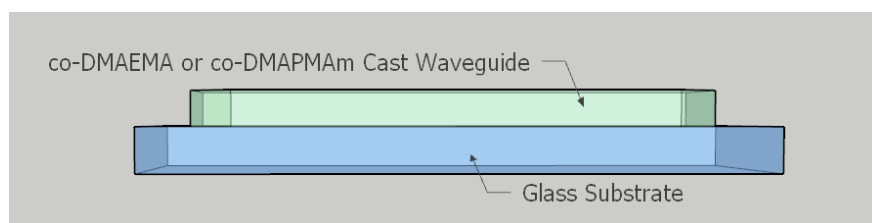
Slide treatment occurred as per the method described in Chapter 3, covered below. Before use in any application, 25 x 25 mm glass slides were sonicated for 30 minutes each in Decon 90 detergent solution, deionised water and ethanol, before drying in air. Substrate slides were cleaned as described above, then were immersed in a 0.2% v:v solution of chloro(dimethylvinyl)silane (CDMVS) in toluene. Slides were then transferred to clean toluene for 5 minutes before drying on soft tissue paper. Microsphere casting slides were produced by spotting clean glass slides in each corner with 1  $\mu$ l of a 1% suspension of microspheres in water and dried at 60° overnight. The integrity of the microsphere deposition on sample slides was verified by visual inspection.

Polymer deposition was performed within a day of slide treatment, and ideally within 2 hours of slide treatment to ensure hydrophilicity. Where delays occurred, CDMVS-treated slides were retained in their toluene wash until required in order to minimise air exposure.

### **5.3.1. Polymer Casting**

For fabrication of cast polyacrylamide, 875  $\mu$ l of deionised water degassed with nitrogen is added to 125  $\mu$ l of acrylamide/bis(acrylamide) 29:1 solution (40% w/v) To this solution is added 1.25  $\mu$ l of TEMED and finally 12.5  $\mu$ l of APS (10% v/w in deionised water) which

initiates free-radical polymerisation. The prepolymer is then immediately vortexed and a 100  $\mu$ l aliquot is deposited in the centre of a CDMVS-treated glass slide. A clean glass slide with appropriate spacer is placed above, followed by a 500 g brass weight. The solution is permitted to gel within the cast until the remaining (non-aliquot) solution is gelled and invertible. Finally, the cast is immersed in deionised water for at least 2 hours before gently prying apart, and is stored dry until required. The intended configuration is shown in **Figure 5.1**



*Figure 5.1 - Cartoon of cast pH-sensitive leaky waveguide layout used in this chapter.*

For fabrication of cast copolymer, a similar overall method is used, however the alternative recipe is applied. Due to the need to tune crosslinker content, an aqueous solution of bisacrylamide (2% w/v) as well as a separate stock of acrylamide (40% w/v) is used. Prepolymer components are added in the following order: comonomer (as appropriate), bisacrylamide, acrylamide, DI water, TEMED, APS. This film production is as per above, however all films were incubated dry at 25° overnight (approx. 16 hours) before use. All films were stored dry and were washed with deionised water before and after use. Where gelation did not occur to a prepolymer solution, the solution is charged with additional acrylamide/bis(acrylamide) 29:1 solution before addition of additional APS/TEMED initiators to force the consumption of potentially hazardous monomers, and subsequently disposed of safely.

### **5.3.2. Sample Preparation and Storage**

Running solutions were produced using a phosphate salt system (phosphoric acid, sodium dihydrogen phosphate, disodium hydrogen phosphate, sodium phosphate). Stock solutions were made to a target concentration of 100 mM, then running solutions made from a 10 mM solution of each. As the ionic strength of a buffer is proportional to its refractive index, the RI of the running solutions was measured and then adjusted to 1.33314 before use. Where effects of buffer concentration was being investigated, this dilution was not performed.

Where interferent solutions were tested, solutions were made at 0.1, 0.2, 0.5, 1, 2, 5, 10 and 20 mg/L solutions. Sodium hypochlorite disregarded the 10 and 20 mg/L solutions, as rising above 5 mg/L indicates overchlorination and may cause other complications (see Chapter 1). Sodium chloride solutions were used as a source of hypochlorous acid (ClOH) ions, and were made to concentrations of 1, 5, 10, 30 and 45 mM free chlorine content. In order to eliminate the effects of acidity or alkalinity, which were found to have significant independent effects on the waveguide response, all solutions were brought up to 10 mM of pH 7 phosphate buffer in addition to their intended chemical content.

Waveguides are stored dry by default, following experiences with polysaccharide slides, and were kept in the dark unless the immediate batch was in use. Likewise, running solutions and buffers were stored in a cool dark place unless expected to be used. Buffers around neutral pH were examined monthly for microbial growth and were disposed of and replaced if any evidence

of contamination was found. For some experiments regarding leaching-out of material, a number of waveguides were stored under deionised water. These samples were maintained safely in a cupboard, as above, and were gently air-dried prior to use.

## **5.4. Results and Discussion**

In Chapter 3, the decision to investigate DMAEMA as a potential waveguide component was decided upon using a spun polymer of 3:2 DMAEMA:polyacrylamide, 250 ppm glutaraldehyde crosslinker and 4000 rpm spin speed. However, it was considered likely that a formulation of superior overall performance may be found. As a result, an assay was performed with the more rapidly manufactured cast gels.

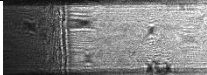



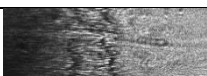
### **5.4.1. Optimisation of DMAEMA**

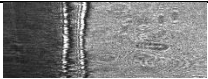
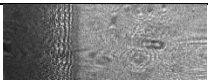
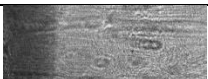

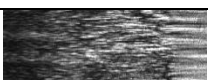

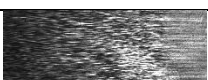
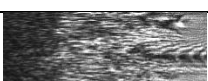
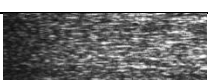
The first stage in this procedure was to perform an assay of viable waveguide formulations. These were performed as bulk gels initially, with suitable gel formulations being taken forwards to assay for viable cast waveguides. In this case, as in Chapter 3, the objective is to fabricate a gel with suitable refractive index contrast to act as a leaky waveguide. Additionally, sufficient stiffness to retain the waveguide shape, but not so stiff as to resist swelling. Finally, the gel is expected to have the highest appropriate density of DMAEMA copolymer should induce sufficiently strong pH-induced swelling capacity.



The results of the initial gel formation survey are shown in **Table 5.1** Error! Reference source not found.. It was rapidly found that DMAEMA and bisacrylamide alone did not form a gel, even at a 10% (w/v) monomer content, except with addition of copious bisacrylamide. The majority of other gels formed properly, particularly where the DMAEMA content was low in comparison to the acrylamide content.

*Table 5.1- Formulation of co-DMAEMA waveguides. A star \* indicates a bulk gel formed, but with poor or no shape-retaining ability.*

Sample ID	Total Monomer (% w/v)	Bisacrylamide (% of total monomer)	DMA /Acrylamide (molar ratio)	Gel	Waveguide profile
Pa2c	5.26	2.24	1.05	Y	
2.1c	4.71	3.33	1.50	N	n/a
2.2c	8.71	1.12	0.27	Y	n/a
2.3c	5.92	2.14	0.56	Y	n/a
2.4c	4.29	6.66	1.50	Visc.*	n/a
2.5c	9.17	1.84	3.53	Visc.*	n/a
1.1c	4.80	3.33	1.50	N	n/a
6.1c	6	2	0.5	Y	
6.2c	6	2	1	Y*	
6.3c	6	3	1	Y	
6.4c	6	4	1	Y	

6.5c	8	3	1	Y	
6.6c	8	4	1	Y	
6.7c	8	6	1	Y	
6.8c	8	4	2	Y	
6.9c	8	6	2	Y	
6.10c	8	8	2	Y	
5.1c	10	2.04	DMA	N	n/a
6.11c	10	4	DMA	Y*	
6.12c	10	6	DMA	Y	
6.13c	10	8	DMA	Y	

Higher quantities of DMAEMA gelled only in the presence of a corresponding increase in acrylamide. In particular, as shown by formulations **5.1c** and **6.11c**, a viable gel without any acrylamide as a backbone polymer is not possible until at least 4 mol% bisacrylamide content, and ideally greater. At this concentration, there is 362 mg/ml bisacrylamide alone within the gel, and a polymer network would have been available given even small amounts of copolymer. This may be attributable to the increase of molar mass of DMAEMA from acrylamide (157.21 as opposed to 71.08), reducing the number of monomer units in the prepolymer solution by a factor of 2.21 for the fraction of PAAm exchanged, however elements in the character of each

polymer may also be involved. Given the copolymer reactivity ratios for acrylamide and DMAEMA, 1.9 and 0.52 respectively,<sup>197</sup> it can be deduced that the co-DMAEMA fraction polymerises more rapidly than its counterparts and so partially excludes acrylamide (and bisacrylamide) from the polymer network during initial growth.

With inclusion of equal quantities acrylamide and DMAEMA, the capacity to gel is significantly increased. particularly, as shown by formulation **Pa2c**, the total monomer content can be halved relative to the only viable DMAEMA polymer and the bisacrylamide content correspondingly reduced to around a quarter. As the DMAEMA fraction is further reduced, the minimum polymer and crosslinker content may be further reduced. As can be better visualised in **Figure 5.2** and **Figure 5.3**, Increasing the bisacrylamide content alone does not appear to alter the minimum gelling conditions to the degree that altering the DMAEMA content does. In order to ensure a suitable gel is produced, the DMA content must be kept low or else the total monomer content must be increased.

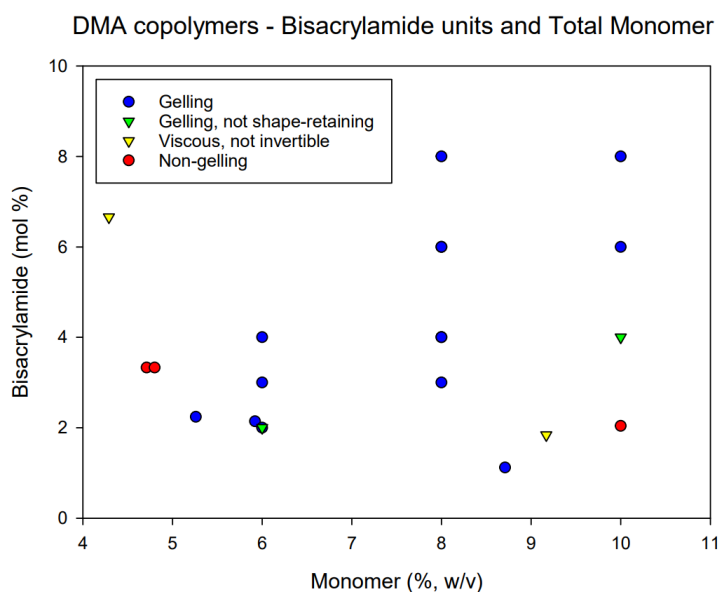


Figure 5.2 - Examining possible relationships between total monomer fraction and bisacrylamide content, for co-DMAEMA gels

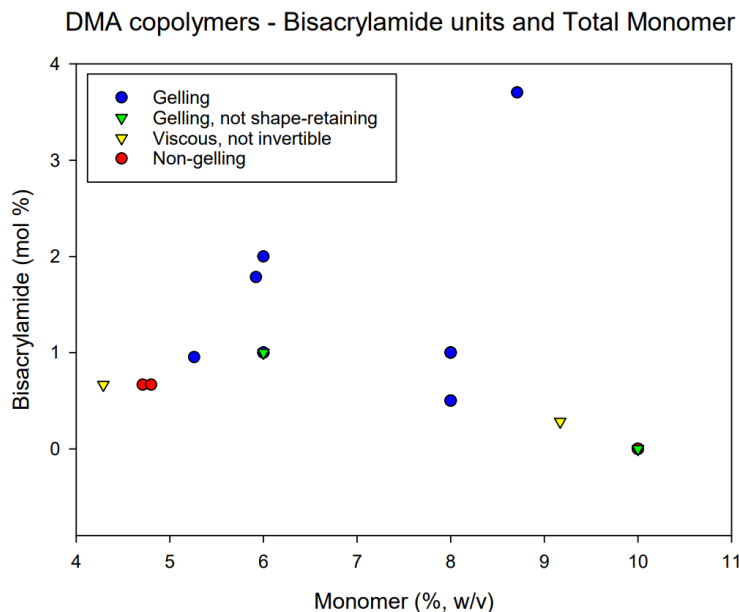


Figure 5.3 - Examining possible relationships between total monomer fraction and copolymer ratio, for co-DMAEMA gels

After demonstration of gel production, cast thin films were manufactured and suitable waveguides were identified. The images taken using these waveguides can be seen in the final column of **Table 5.1**. Formulations that provided no leaky mode whatsoever were disregarded, as were gels that were too dense to support a clearly legible mode or too rare to support more than a transient interference pattern. Two formulations remained, 6.4c and 6.5c. Of note is that the formulations are similar but for the total monomer content, although they provide the same final bisacrylamide content (0.019 mmol/ml) This indicates an optimum for future potential waveguide production. Also of note is that none of the tested formulations provided a single-moded waveguide, however this did not cause notable complications as the final leaky mode (furthest from the TIR) could be analysed instead (see below). While the solution made at 8% (w/v) polymer content provides the clearer and more legible mode appearance, it was felt that

the 6% (w/v) gel may provide a greater swelling capacity and so greater pH sensitivity. As a result, both were taken forwards in parallel.

The copolymer formulations taken forward were then tested for pH sensitivity using phosphate buffers, as per for cast acrylamide. As is previously shown in Chapter 3, acrylamide-bisacrylamide gels feature little to no pH sensitivity without an additional component and so can be disregarded as potential causes for pH response. Both formulations saw a decrease in response as the pH increased, corresponding with a reduction in swelling as dimethylamino groups are induced to deprotonate.

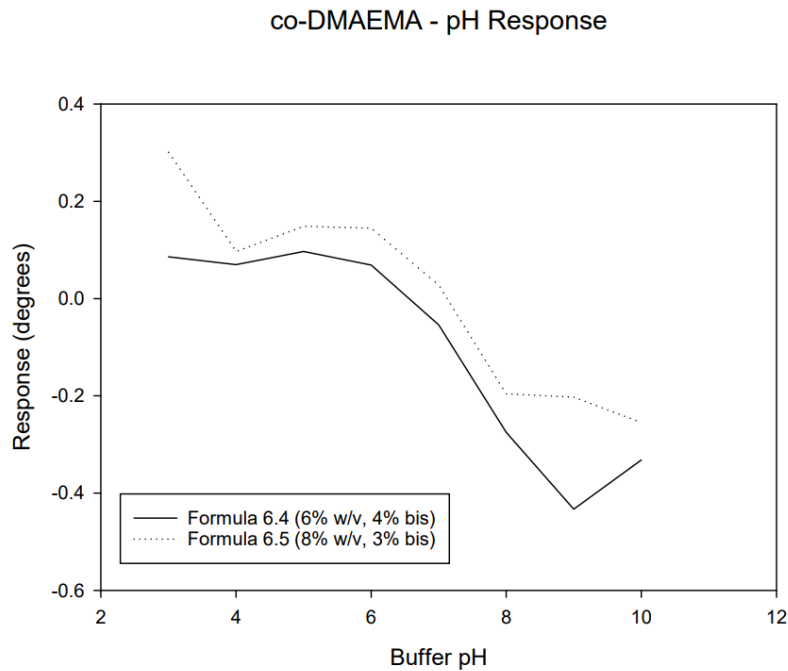


Figure 5.4 - pH sensitivity curve of co-DMAEMA cast waveguide, formulas 6.4 and 6.5 (defined in description). Note difference in overall response over pH 8-10 range.

The pH sensitivity curves found are provided in **Figure 5.4**. The gels made from formulation 6.5 (8% w/v total monomer, 3% bisacrylamide) were found to be unpredictable, especially outside the range of pH 4-8. In addition, response values for pH 3 or pH 9-10 were found to vary not just in response but in general character, with some (but not all) films providing a strong negative response at pH 3 which could not be explained by functional group ionisation characteristics alone. Such malfunctions were deemed too inconsistent to examine as a whole, as the pattern of response varied from waveguide to waveguide despite the relative stability of the pH 5-9 region.

Formulation **6.5** also provided a smaller response in all, with a magnitude of 0.403 degrees (giving a sensitivity slope of 0.081 degrees /pH unit) as opposed to the 0.530 degrees (with a sensitivity curve of 0.132 degrees /pH unit). While on the whole Formulation 6.5 appears to cover a broader area, to be expected given the greater number of ionisable units expected to be contained in the same volume of gel, it lacks sensitivity. The sensitivity curve of Formulation **6.4** is not only larger in magnitude, as to be expected given the less dense gel, but also more clearly linear. Greater range permits effective sensor use in more environments and conditions. Finally, both formulations provided a similar apparent  $pK_{aH}$  (7.38 and 7.20, respectively), both close to the  $pK_{aH}$  of DMAEMA monomer (7.3).<sup>198</sup> The lack of change in  $pK_{aH}$  indicates no significantly greater difficulty in ionising 50% of the dimethylamino groups relative to the free monomer, and in turn indicates the dimethylamino groups do not take additional proton availability to become ionised.

After examining the difference in performance between the two viable formulations, it was considered appropriate to continue with Formulation 6.4 as the best available for fabricating waveguides.

### 5.4.2. Sensor Longevity

The longevity of the waveguides was then analysed by immersing in deionised water to replicate the effects of prolonged operation. After 4, 18 and 48 hours the waveguide was extracted, and its pH sensitivity assayed as per Section 5.4.1. As displayed in **Figure 5.5**, pH sensitivity was lost over time due to this immersion.

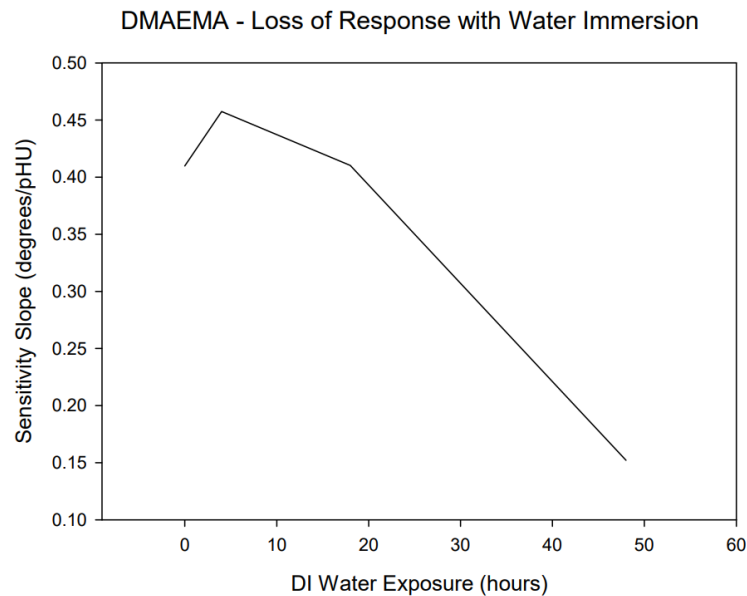
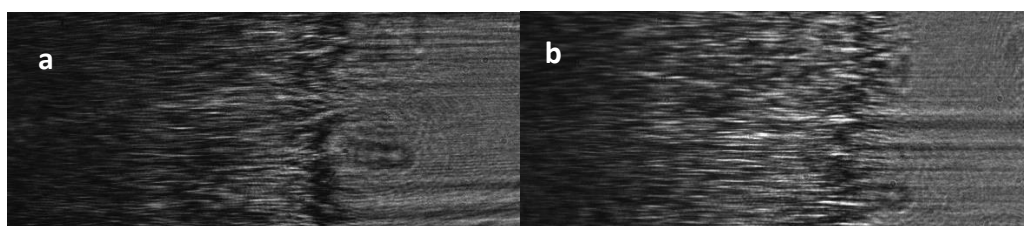


Figure 5.5 - Losing pH sensitivity in co-DMAEMA waveguides through immersion in water.

While it is possible that more sensitivity may be lost with additional immersion time, most waveguides failed to maintain a leaky mode as immersion times passed 48 or even 18 hours. In addition, many waveguides that underwent this process also exhibited an increase in refractive index contrast and an appearance of a denser gel. This may be seen in **Figure 5.6**, where the resonance dip representing the leaky mode retreats from the TIR line. A broader and more intense distorted pattern also appears, not unlike the appearance of very dense waveguides seen in **Table 5.1**. From this it can be inferred that the properties of the polymer network are altered as the sensitivity drops, and particularly that the waveguide is growing more dense as the sensitivity drops.



*Figure 5.6 - Appearance of a co-DMAEMA waveguide before (a) and after (b) water immersion. Note the migration of resonance angle from the TIR, and the expanding area of noise in the intervening space.*

### **5.4.2.1. Understanding Sensitivity Loss**

The behaviour of the co-DMAEMA waveguides immersed in water, above, is consistent with gradual leaching of the dimethylamino-bearing component into the bulk solution.

A possible cause of this behaviour is that DMAEMA, as an amphiphilic cationic copolymer, may self-assemble into a stable nanoparticle, with the polymer backbone forming a



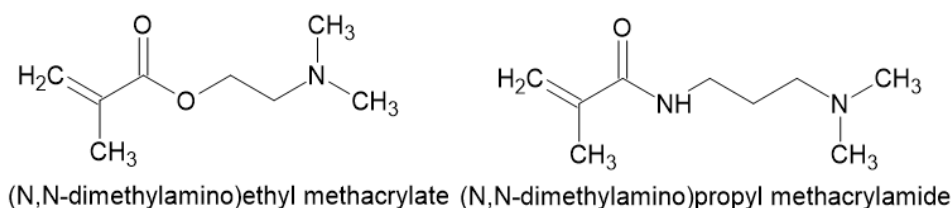
hydrophobic core.<sup>199</sup> Such behaviour has been used to develop core-shell nanoparticles based on DMAEMA among other polymer blends, where it excels as a pH-responsive drug delivery vehicle.<sup>200</sup> This leaching out also explains the change in mode position and appearance. As the DMAEMA leaches out, acrylamide and bisacrylamide remains as a densely crosslinked polymer network that may contract and appear as a much more dense waveguide.

Likewise, the copolymer reactivity ratios of DMAEMA and PAAm play a part in ensuring the microparticles form. Some DMA will react with the slower acrylamide and be incorporated into the polymer backbone, thereby remaining in the hydrogel even after loss of these microparticles. This means that at least theoretically, a small amount of DMAEMA would remain in the depleted gel. This effect would be exacerbated by the interior location of the polymer backbone within the nanoparticle, where it is inaccessible to acrylamide monomer or suitable chains.<sup>201</sup>

As indicated by the disrupted shape of the resonance line in immersed co-DMAEMA gels, the position of the particulates may not be evenly distributed throughout the film. Why this may be is not fully known, and would present an excellent opportunity for further research sadly not performed due to time and scope constraints.

### **5.4.3. Adopting DMAPMAm**

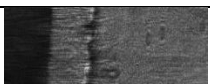

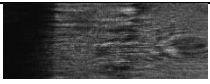
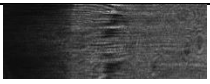
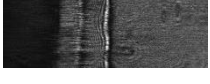
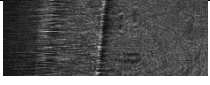
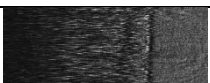
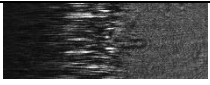
Given shortcomings with co-DMAEMA waveguides, a structurally similar molecule was selected to act as a less amphiphilic substitute. N,N-(dimethylamino)propyl methacrylamide (DMAPMAm, **Figure 5.7**) is a tertiary amine-bearing methacryl monomer of similar weight. The main difference between the selected molecules is the loss of the acrylate unit in favour of acrylamide, or rather the addition of a nitrogen as a bridge between the polymer backbone and pendant group. This group allows the bridging unit between to both donate and accept hydrogen bonds, reducing hydrophobicity near the polymer backbone and so limiting the forming monomer's capacity to form microparticles. Lengthening the pendant group by one carbon, performed due to issues with sourcing a suitable (dimethylamino)ethyl monomer, may have an unexpected effect and was to be investigated should any issues be encountered.<sup>199</sup>

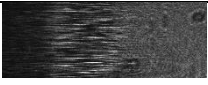



*Figure 5.7 - Prior comonomer (N,N-dimethylamino)ethyl methacrylate (DMAEMA, left) alongside newly introduced monomer N,N-(dimethylamino)propyl methacrylamide (DMAPMAm, right). Note the slightly longer pendant group length along with the switch from ester linkage to an acrylamide linkage similar to the structure of the base polymer.*

In order to expedite the manufacture and optimisation process for the new copolymer, a gelling study similar to that performed for DMAEMA was performed. As the majority of formulations gelled without issue, only a selection of total results are given in **Table 5.2**, below.

Table 5.2 - Formulation of co-DMAPMAM waveguides, initial test parameters. A star \* indicates a bulk gel formed, but with poor or no shape-retaining ability. A waveguide profile of 'n/a' indicates no waveguide could be produced.

Total Monomer (% w/v)	Bisacrylamide (% of total monomer)	DMAM /Acrylamide (molar ratio)	Gel	Waveguide profile
10	4	DMAM Only	N	n/a
10	6	DMAM Only	N	n/a
10	8	DMAM Only	Visc.*	n/a
6	2	0.5	Y	
6	3	0.5	Y	
6	4	0.5	Y	
6	2	1	Visc*	n/a
6	3	1	Visc*	n/a
6	4	1	Y*	
8	3	1	Y	
8	4	1	Y	
8	6	1		
8	3	2	N	n/a
8	4	2	Visc*	

8	6	2	Y	
8	8	2	Y	

As can be determined from **Table 5.2**, particularly in contrast with the previous copolymer interrogated in **Table 5.1**, the polymerisation of co-DMAPMAM was found to occur at lower concentrations of total monomer, indicating more suitable integration of the copolymer into the gel. As the new polymer formulation appeared more forgiving, particularly for generating new waveguides, the decision was made to move directly on to assessing pH sensitivity curves.

The priorities for selection of the optimal waveguide were selected based on the output of the co-DMAEMA formulations 6.4 and 6.5 (see Section 5.4.1). As both the span of linear range and magnitude of pH response were shown to change with the formulation, both were taken forward as measured of the efficacy of a co-DMAEMA formulation, with sensitivity the deciding factor. A bisacrylamide content of 3% (molar fraction of total monomer) was selected and held at, in order to maintain parity between other formulations. As can be seen from **Table 5.3a**, the sensitivity ranges achieved were shifted lower than those of the former copolymer, indicating a slightly lower overall  $pK_aH$ . This is despite a higher overall  $pK_aH$  of 8.9, itself possibly due to the slightly longer pendant chain between the electronegative ether or amide unit and the dimethylamino unit. An optimal range was found around the 5 or 5.31% (w/v) polymer content.<sup>202</sup>

*Table 5.3 - Tabulated summaries of the effects of total monomer and DMAPMAM fraction upon the range of sensitivity (a) and the linear sensitivity slope over that range (b). A greener colour indicates more ideal properties, a broader range in table a and greater sensitivity in table b.*

a. Sensitivity Range (pH Units)		Polymer Content (w/v)			
		4%	5%	5.31%	6%
DMAM units per monomer	0.1	4-7	4-7	4-8	4-7
	0.15	4-7	4-8	4-8	4-7
	0.2	4-7	4-8	4-8	4-7
	0.25	4-8	4-7	4-7	4-7
	0.333	--	4-8	4-7	4-7
	0.4	--	4-8	--	--

b. Sensitivity Slope (Deg/pHU)		Polymer Content (w/v)			
		4%	5%	5.31%	6%
DMAM units per monomer	0.1	0.113	0.104	0.062	0.084
	0.15	0.133	0.090	0.092	0.099
	0.2	0.096	0.091	0.106	0.104
	0.25	0.070	0.0797	0.056	0.085
	0.333	0	0.073	-0.021	0.018
	0.4	0	0.026	0	0

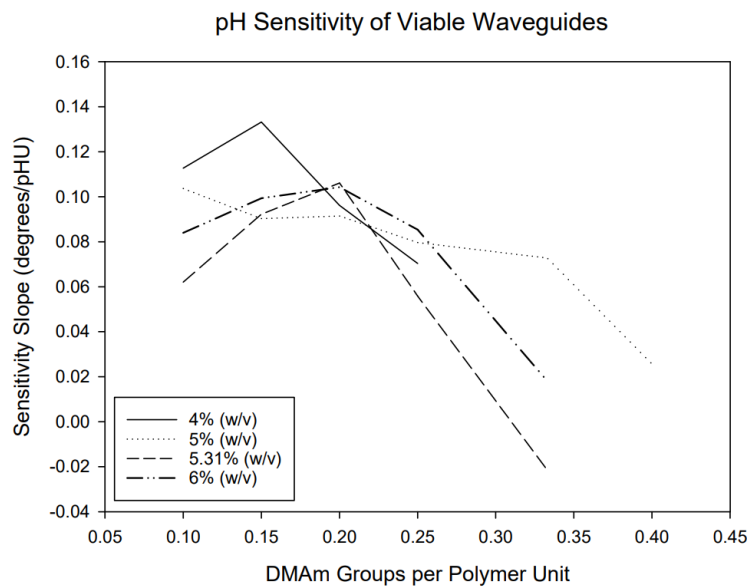


Figure 5.8 - pH sensitivity slopes for assayed co-DMAPMAM waveguides, ordered in terms of polymer backbone units per dimethyl moiety.

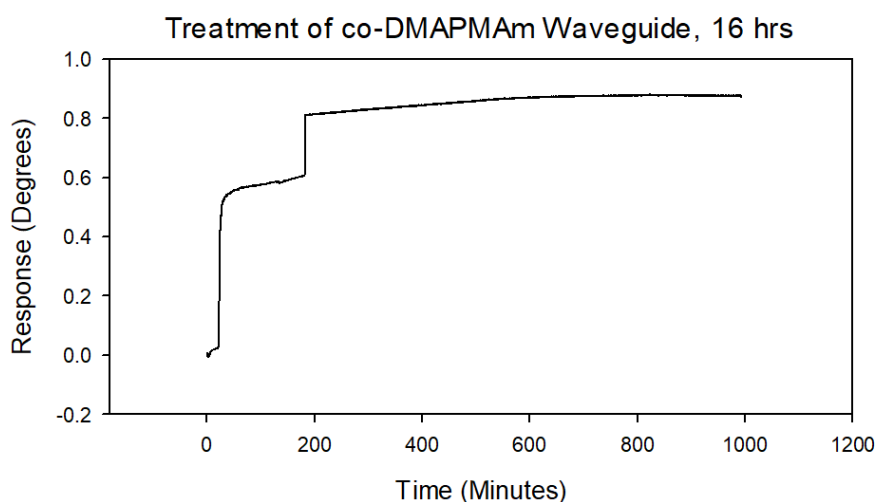
The effect of the concentration of DMAPMAM can be seen in **Table 5.3b**. The sensitivity is here provided over the range described in the table immediately preceding. The same data is

also presented more legibly as **Figure 5.8**, demonstrating trends particularly within each polymer density. As the DMAPMAM content increases, so does the sensitivity as increasing charge densities provide greater repulsion. However, at a point (typically near 0.2 dimethylamino units per monomer unit) the sensitivity falls off sharply with increasing copolymer content. This relationship is broadly related to the concentration of polymer, with the point of the drop in sensitivity occurring at lower concentrations for a less concentrated hydrogel and vice versa. As a result, this relationship is likely related to the incorporation of DMAPMAM into the polymer network, similar to the previous issues with DMAEMA but significantly less pronounced.

While the optimal density of polymer was found to lie in the general range of 5 or 5.31% (w/v) polymer content, the broadly optimal fraction of DMAPMAM was found to be 0.15 or 0.2 units per total monomer, or 5 – 6.667 monomer units per pH sensitive unit. Within this region, the best sensitivity slope detected can be found with a 5.31% (w/v) polymer, of which 0.2 of monomer units are DMAPMAM. Compared with the sensitivity slopes reported by co-DMAEMA waveguides over the pH 5-9 region, this result is lower and so less effective. In addition, the altered alters the potential further applications for the sensors – losing linear range at alkaline sensitivities may be less effective in environments of higher pH such as biosensing<sup>203, 204</sup> or some wastewater treatment processes, where abnormal pH can cause harm to important microbial species within activated sludge.<sup>7, 205</sup>

### **5.4.3.1. Longevity and Repeatability**

In order to test the viability of co-DMAPMAM sensors, a waveguide of the above optimal formulation was primed with sodium chloride solution and then remained under a recirculating running buffer for 16 hours. The results of this test can be seen in **Figure 5.9**. One caveat to this test is that due to running unsupervised for a while, imperfections arose with the testing apparatus and the formation of an air bubble was not detected in the running solution until 182 minutes in (visible as a large apparent jump in response as the air bubble is cleared and its optical distortion is removed). As can be determined, the response achieved did not fall during the course of the analysis, as would have been expected based on the behaviour of the previous sensor. The likely reason for this improvement is given in Section 5.4.3 and has already been discussed. Additionally of note, however, is the gradual rise in response which terminates after around 720 minutes (12 hours). As co-DMAPMAM waveguides are still stored dry, this may be an artefact of gradual swelling as the hydrogel fully hydrates. Superior sensitivity may in future be achievable by storing these more stable waveguides wet.



*Figure 5.9 - Extended immersion of co-DMAPMAM waveguide under pH 7 running buffer. Bubble in flow cell until approx. 180 minutes. Initial response of 0.0 degrees represents a 10 mM NaCl charging/stabilisation solution applied before the running buffer, in order to ensure proper filling of the delivery capillary tubes and flow cell before data acquisition could begin.*

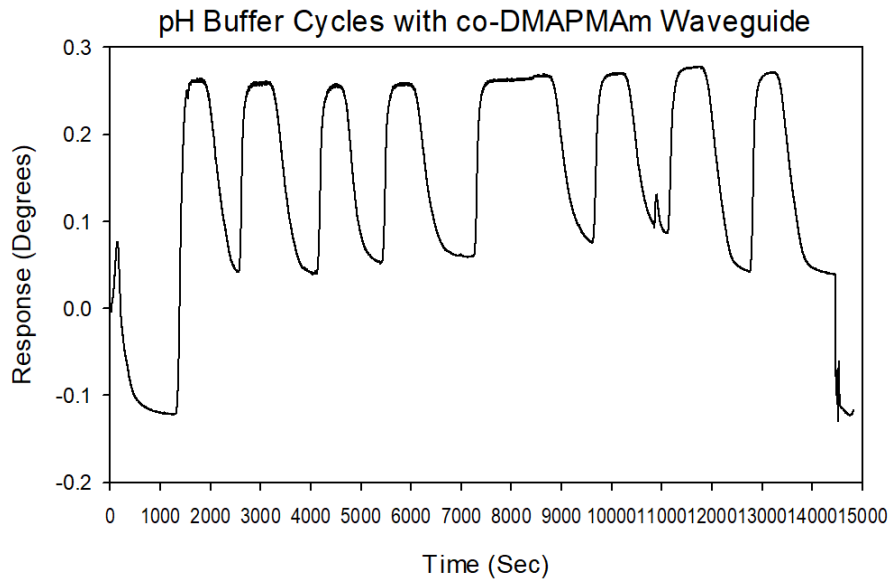


Figure 5.10 - cyclic treatment of waveguide between pH 4 and 7 running buffers, 8 repetitions. Note the reduced apparent response of repetitions 6-7. Initial response of 0.0 degrees represents a 10 mM NaCl charging/stabilisation solution applied before the running buffer, as above.

In addition, in order to ensure the repeatability of pH measurements and that no sensitivity is lost, a repeatability study was performed by cycling a waveguide through pH 4 and 7. The output of this test is shown in **Figure 5.10**. As can be shown, no significant change in response integrity was experienced, particularly in terms of returning to pH 7. There is however the issue of response time – while moving to pH 7 is generally rapid, on the order of 200 seconds or less between regions of flat response, it was found that moving to pH 4 was a much slower affair (up to 700 seconds). At certain points, notably repetitions 5 and 6, this period was not properly judged at the time of performing the experiment and so the return to pH 4 was cut short. While an automatic rather than manual buffer change system may have directly alleviated the issue it does here indicate the difference in response times. This non-symmetrical swelling and deswelling behaviour has parallels in other applications of swellable hydrogels,<sup>206</sup> and had been linked to the way compressive stresses diffuse through the hydrogel.<sup>207</sup>



### 5.4.3.2. Sensitivity with Buffer Strength

While co-DMAPMAM waveguides are not entirely superior to co-DMAEMA, they are suitable for pH sensing in buffer and appear to be resilient to prolonged immersion. However, it is important to investigate whether sensitivity is affected by the strength of the buffer used. As the ionic strength of a buffer affects the buffer's capacity to induce osmotic pressure, and correspondingly the rate and degree of swelling,<sup>206</sup> the current choice of RI-adjusted 10 mM buffers was verified by assessing the effects of non-stabilised buffers of different strengths.

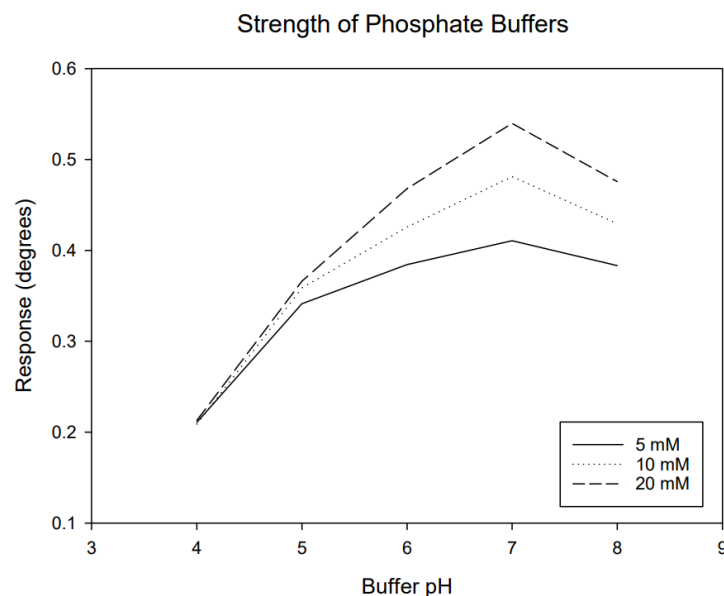


Figure 5.11 - pH response of co-DMAPMAM Waveguides at different buffer concentrations

The interrogation of waveguides by different buffer strengths (**Figure 5.11**) demonstrated a positive relationship between buffer strength and response strength. The pH sensitivity slope over the 4-7 region rises from 0.064 degrees/pHU (5 mM) to 0.088 (10 mM) and then to 0.108 (20 mM). There is no significant change in the range or pattern of response due to the shift in

buffer ionic strength, particularly the peak at pH 7 which caps the current pH response range. However, the peak response at pH 6-8 increases gradually as buffer content increases, with no significant change in response is detected at pH 5 or below. As the buffer strength increases, the response curve in the pH 5-7 region also approaches a linear relationship. As to why, it may be possible that an increasing buffer strength provides greater availability of protons shed by phosphoric acid, allowing formation of  $-N(CH_3)_2H^+$  groups that ordinarily would need to scavenge  $H^+$ . As buffer strength increases, so too does the degree of protonation. This increased availability has little effect below approx. pH 6, as few enough dimethylamino groups are protonated that dilute buffer (or even water) can meet this demand. However, changes in osmotic pressure may have its own effect and will be analysed separately, below.

Comparing the co-DMAPMAM waveguides with data received from co-DMAEMA waveguides (**Figure 5.4**), it can be seen that an apparent inversion of response has occurred. While the latter gel demonstrated a properly cationic character, deswelling with increasing proton scarcity, the co-DMAPMAM waveguides appear to be anionic in nature. Unfortunately at this late stage of the project all effort was devoted to generating a working pH-sensitive sensor in favour of making proper investigations – this was in retrospect a significant error. Future research into pH-responsive leaky waveguides must include some analysis of this unexpected behaviour. For the time being, however, experiments were performed investigating the resilience of the current single-layer sensor to expected interferants.

#### **5.4.4. Effects of Interferants**

In order to test the best-result waveguide in conditions more in line with real samples, a shortlist of probable interferants was selected for testing. **Sodium chloride** was selected to demonstrate the effects of salinity, but also to identify the possible impact of osmotic pressure on the waveguide's behaviour. **Calcium chloride** was selected as a proxy for water hardness, as efforts to produce a  $\text{CaCO}_3$  solution free from other salts and suitable for pH stabilisation were not successful in the time available. Particularly, carbonate addition would offer the possibility of examining how the sensor behaves in the presence of divalent cations (as chlorides and phosphates show the effects of mono- and trivalent anions). **Aluminium sulphate** was selected due to its role as a coagulant in the clarification stage of water treatment,<sup>208</sup> but also as a means of testing for the effects of the divalent  $\text{SO}_4^{2-}$  anion, which may have a binding effect of co-DMAPMAm (see the comparative examination of buffers in Chapter 5). **Urea** was selected as a relatively simple marker for human waste, to be expected in municipal wastewater but also on occasion in sites such as swimming pools. **Sodium hypochlorite** (or hypochlorous acid) was selected as a source of free chlorine, present in potable and waste water and necessary for suppressing pathogens as described in Chapter 1. Finally, a generic form of **humic acid** was selected as a general marker for soil contamination, present in natural water courses and any other water source that comes into contact with the natural environment.

As some of the selected materials are acidic or have a buffering capacity of their own, they each were made up in a 10 mM solution of pH 7.0 phosphate buffer to eliminate these effects.

The outcomes of the interferant studies, demonstrated in **Figure 5.12**, were as follows.

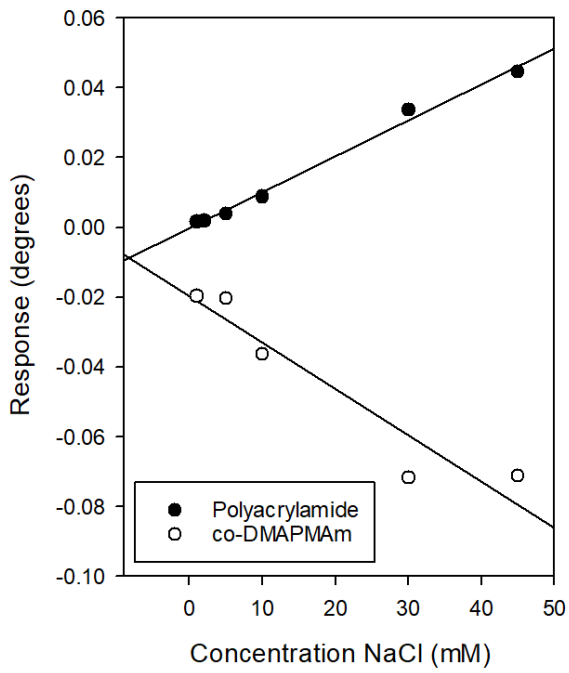
Exposure of the waveguide to sodium chloride (**Figure 5.12a**) provided a modest negative trend in response, at  $-1.3 \times 10^{-3}$  degrees  $\text{mg}^{-1} \text{L}^{-1}$ . This trend is however not represented in PAAm,

where a positive shift of  $1.0 \times 10^{-3}$  degrees  $\text{mg}^{-1} \text{L}^{-1}$  was found due to the effects of RI, and is not related to the solution refractive index. This negative trend is attributable to charge screening by the increasing proportion of ions in solution, able to dampen electrostatic forces between polymer strands.<sup>209</sup> Regarding urban wastewater, high salinities can be caused by the use of seawater for toilet flushing in marine areas, the utilization of salt for outdoor snow-melting strategies, or by entrance of marine water in the sewage systems in coastal or island areas.<sup>210</sup> High-salinity wastewater falls in the 20-50 g/L range<sup>211, 212</sup> which lies considerably above the range measured here, however this may be considered an opportunity for further analysis if necessary. At these concentrations, a considerable response in the range -0.44 to -1.11 degrees may be expected – enough to overtake any and all pH response.

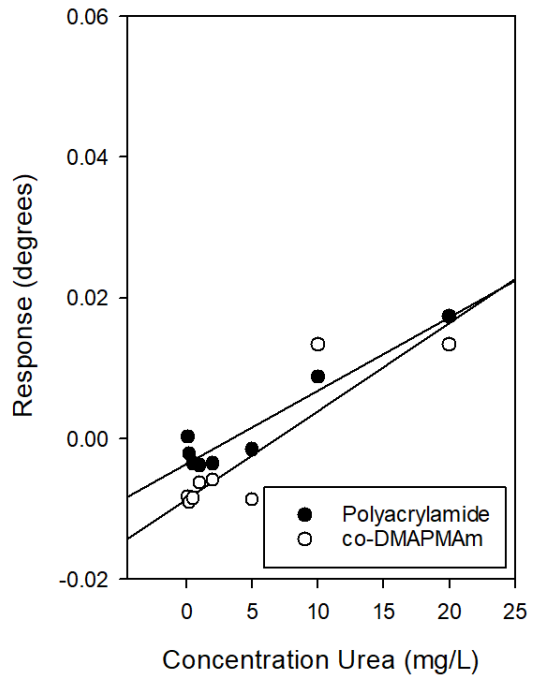
For the addition of urea (**Figure 5.12b**), a response gradient of  $1.3 \times 10^{-3}$  degrees  $\text{mg}^{-1} \text{L}^{-1}$  is found, commensurate with the refractive index increase of the buffered interferent solutions and not significantly different from that of cast polyacrylamide at  $1.04 \times 10^{-3}$  degrees  $\text{mg}^{-1} \text{L}^{-1}$ . As urea has zwitterionic character and may readily act as a hydrogen bond acceptor,<sup>213</sup> it may be expected that urea would interfere with the gel swelling capacity by screening or propagating charges from the dimethylamino pendant groups. However, while urea addition has in the past been shown to increase the water retention of an acrylic acid copolymer, it was considered to do so by forming salts with the acrylic acid groups and so altering the pH responsivity of the system.<sup>214</sup> In another study it was found that up to 20 mmol Urea had almost no effect on the swelling capacity of a carboxyl-bearing polymer,<sup>215</sup> and urea ammonium chloride was found to leach at similar rates from cationic and anionic polymers.<sup>216</sup> As a result, and from a lack of permanent shift in resonance line position after the urea treatment (see humic acid, below) it

can be gathered that no significant interactions occur and the polymer is therefore largely indifferent to urea contamination.

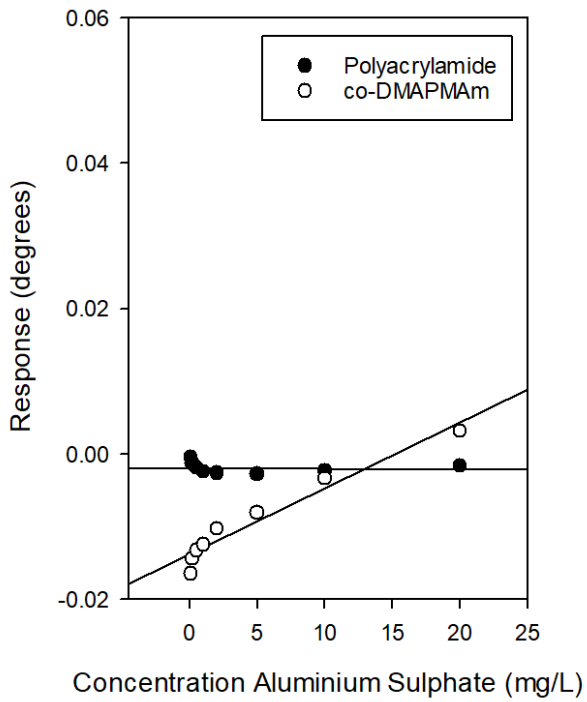
a. Sodium Chloride



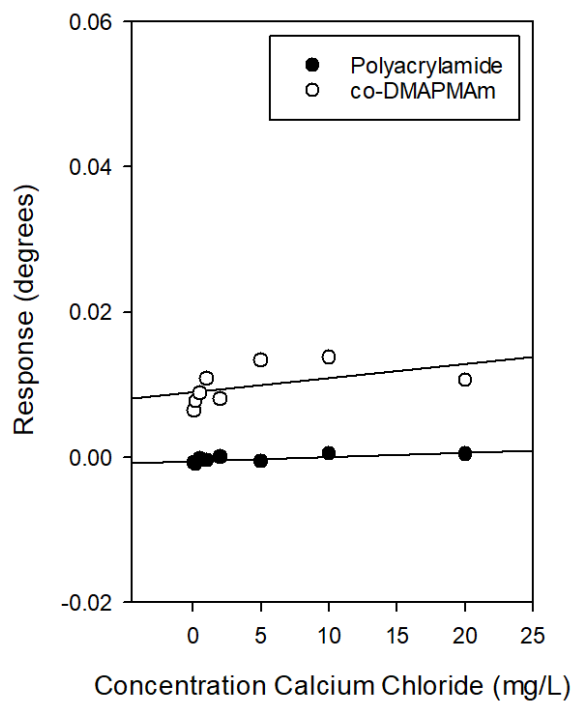
b. Urea



c. Aluminium Sulphate



d. Calcium Chloride



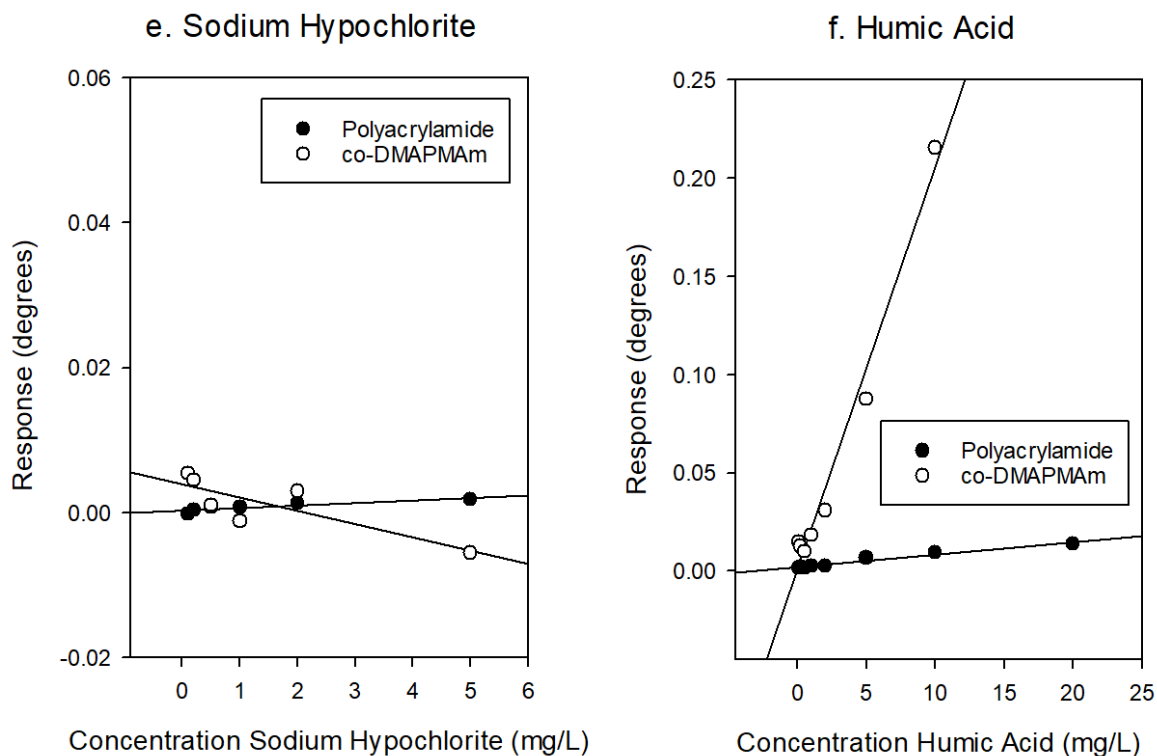


Figure 5.12 - Selected interferant studies performed upon cast co-DMAPMAM waveguides. Black dot indicates reference material (cast polyacrylamide) ran in parallel.

Aluminium sulphate exposure occurred under similar conditions. a positive shift of  $0.91 \times 10^{-3}$  degrees  $\text{mg}^{-1} \text{L}^{-1}$  is found, as seen in **Figure 5.12c**, also in line with the refractive index increase of the buffered interferents themselves. Divalent cations have a greater inhibitory effect on polyanionic polymer swelling than monovalent cations, as they are able to interact with multiple charge sites and tie them together<sup>215</sup>, which would result in a negative response pattern as the waveguide's pores are reversibly bound together by the sulphate ions, much as was detected with phosphate buffer interrogation of chitosan films (Chapter 5). In addition, aluminium sulphate is used as a coagulant alongside polyacrylamide or anionic polyacrylamide flocculant, neutralizing colloidal electrostatic charges and so allowing the aggregation of microparticles into larger microflocs that may be bound together by adsorption onto the long polyacrylamide chain.<sup>208</sup> In the case of aluminium sulphate as-is, no such interaction occurs for the polymer,

much as for linear polyacrylamide. This is likely due to the lack of colloidal material to coagulate in the first place, and may not be the case should this sensor be used on (or immediately before) the clarification stage of wastewater treatment.<sup>217</sup> Overall, the waveguide appears to suffer no significant interactions with aluminium sulphate coagulant.

Calcium chloride exposure (**Figure 5.12d**) resulted in little-no response detected. A small increase in response was detected, occurring over less than 0.01 degrees and equating to only 8 pixels in raw collected data, dwarfed entirely by the expected effect of refractive index alone. Di- or multivalent metal ions such as calcium typically interact with acidic chelating groups, rather than the dimethylamino groups available, so little specific interactions may be expected.<sup>218</sup> That the polyacrylamide and calcium chloride sensor response is equally minimal may indicate a common cause – however due to unexpected time constraints at the end of the project there was no opportunity to investigate further.

Exposure to free chlorine, here in the form of hypochlorous acid, provided a negative response trend not followed by that of the polyacrylamide sensors (**Figure 5.12e**). As the state of hypochlorous acid in water is quite complex and contains a number of both neutral and negatively charged species, terminating in release of chlorine gas or  $\text{ClO}_3^-$  chlorate ions,<sup>219</sup> a thorough understanding of the relationship between free amine content and sensor response would require a more in-depth analysis given any of the available ions present. However, by comparison with the negative response trend of sodium chloride, a similar decrease of  $-1.8 \times 10^{-3}$  degrees  $\text{mg}^{-1} \text{L}^{-1}$  was provided. In the absence of more complex relationships between co-DMAPMAM hydrogel and the hypochlorous acid system at neutral pH, which would bear



further investigation on its own terms, it appears that the monovalent negatively charged species present behaved similarly to monovalent charges of chloride ions.

Uniquely among the interferants tested and as shown in **Figure 5.12f**, humic acid (**Figure 5.13**) exposure provided a strong positive response, significantly greater than for any other interferant, and significantly outsize the response of an appropriate polyacrylamide leaky waveguide. Of particular note is the pattern found at higher values, particularly after 10 mM, at which the pH sensitivity rose considerably the longer the humic acid solution was passed over the sensor. After this point, the sensor does not return to baseline upon washing with pH 7 buffer or sodium chloride. By visual observation (**Figure 5.14**), it can be seen that the waveguide is discoloured over the area encapsulated by the flow cell, even after extensive washing. It can therefore be inferred that humic acid, part of a family of acid dyes, is capable of binding to the dimethylamino pendant groups and incorporating itself into the hydrogel to create a dye-doped leaky waveguide (DDLW). The permanent 'increase' in response represents both the increased refractive index of the additionally-decorated waveguide environment, and the absorbing effects of the dye. The presence of this binding capacity holds some negative connotations for the sensor's lifetime in the natural environment such as rivers, where humic acids may leach into waterways from the soil, but also downstream of industrial processes where remnant dyes or similar molecules may be released.

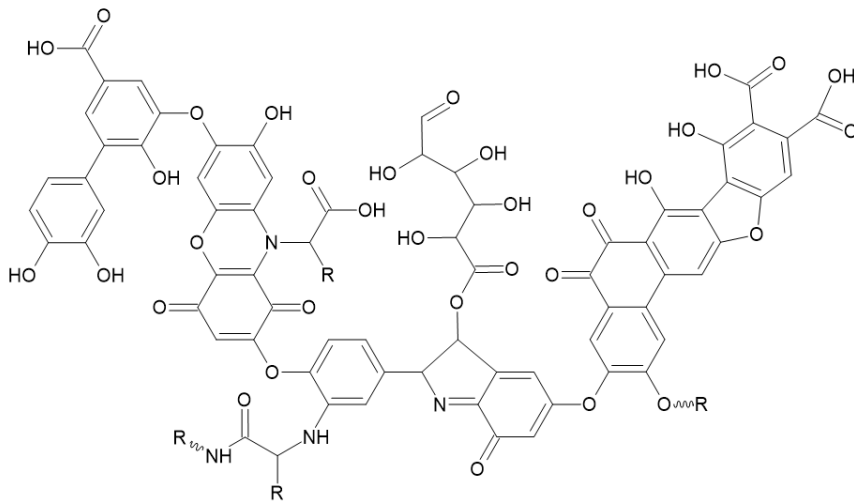


Figure 5.13 - Base structure of humic acids, a form of biomolecule associated with soils and tree roots. Note the proliferation of carboxylic groups.

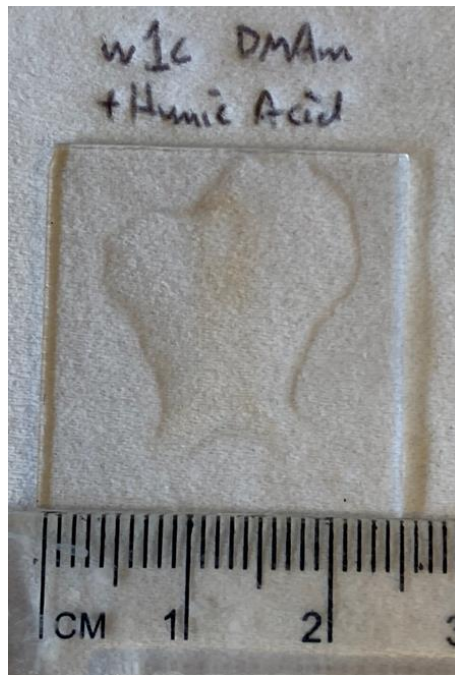


Figure 5.14 - Waveguide after humic acid treatment. Brown discoloration most visible at original location of flow cell inlet, upper centre of image.

## 5.5. Summary

In this chapter, the viability of a pH-sensitive sensor of synthetic origin was confirmed and the dimethylamino functional group was shown to be a suitable component upon which to base the sensor's efficacy. Copolymer hydrogels of *N,N*-(dimethylamino)ethyl methacrylate and *N,N*-(dimethylamino)propyl methacrylamide were assayed and optimised for pH response and their longevity in the short (day-scale) term assessed. The more stable sensor was then tested with a selection of interferants and the suitability of the sensor for in situ pH monitoring in some manner addressed.

It should be noted that while the synthetic waveguide manufactured from co-DMAPMAM is effective, it is far from the most sensitive or broad-ranged sensor demonstrated in this document. Chitosan (Chapter 4) achieved a greater pH sensitivity curve at 0.365 degrees/pHU, compared with the sensitivity of the selected DMAPMAM gel at 0.091 degrees/pHU, and did so over a linear range that typically extended further into the weak alkaline region than dimethylamino gels have been demonstrated to achieve. Further work for this chapter would therefore emphasise additional optimisation passes of the pH-sensitive waveguide, or alternatively selecting (and as necessary synthesising) additional dimethylamino-bearing polymers which may achieve a superior performance. The following chapter will progress with the formulation of co-DMAPMAM waveguides demonstrated above.

## **Chapter 6. AN INTERNALLY REFERENCED SYNTHETIC LEAKY WAVEGUIDE**

### **6.1. Introduction**

A synthetic waveguide material has, in Chapter 5, been selected. While a leaky waveguide using both pH-responsive and -inert synthetic materials has been demonstrated, however, an internally referenced sensor has yet to be manufactured. The feasibility of manufacturing a pH-responsive internally referenced sensor had also been demonstrated in Chapter 5. This chapter will therefore address the combination of copolymer gels of *N,N*-(dimethylamino)propyl methacrylamide (DMAPMAm) with an acrylamide reference gel to fabricate the stacked sensor. As per previous chapters, Sections 6.2 and 6.3 provide the methods, materials, and procedures used in this chapter. Section 6.4.1 discusses the manufacture and optimisation of the spincoated co-DPAPMAm-polyacrylamide stacked leaky waveguide. The pH sensitivity of the stacked sensor and its properties at neutral pH, the upper terminus of its sensitivity curve, are investigated in Section 6.4.2. The utility of the internal referencing scheme is briefly demonstrated in Section 6.4.3 with the capacity of the sensor to subtract refractive index changes from pH response. Finally, Section 6.4.4 discusses the effect of selected interferents examined in Chapter 6 upon the stacked sensor, relative to each waveguide layer alone.

## **6.2. Materials**

### **6.2.1. Chemicals and Materials**

Acrylamide 40% (w/v), N,N-methylene bisacrylamide (bisacrylamide) 2% (w/v) and premixed acrylamide/bisacrylamide blends for gel electrophoresis (40% w/v) were procured from Sigma Aldrich (UK). Also from the same supplier were mono- and dibasic sodium phosphate.

Decon 90 and sodium chloride were procured from Fisher Scientific (UK).

Phosphoric acid, trisodium phosphate, aluminium sulphate and humic acid were procured from Acros Organics (UK).

(N-dimethylamino)propyl methacrylamide (DMAPMAm) was procured from ABCR (Germany).

Chloro(dimethylvinyl)silane (CDVMS) was purchased from TCI Chemicals (UK).

Glass microscope slides (to standard ISO 8037/1) and sodium hypochlorite ~14% were purchased from VWR (UK).

### **6.2.2. Instrumentation**

The majority of analysis occurred using a waveguide apparatus, described in Chapter 3. A flow rate of 1.50 ml/min was used throughout. Solution refractive indices were found using a Bellingham Stanley RFM970-T refractometer, the specifications of which are given in Chapter

4. Likewise, the pH of running buffers and other test solutions was found using a Hanna HI 2210 benchtop electrochemical pH meter previously discussed.

## **6.3. Experimental Procedure**

### **6.3.1. Polymer Casting**

For fabrication of cast polyacrylamide, 875  $\mu\text{l}$  of deionised water degassed with nitrogen is added to 125  $\mu\text{l}$  of acrylamide/bis(acrylamide) 29:1 solution (40% w/v) To this solution is added 1.25  $\mu\text{l}$  of TEMED and finally 12.5  $\mu\text{l}$  of APS (10% v/w in deionised water) which initiates free-radical polymerisation. The prepolymer is then immediately vortexed and a 100  $\mu\text{l}$  aliquot is deposited in the centre of a CDMVS-treated glass slide. A clean glass slide with appropriate spacer is placed above, followed by a 500 g brass weight. The solution is permitted to gel within the cast until the remaining (non-aliquot) solution is gelled and invertible. Finally, the cast is immersed in deionised water for at least 2 hours before gently prying apart and is stored dry until required.

For fabrication of cast copolymer, a similar overall method is used, however the alternative recipe is applied. Due to the need to tune crosslinker content, an aqueous solution of bisacrylamide (2% w/v) as well as a separate stock of acrylamide (40% w/v). Prepolymer components are added in the following order: comonomer (as appropriate), bisacrylamide, acrylamide, DI water, TEMED, APS. This film production is as per above, however all films were incubated dry at 25° overnight (approx. 16 hours) before use. All films were stored dry and were washed with deionised water before and after use.

Where gelation did not occur to a prepolymer solution, the solution is charged with additional acrylamide/bis(acrylamide) 29:1 solution before addition of additional APS/TEMED initiators to force the consumption of potentially hazardous monomers, and subsequently disposed of safely.

In order to deposit polyacrylamide onto the cast gel, a method similar to that used in Chapter 4 was employed. Briefly, the cast waveguide serving as the lower layer was immersed in deionised water for approx. 5 minutes, and then all excess water was wicked away by placing an absorbent material to the edge of the slide. The polymer solution is prepared by dissolving linear polyacrylamide into 100 mM acetic acid to 4% (w/v), and an aliquot of 99.5  $\mu$ l polymer is taken. To this is added 0.5  $\mu$ l of 5% (v/v) glutaraldehyde crosslinker, and the polymer solution is vortexed briefly before addition onto the cast waveguide. Finally, the solution is carefully spread across the waveguide surface with the flat of a pipette tip, and then spin-coated for 60 seconds at an acceleration speed of 100 rpm/sec. The spin speeds assessed are provided in their context in **Table 6.1** (below).

### **6.3.2. Sample Preparation**

Running solutions were produced using a phosphate salt system (phosphoric acid, sodium dihydrogen phosphate, disodium hydrogen phosphate, sodium phosphate). Stock solutions were made to a target concentration of 100 mM, then running solutions made from a 10 mM solution of each. As the ionic strength of a buffer is proportional to its refractive index, the RI of the

running solutions was measured and then adjusted to 1.33314 before use. Where buffer concentration was being investigated, this dilution was not performed.

Where interferent solutions were tested, solutions were made at 0.1, 0.2, 0.5, 1, 2, 5, 10 and 20 mg/L solutions. Sodium hypochlorite (again used as a source of hypochlorous acid) disregarded the 10 and 20 mg/L solutions, as rising above 5 mg/L indicates overchlorination and so the intended use cases would have other problems. Sodium chloride solutions were made to concentrations of 1, 5, 10, 30 and 45 mM free chlorine content. In order to eliminate the effects of acidity or alkalinity, which were found to have significant independent effects on the waveguide response, all solutions were brought up to 10 mM of pH 7 phosphate buffer in addition to their intended chemical content.

Waveguides are stored dry by default, following experiences with polysaccharide slides, and were kept in the dark unless the immediate batch was in use. Likewise, running solutions and buffers were stored in a cool dark place unless expected to be used. Buffers around neutral pH were examined monthly for microbial growth, and were disposed of and replaced if any evidence of contamination was found. For some experiments regarding leaching-out of material, a number of waveguides were stored under deionised water. These samples were maintained safely in a cupboard, as above, and were gently air-dried prior to use.

## **6.4. Results and Discussion**

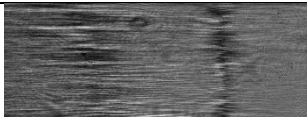
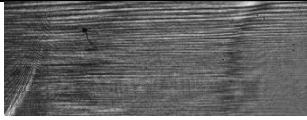



In Chapter 5, a synthetic cast waveguide suitable for pH sensing, based on dimethylamino groups was proposed and explored. A copolymer of (dimethylamino)ethyl methacrylamide (co-DMAPMAM) was selected as the ionisable component. Below is described the development of a stacked leaky waveguide sensor using this material as a base. Section 6.4.1 and 6.4.2 describes the fabrication process and pH sensitivity assays, respectively. Section 6.4.3 will present and discuss the utility of the reference layer in pH sensitivity assays. Finally, Section 6.4.4 will examine the interferant studies performed on the stacked waveguide in the context of both the single-layer and cast polyacrylamide waveguides presented in Chapter 5.

### **6.4.1. Stacked co-DMAPMAM Waveguide Fabrication**

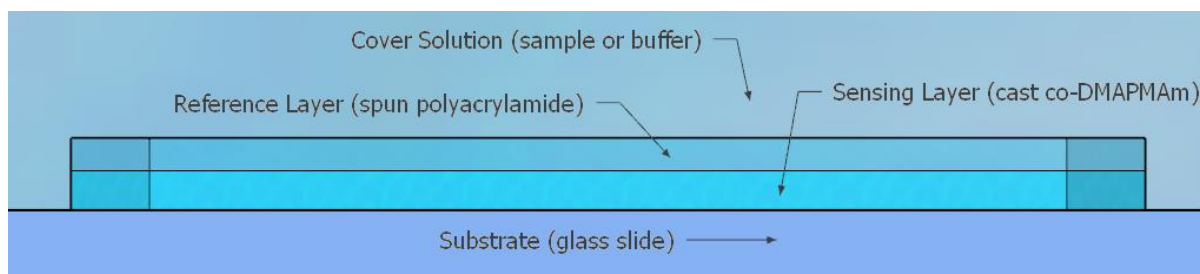
Due to time pressure, an alternative to the relatively time-consuming pH-sensitive linear polymer process (explored in Chapter 3) was sought. In place of developing a linear polymer to spin onto cast polyacrylamide, a cast co-DMAPMAM waveguide was to be used as the cast layer of known characteristics while an acrylamide homopolymer is spin-coated above. This modified process, while novel for stacked sensors within this thesis, does not differ from the methodologies previously demonstrated. The linear homopolymer was developed as per the description given in Chapter 3, and the cast co-DMAPMAM gel was made to the formulation described in Chapter 5.

Table 6.1 - Spin characteristics of PAAm reference layer for stacked co-DMAPMAm waveguides. Sample agarose-chitosan waveguide provided as an image comparison.

Linear Polymer Content (w/v)	Glutaraldehyde Content (ppm)	Spin Speed (rpm)	Output
4%	250	3000	n/a
4%	250	4000	
4%	250	5000	
Agarose + Chitosan (for comparison)	--	--	

While the general conditions for cast polyacrylamide were used as per production of spun polyacrylamide alone (see Chapter 3), some optimisation was still required. As a number of variables were available, it was decided to keep to spin-coater rotation speed alone unless other changes or properties were required. As **Table 6.1** shows, three speeds known to provide effective PAAm waveguides were chosen and evaluated. 4000 and 5000 rpm provided waveguides suitable for further study, however the slower and therefore thicker 3000 rpm films did not. In the latter case, the image was very confused and neither mode could effectively be monitored. **Figure 6.2** (below) confirms that the broader and messier resonance line closer to the TIR is that of the PAAm layer, while the finer resonance line with remnants of a pale fringe is that of the co-DMAPMAm cast gel. Comparison can also be drawn with chitosan layered onto agarose, for which a sample image has been appended onto **Table 6.1** for ease of reference.

The decision to place the sensing layer below of reference layer may have aided the effectiveness of the sensor in one regard – the PAAm gel, while containing smaller pores than cast gels or crosslinked polysaccharides as shown by porosity tests in Chapter 4, is of a lower density by weight (4% w/v) than that of the co-DMAPMAm gel (5.31% w/v) and so should be the rarer formulation. (Unfortunately, due to the not inconsiderable toxicity of acrylamide monomer and the lack of suitable refractometry equipment for thin hydrogel films, this was not verified). Therefore, as shown in **Figure 6.1** Error! Reference source not found., a rarer upper layer may not interfere with the ability of the lower layer to contain a leaky mode. However, this may create issues with effective correction or isolation from interferents, as the reference layer is not independently reported.



*Figure 6.1 - The layout of the DMAm-PAAm stacked leaky waveguide as tested in this chapter.*

It is hoped that due to the previously demonstrated role of polyacrylamide as an unproblematic and relatively resilient material for sensor waveguides, it can still be used to extract nonspecific interactions or responses from the solutions at large. In addition, as the crosslinked linear polyacrylamide is less porous, it is expected that large molecules such as proteins that may interact with the polycationic cast gel will be unable to penetrate through the less porous and

inert spun polyacrylamide layer. However, the role of spun polyacrylamide as a guard gel was not explored due to further time constraints.

## 6.4.2. pH Sensitivity of Stacked Sensor

With the stacked waveguide manufactured, an assay of pH sensitivity was performed, using a methodology identical to that used in Chapter 5. Initially, a pH sensitivity test was performed as per the method used in previous chapters. As can be noted from **Figure 6.2** and was mentioned in Section 6.4.1 above, the nearer mode to the TIR showed minimal signs of pH sensitivity, similar to polyacrylamide, while the further mode from the TIR behaved similarly to single-layer co-DMAPMAM waveguides – this confirms the main action of the two respective modes.

A range of pH 4-7 was found, similar to that of the single-layer co-DMAPMAM waveguide in both apparent position and terminus of the sensitivity slope at around pH 7. Likewise, the intensity of the achieved curve is similar, at 0.091 degrees/RIU. These factors are in contrast to the properties of polysaccharide copolymers (Chapter 4), where pH sensitivity range broadened with inclusion of polyacrylamide or agarose. This may be due to the reference layer now being buried under the sensing layer, unlike agarose-chitosan or polyacrylamide-chitosan stacked waveguides. Some very small drift in the reference layer's pH response can also be seen. However as the reference mode is not moving with or in counterpoint to the sensing layer, it is unlikely to be evidence of incomplete segregation of modes in their respective layers.

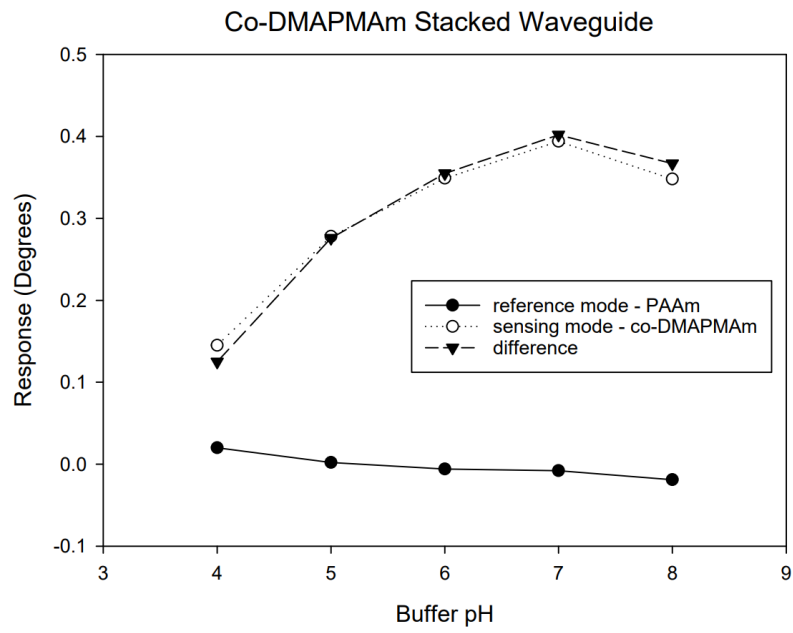


Figure 6.2 - pH sensitivity curve of internally referenced co-DMAPMAm waveguide

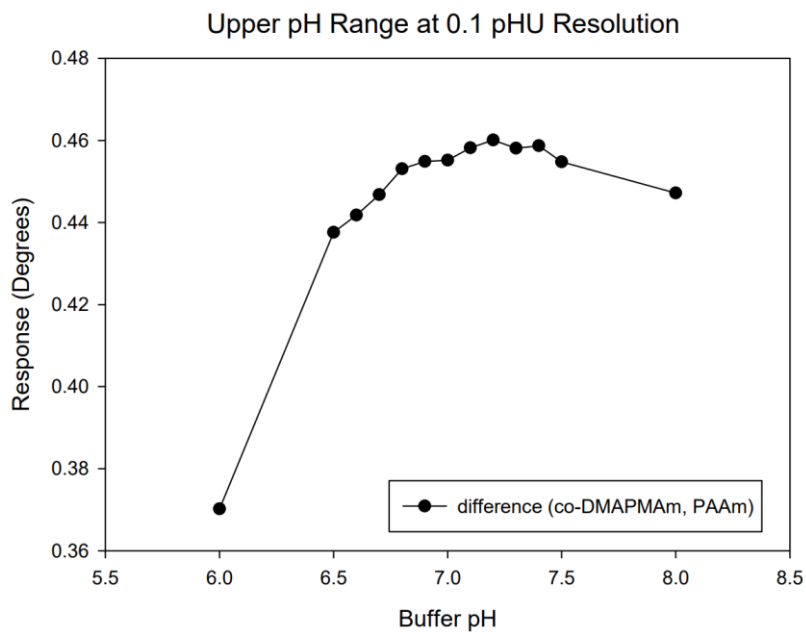


Figure 6.3 - pH sensitivity curve of waveguide at the pH 6.5-7.5 region

While it had been previously established in Chapter 5 that the upper limit of the pH sensitivity curve is stable with regards the strength of the buffer used, it is worth investigating what occurs around this point in finer detail. For this purpose, phosphate buffers of strength 10 mM and pH 6.5-7.5 were produced at 0.1 pH intervals and the corrected response of a stacked waveguide assessed. The result can be seen in **Figure 6.3**. The maximum (and subsequent falling-away) of resonance line shift can be seen at around pH 7.2, however at these smaller response intervals, small differences such as measurement uncertainties in buffer generation are more prominent. The visible error bars of 1 standard deviation are experimentally derived and cast some doubt on the utility of the finer-grade sensitivity of the sensor. A transition from pH-mediated increase in response to the gradual swelling reduction caused by osmotic pressure may also be seen as the pH increases. The tailing-off in response indicates that in the pH 6.5-7.4 region both phenomena are in play simultaneously, causing the tailing-off of pH sensitivity as seen.

One factor that emerged during analysis of stacked waveguides is the presence of small shifts in the reference layer that follow or contrast the response pattern of the sensing layer. **Figure 6.2** shows little to no response, however **Figure 6.4** (below) demonstrates a trend in counterpoint to the sensing layer. As of writing we have no experimental means of interrogating this behaviour. However, it is suspected that one of two factors may be in play. First, the linear polymer of the reference layer is partially interpenetrating into the sensing layer during the crosslinking process. Alternatively, the leaky mode contained in the reference layer extends partially into the sensing layer, indicating incomplete capture of the reference mode in the polyacrylamide homopolymer gel.

### 6.4.3. Internal Referencing and Eliminating RI Interference

While the components necessary for an internally referenced sensor have been assembled and pH sensitivity demonstrated, it has yet to be proven that the polyacrylamide layer is an effective tool for elimination of nonspecific sensor response. To address this, a small number of sensors were introduced to a phosphate buffer range including two buffers doped with 1% (v/v) glycerol.

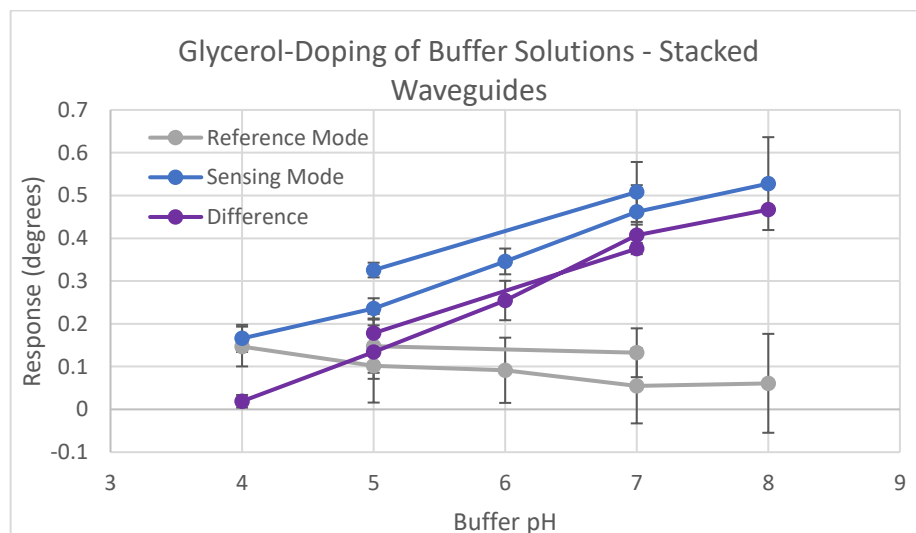


Figure 6.4 - effect of glycerol-doping pH buffers for co-DMAPMAM stacked waveguides

The change in response caused by the glycerol doped buffers was assessed by direct comparison with non-doped buffers. **Figure 6.4** shows the effects of RI interference on the reference and sensing modes. The increase of around 0.06 degrees in the polyacrylamide layer and 0.07 degrees in the cast co-DMAPMAM layer are comparable to the refractive index shift actually recorded in the buffers, indicating suitable functionality. Subtracting the reference mode from

the sensing mode gives a similar outcome to that of the non-doped buffers, within 1 standard deviation of one another, and from the mean RI shifts accounts for all but 9.7% of the difference between doped and undoped buffers. With a suitable RI correction system, the effects of nonspecific interaction can be eliminated from the sensor's response, improving confidence in the data it provides.

However, there is a small gradient in the apparent RI sensitivity of the cast co-DMAPMAm layer which is not reflected in the PAAm layer, falling from a 0.09 degree shift to 0.05, and accounting for much of the deviation from the non-doped buffers after reference correction. This is unexpected - as the gel deswells in alkaline media it should be able to admit a lower total amount of glycerol-doped buffer inside, however the volume fraction of glycerol per the waveguide interior would not be expected to change with it. Future experiments to investigate this effect would have been advantageous.

#### **6.4.4. Chemical Interferants**

The selection of interferent was described in greater detail in Chapter 5, and the same chemical interferents were selected for analysis of internally referenced sensors to provide a greater understanding of the sensing regime in general. Briefly, sodium chloride as a measure of salinity and of inducing osmotic pressure on the waveguide, calcium chloride as a proxy for water hardness, aluminium sulphate to represent chemical coagulants in water treatment as well as to introduce the divalent sulphate anion, urea as a marker for municipal wastewater, and humic acid as a measure for soils or plant infiltration into the water.



Due to setbacks plus time constraints limiting the opportunity to examine chlorine sensitivity (see Chapter 7 for further details), sodium hypochlorite was deemed less important a variable to examine at this stage and so was substituted for additional replicates of other tests. For the sake of easy reference between single-layer and stacked waveguides, data from **Figure 5.12** has been replicated along with the appropriate data from stacked waveguides.

With sodium chloride (**Figure 6.5**), a negative response found in both co-DMAPMAm layer and the reference-corrected data, albeit a gentler pattern with a slope of 1.98 and 1.93 mDegrees/mM respectively. A particularly strong sensing mode response can be seen compared with the single-layer gel, particularly at low concentrations where the resonance line shift would be expected to track closer to that of pH 7 buffer (meaning a relative response closer to 0.0 degrees at almost 0 mM NaCl). Without this lower concentration, and particularly when looking at the reference-corrected values, NaCl of the stacked waveguide mirrors that of the single-layer waveguide. This may be an artifact of the phosphate buffer used, and a gradual change in dominant ion due to the introduction of NaCl to the buffered solution.

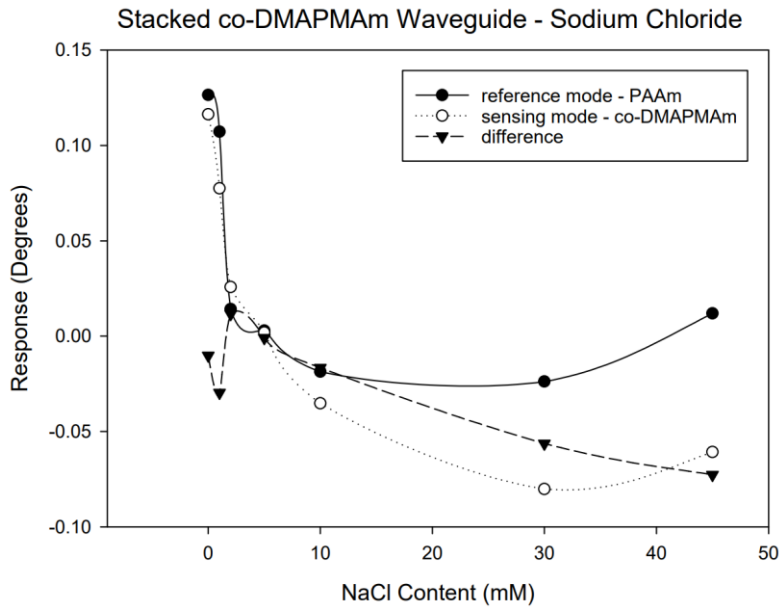


Figure 6.5 - Sodium chloride interferent studies performed on (a) internally referenced and (b) separate single-layer leaky waveguides.

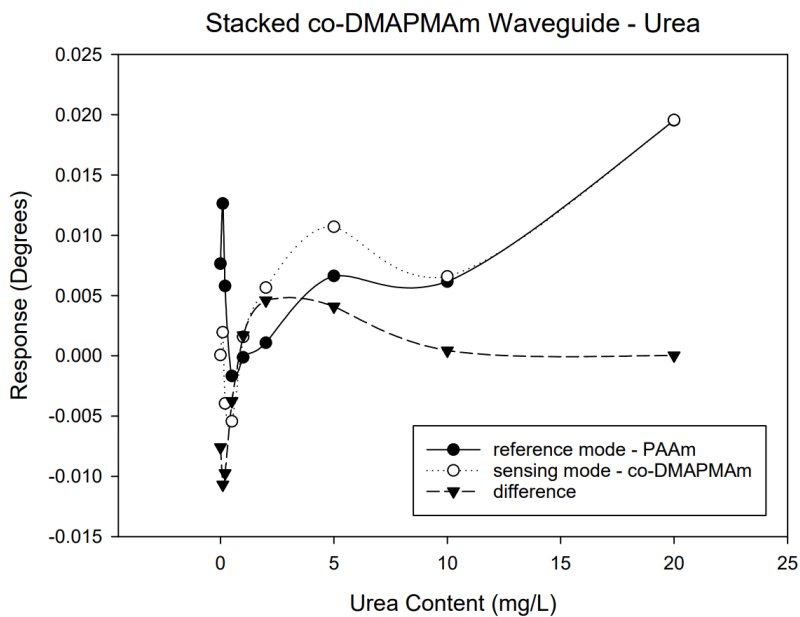


Figure 6.6 - Urea interferent studies performed on (a) internally referenced and (b) separate single-layer leaky waveguides.

The urea response of the stacked waveguide (**Figure 6.6**) is more conventional, and the response of both sensing and reference modes mirrors that of the single-layer and reference waveguides. As the urea concentration rises, the response of each mode also rises. The

reference-corrected response slope is therefore minimal at 0.3 mDegrees/mM, indicating no special property of response is occurring other than nonspecific refractive index effects. The small difference between reference and sensing modes demonstrates a suitable ability to eliminate urea contamination from pH data.

Aluminium sulphate response on single-layer waveguides had been minimal, with a very small positive trend on co-DMAPMAM that may prove difficult to differentiate from sources of instrumental or measurement error (**Figure 6.7**). On the stacked leaky waveguide, little to no response can be discerned in either reference or sensing layers. Needless to say, the reference-corrected trend is flat and so any potential aluminium sulphate contamination may be considered eliminated should any be detected in future.

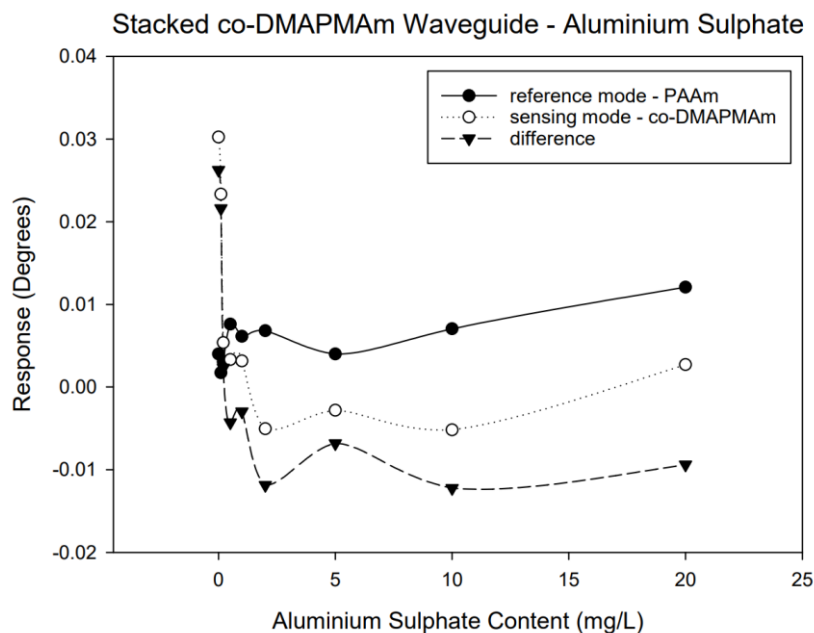


Figure 6.7 - Aluminium sulphate interferent studies performed on (a) internally referenced and (b) separate single-layer leaky waveguides.

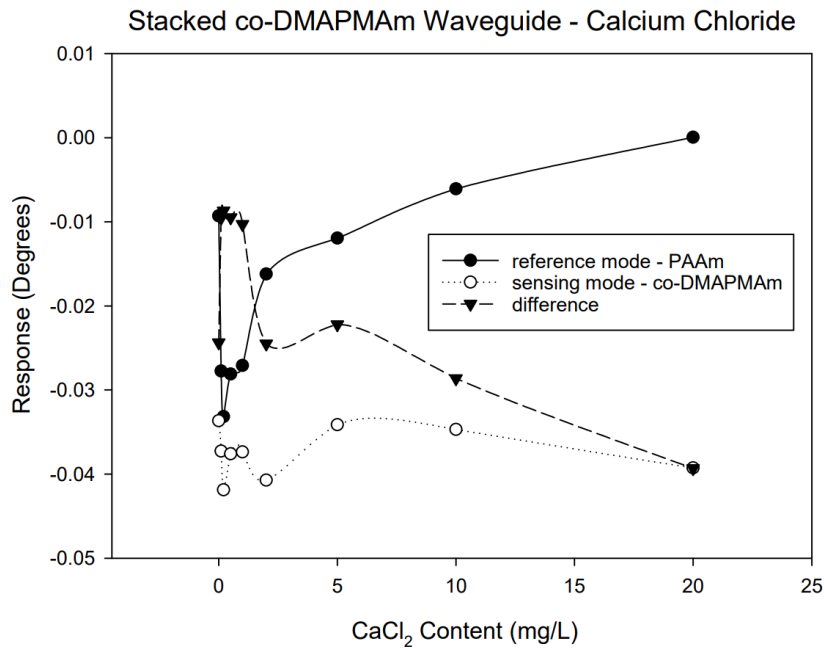


Figure 6.8 - Calcium chloride interferent studies performed on (a) internally referenced and (b) separate single-layer leaky waveguides.

The calcium chloride sensitivity of the stacked waveguide (**Figure 6.8**) deviates from the results of the single-layer tests. A small positive trend of 0.13 mDegrees/mM from the reference layer and small negative trend of 0.17 mDegrees/mM from the sensing layer can be seen instead. The former is particularly interesting when compared with the response from cast polyacrylamide, which is effectively zero. The trends apparent from the stacked leaky waveguide with calcium chloride are in fact similar to the trends found in the single-layer counterparts for sodium chloride (**Figure 6.5b**), with a rising reference response due to refractive index alone and a falling sensing response due to charge screening effects.

As was discussed in Chapter 6, a large degree of response of the co-DMAPMAM cast film to humic acid (**Figure 6.9**) is sadly inevitable in the current sensing regime, due to the staining effect of humic acid on the gel. The sensing mode in the stacked waveguide exhibits a similar

response pattern with broadly unpredictable extents. The latter is due in part to small variations in the exposure time as each dose was applied until all evidence of solution exchange in the flow cell was eliminated, itself an unavoidable part of the sensor response rate. Of particular note, however, is the behaviour of the reference layer which exhibits almost precisely half the response integrity of the sensing layer (**Figure 6.9a**), and results in the reference-adjusted sensitivity matching the positive (and largely permanent) sensitivity slope of the reference layer. The change in response of the reference layer indicates that the two modes are not entirely independent – as discussed in Section 6.4.2 the cause may be due to interpenetration of the two polymer networks at the interface, or due to the reference mode being insufficiently contained in the polyacrylamide waveguide layer.

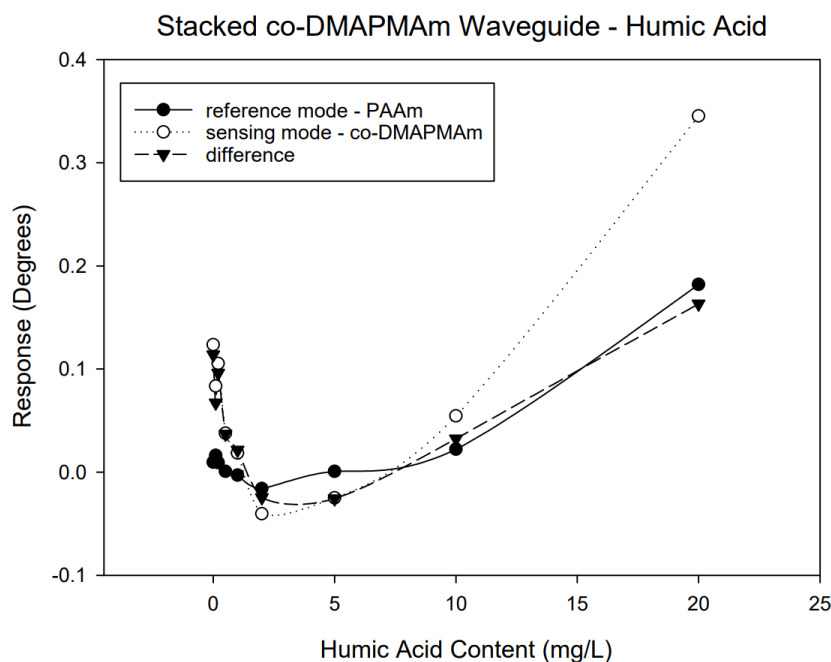


Figure 6.9 - Humic acid interferent studies performed on (a) internally referenced and (b) separate single-layer leaky waveguides.

When considering the overall utility of the internal referencing scheme for elimination, there appears to be mixed results. The internal referencing scheme was proven to be more effective with nonionic materials, particularly glycerol and urea, which do not interact with the ionic component of the co-DMAPMAM waveguide. Some issues were encountered with inorganic salts, especially sodium and calcium chloride, which interact directly or indirectly with the ionised dimethylamino groups in co-DMAPMAM gels and so alter the stacked sensor's response to provide a negative response. With the acidic dye humic acid, the sensor is particularly susceptible and sustains permanent alteration – the internally referenced sensor would be largely unable to operate in an environment containing humic acid. The outlier remains aluminium sulphate, which uniquely appears to not only interact minimally with the sensor but also be largely undetectable to polyacrylamide despite its refractive index.

There are therefore clear limitations to the reference layer in a practical context, and additional research is recommended before its limitations may be fully understood.

## **6.5. Summary**

In this chapter, the viability and pH sensitivity of synthetic, stacked leaky waveguides was demonstrated. Application of a linear polyacrylamide layer for internal referencing for pH is possible, and by a blank correction process the response curve of the pH-responsive leaky waveguide can be corrected to within 9.7% of the original result. The sensor is also impervious to nonionic contaminants, however susceptible to interference by inorganic salts and amine-reactive dyes.

Development of the stacked sensor has been brought to the point of an optimised and effective hydrogel, however there are limitations still to be explored, particularly the low overall response compared with the rarer and less ion-dense chitosan. In addition, there is the varied picture of interferant studies, where inconsistencies especially in sodium and calcium chloride response may need to be investigated further. Further attention would need to be paid to phenomena not properly investigated, as well – the most prominent of these is the behaviour of the polymer networks at their interface and the possibility of interpenetration that may have implications for the distinction between the two modes. Monitoring this interface may be possible by computational or by experimental means.

Future work for this sensor design would also provide those research avenues that could not be investigated due to time constraints, such as longer-term sensor longevity on the order of weeks or months. In addition, the acidic bounds of the pH sensitivity curve for co-DMAPMAM were not identified – although some experiments were performed looking into sensitivity below pH 3, severe inconsistencies were encountered that rendered precise assays impossible. With the use of the stacked sensor, along with finer measurements, an investigation could be performed to better understand what occurs at this range.

## **Chapter 7. CONCLUSIONS AND FUTURE WORK**

### **7.1. Introduction**

The aim of this chapter is to provide some summary of findings and potential significance of the work performed for the project. Suggested directions for future work are also indicated, including where attention will be placed for correction or resubmission of the thesis in addition to the examiner's comments. Sections 7.2 and 7.3 present the conclusions and the suggested future work respectively.

### **7.2. Conclusion**

The pH of water supply has consequences for microbial growth, precipitation, coagulation, disinfection and more, and has consequences for industrial, household and environmental factors. Within wastewater treatment an abnormal pH can endanger the microbial content of activated sludge treatment, hinder flocculation and settling, disrupt metal processes and may lead to plumbosolvency in water discharge or supply. The field of pH monitoring is presently well served by a range of both traditional and new sensing schemes and products, however there is room for further improvement. Given the original intention to incorporate pH detection into a free chlorine sensor, some sensing schemes are unavailable. Colorimetric sensors offer wide and rapid reporting but risk leaching-out (in aqueous media) or bleaching (by free chlorine) of the sensing moiety. Fluorometric sensors are precise but suffer from narrow pH ranges and both



bleaching and quenching. Chemomechanical sensors were therefore selected due to their wide ranges and (with optical rather than mechanical transduction) reasonable response times.

A need was therefore identified for a pH-responsive chemomechanical sensor and transduction scheme, and the leaky waveguide was selected as the core of the sensor design. Changes in pH create electrostatic swelling of a soft material, while a leaky mode confined within the material is monitored and therefore the degree of swelling reported in real time. It was originally intended that pH and free chlorine measurements could be combined by using common-path optical transduction, however the option existed to develop an internally referenced sensor for one or both by measuring nonspecific sensor response (indicating refractive index) with additional inert waveguide material.

To meet this need, an experimental means of producing polyacrylamide leaky waveguides was developed to act as a sensor base. Following optimisation, a regime for casting of polyacrylamide hydrogel waveguides and spincoating of linear polyacrylamide was developed and refractive index sensitivities in the 130-150 degrees/RIU range were demonstrated. By addition of ionisable copolymers to the linear polymer recipe, spin-coated hydrogels were shown to exhibit pH-dependent response and a linear range of up to 5 pH units was demonstrated.

In order to form a testbed for internally referenced, pH-sensitive waveguides, a polysaccharide-based sensor design was constructed using pH-inert agarose and cationic chitosan. Multilayered waveguides were produced by sequential spincoating, and both a buried (agarose) and upper

(chitosan) leaky mode were visualised and could be monitored through dye-doping. A pH sensor of sensitivity 0.280 degrees was produced, dependent on the selection of buffer, and a typical linear range of pH 4-8. By substituting agarose for linear polyacrylamide, a sensitivity of 0.273 degrees/pHU was retained with the more hard-wearing material.

A fully synthetic waveguide was requested despite the apparent effectiveness of chitosan. *N,N*-dimethylamino moieties were selected as the ionisable group to impart pH sensitivity, and optimisation processes were independently pursued with an acrylate and acrylamide comonomer. The former provided superior initial sensitivity at 0.132 degrees/pHU and a  $pK_aH$  closer to neutral at 7.38 but suffered from leaching in water which limited effective use. The latter was shown to produce a stable pH-sensitive waveguide of sensitivity 0.091 degrees/pHU and a typical linear range of pH 4-8. Additional studies of repeating buffer cycles and varying phosphate buffer concentration were performed. Stacked synthetic waveguides for pH sensitivity were then fabricated by spincoating linear polyacrylamide onto a cast pH-sensitive thin film. The sensor retains a pH sensitivity of 0.091 degrees/pHU, and a tested range of pH 4-8. Sensitivity to selected interferants was also assessed for both single-layer and internally referenced dimethyl-amino bearing leaky waveguides. The sensor was shown to be susceptible to dye staining and interference from monovalent salt solutions but effectively eliminated nonspecific interactions.

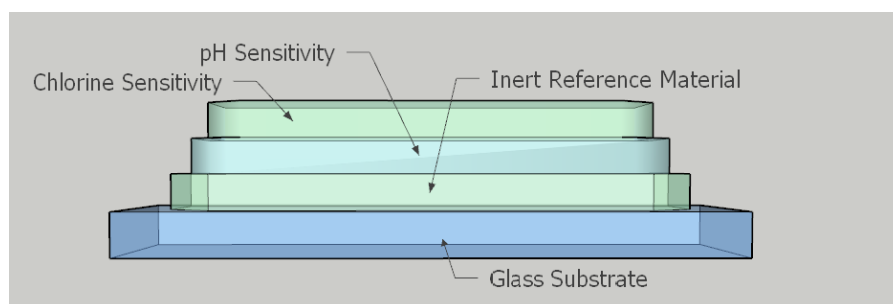
Due to unfortunate delays and an unanticipated reduction in scope, the product of this thesis is not entirely mature. However, applications for its findings may be found, especially in terms of utilising common-path internal referencing schemes, as discussed below.

### 7.3. Future Work

Regretfully the body of work intended to support this thesis was left incomplete due to factors such as the Covid-19 pandemic and its fallout. The sensing of free chlorine, as a direct continuation of this project's original aims, may be a good next step for this research. It was originally planned to use a cyanuric acid moiety as a sensing moiety to reversibly bind free chlorine molecules, forming the more optically dense cyanuric chloride moiety, a property normally employed for chlorine stabilisation in swimming pools by addition of cyanuric acid. Addition of cyanuric chloride to an amine-bearing linear polymer by a facile nucleophilic substitution was theorised and attempted, but due in part to global events in 2020 there was little opportunity to diagnose and resolve initial issues encountered with the reaction. An interesting issue to resolve would be protecting the cyanuric moiety from polymerisation or crosslinking reactions, or else avoiding damaging the hydrogel during the addition of the cyanuric pendant group.

With more than one analyte to detect, the opportunity may open to perform multiparameter measurements. While the creation of multiple selectively-treated channels has been reported by this research group in the past,<sup>19</sup> the stacked waveguide framework potentially permits a triple-layer stacked waveguide (**Figure 7.1**) by multiple spin-coating phases, demonstrated to be viable through the effectiveness of agarose-chitosan stacked leaky waveguides in Chapter 4. Such a layout was originally envisioned as a means of packaging pH and chlorine detection along with the internal referencing scheme, and would offer additional functionality to RI-

corrected common-path sensing without requiring techniques such as area-selective activation of photolabile groups. The technology, once demonstrated, may also be broadened out by incorporating recognition groups for other analytes in turn.



*Figure 7.1 - Demonstration of the layout of a hypothetical multianalyte stacked leaky waveguide, using pH and free chlorine sensitivity as model analytes.*

A number of minor elements and noted phenomena remain unexplored, particularly the behaviour of swelling and deswelling leaky waveguides, and future research may well be directed towards them. The most significant of these is the apparently inverted pH sensitivity curves encountered when comparing co-acrylic acid spun polymers with acidified gels during early tests (**Figure 3.22**) or in direct comparison between the behaviour of co-DMAEMA and co-DMAPMAm waveguides (**Figure 5.4** and **Figure 5.8**) – despite bearing the same pH-responsive functional groups, and in the case of acrylic acid bearing gels displaying the same (if inverted) pH sensitivity curve. Understanding the underpinnings of this behaviour should pave the way for better understanding of the sensor as a whole.

Other factors worth investigating include the longer-term longevity of sensors, especially determining whether the superior chitosan-based sensor may be viable after prolonged storage

or use. The question of the lower bound of the co-DMAPMAm sensitivity curve also remains unanswered due to the waveguides providing contradictory results and in cases being permanently damaged, therefore a more delicate test may be required to map its sensitivity curve overall. The listed gel thicknesses are also to be considered estimations - as mentioned in Section 3.2.3.1, swelling of the hydrogel will occur and so the cast thickness is considered a guideline thickness. More accurate data will require the research group to procure or access instrumentation capable of accurately determining the thickness of a transparent, waterlogged and deformable surface usually deposited onto another transparent surface – ellipsometry has recently been recommended.

Utilising the core achievement of the thesis as-is, the development of a scheme for internal referencing with hydrogel waveguides, was performed in parallel by other researchers within the unit. One promising method employs young interferometry, along with prefocusing of the analyte by electrophoresis.<sup>18</sup> An internal referencing scheme has also been utilised with a single-layer chitosan waveguide by photofunctionalisation, creating a visualisable grating for comparative monitoring of both the binding site rich and -poor areas of a single slab waveguide in an effective single-channel apparatus.<sup>19</sup> An internally referenced sensor of the type proposed in this project has the advantage of low cost, being manufactured from a microscope slide and relatively easy to procure reactants, and so may be suitable for biosensing of analytes in blood or other fluids where safe and rapid disposal of a contaminated sensor chip is a necessity.

Leaky waveguides are an active field, with phenomena such as diffraction modes still being discovered<sup>98</sup> and utilised,<sup>19, 99</sup> and so investigation of the internally referenced waveguide itself

may provide further advantages. It has been already mentioned that the interaction of polymer networks at the interface has not been experimentally investigated – exploration of the interface between hydrogels along with a more thorough understanding of the waveguide refractive index with depth may provide interesting insights into how the stacked hydrogel leaky waveguide functions, and perhaps find additional advantages specific to the design.

Finally, the option for constructing an effective pH sensor for waveguide operation remains open. In environments where salinity could be controlled for or is an unlikely factor, a chitosan based stacked leaky waveguide could leverage its wide linear range. Production of a compact, relatively inexpensive 3D-printed leaky waveguide instrument has already been reported,<sup>21</sup> making the option of sensitive on-line monitoring of pH more achievable still.

## REFERENCES

1. A. U. Alam, D. Clyne, H. Jin, N.-X. Hu and M. J. Deen, *ACS Sensors*, 2020, **5**, 412-422.
2. M. Hosseini, R. Heydari and M. Alimoradi, *Spectrochimica Acta Part A: Molecular and Biomolecular Spectroscopy*, 2014, **128**, 864-867.
3. D.-Y. Kim and H. J. Kim, *Sensors and Actuators B: Chemical*, 2015, **206**, 508-515.
4. A. Q. Maclin, M. D. Kim, S. A. Dergunov, E. Pinkhassik and E. Lindner, *Electroanalysis*, 2015, **27**, 733-744.
5. H.M. Department for Environment Food and Rural Affairs, *Journal*, 2015.
6. A. D. Eaton, L. S. Clesceri and A. E. Greenberg, *Standard Methods for the Examination of Water and Wastewater*, American Public Health Association, Washington, 19 edn., 1995.
7. C. B. Binnie and M. Kimber, *Basic Water Treatment*, Thomas Telford, London, 4 edn., 2009.
8. B. M. Gawlik and L. Alcalde-Sanz, *Joint Research Centre (European Commission)*, 2018.
9. D. L. Harp, *Current Technology of Chlorine Analysis for Water and Wastewater*, HACH Company, 1995.
10. European Council Directive, *Journal*, 1998.
11. UK Drinking Water Inspectorate, *Journal*, 2020.
12. American Public Health Association, *Standard Methods of Water Analysis*, Lancaster Press, Lancaster, 1905.
13. J. Xu, K. Feng and M. Weck, *Sensors and Actuators B: Chemical*, 2011, **156**, 812-819.
14. Y. Wu, N. Tam and M. H. Wong, *Marine pollution bulletin*, 2008, **57**, 727-734.
15. S. Zou, X. Wang, Y. Chen, H. Wan and Y. Feng, *Energy Conversion and Management*, 2016, **112**, 226-235.
16. R. Wang, M. Yan, H. Li, L. Zhang, B. Peng, J. Sun, D. Liu and S. Liu, *Advanced Materials*, 2018, **30**, 1800618.
17. Y. Xiong, J. Tan, C. Wang, J. Wu, Q. Wang, J. Chen, S. Fang and M. Duan, *Sensors and Actuators B: Chemical*, 2017, **245**, 674-682.
18. R. Gupta, E. Labella and N. J. Goddard, *Sensors and Actuators B: Chemical*, 2020, **321**, 128491.
19. A. K. Pal, N. J. Goddard, H. J. Dixon and R. Gupta, *Biosensors*, 2020, **10**.
20. R. Gupta, A. K. Pal and N. J. Goddard, *Journal of Physics: Conference Series*, 2021, **1919**, 012002.
21. N. J. Goddard, H. J. Dixon, N. Toole and R. Gupta, *IEEE Transactions on Instrumentation and Measurement*, 2020, **69**, 6390-6398.
22. P. Kassal, M. Zubak, G. Scheipl, G. J. Mohr, M. D. Steinberg and I. Murković Steinberg, *Sensors and Actuators B: Chemical*, 2017, **246**, 455-460.
23. S. Trupp, M. Alberti, T. Carofiglio, E. Lubian, H. Lehmann, R. Heuermann, E. Yacoub-George, K. Bock and G. J. Mohr, *Sensors and Actuators B: Chemical*, 2010, **150**, 206-210.

24. J. Guo, B. Zhou, C. Yang, Q. Dai and L. Kong, *Advanced Functional Materials*, 2019, **29**, 1902898.
25. S. K. Krishnan, E. Singh, P. Singh, M. Meyyappan and H. S. Nalwa, *RSC advances*, 2019, **9**, 8778-8881.
26. M. Franke, S. Leubner, A. Dubavik, A. George, T. Savchenko, C. Pini, P. Frank, D. Melnikau, Y. Rakovich, N. Gaponik, A. Eychemüller and A. Richter, *Nanoscale Research Letters*, 2017, **12**, 314.
27. J. Guo, Y. Luo, C. Yang and L. Kong, *Opt. Lett.*, 2018, **43**, 5443-5446.
28. L. H. H. Hsu, E. Hoque, P. Kruse and P. R. Selvaganapathy, *Applied Physics Letters*, 2015, **106**, 063102.
29. K. Deng, C. Bellmann, Y. Fu, M. Rohn, M. Guenther and G. Gerlach, *Sensors and Actuators B: Chemical*, 2018, **255**, 3495-3504.
30. R. Tabassum and B. D. Gupta, *Analyst*, 2015, **140**, 1863-1870.
31. S. K. Mishra, B. Zou and K. S. Chiang, *IEEE Journal of Selected Topics in Quantum Electronics*, 2017, **23**, 1-5.
32. P. Salazar, M. Martín, F. J. García-García, J. L. González-Mora and A. R. González-Elipe, *Sensors and Actuators B: Chemical*, 2015, **213**, 116-123.
33. H. Sharma, N. Kaur, A. Singh, A. Kuwar and N. Singh, *Journal of Materials Chemistry C*, 2016, **4**, 5154-5194.
34. D. Chang, K. Tram, B. Li, Q. Feng, Z. Shen, C. H. Lee, B. J. Salena and Y. Li, *Scientific Reports*, 2017, **7**.
35. W. Xu, S. Lu, Y. Chen, T. Zhao, Y. Jiang, Y. Wang and X. Chen, *Sensors and Actuators B: Chemical*, 2015, **220**, 326-330.
36. A. Leber, B. Cholst, J. Sandt, N. Vogel and M. Kolle, *Advanced Functional Materials*, 2019, **29**, 1802629.
37. A. T. Palin, *Journal (American Water Works Association)*, 1957, **49**, 873-880.
38. A. O. Beckman, *Journal*, 1936.
39. M. I. Khan, K. Mukherjee, R. Shoukat and H. Dong, *Microsystem Technologies*, 2017, **23**, 4391-4404.
40. Y. Qin, H.-J. Kwon, M. M. R. Howlader and M. J. Deen, *RSC Advances*, 2015, **5**, 69086-69109.
41. C. Wu, X. Liu and Y. Ying, *ACS sensors*, 2021, **6**, 1446-1460.
42. G. Gerlach and K.-F. Arndt, *Hydrogel sensors and actuators: engineering and technology*, Springer Science & Business Media, 2009.
43. R. Peltomaa, B. Glahn-Martínez, E. Benito-Peña and M. C. Moreno-Bondi, *Sensors*, 2018, **18**, 4126.
44. M. Zourob, S. Elwary and A. P. Turner, *Principles of bacterial detection: biosensors, recognition receptors and microsystems*, Springer Science & Business Media, 2008.
45. J. Escorihuela, M. A. n. González-Martínez, J. L. López-Paz, R. Puchades, A. Maquieira and D. Gimenez-Romero, *Chemical Reviews*, 2015, **115**, 265-294.
46. T. M. Jørgensen, S. T. Jepsen, H. S. Sørensen, A. K. Di Gennaro and S. R. Kristensen, *Sensors and Actuators B: Chemical*, 2015, **220**, 1328-1337.
47. M. N. Kammer, I. R. Olmsted, A. K. Kussrow, M. J. Morris, G. W. Jackson and D. J. Bornhop, *Analyst*, 2014, **139**, 5879-5884.
48. A. Kussrow, C. S. Enders and D. J. Bornhop, *Analytical chemistry*, 2012, **84**, 779-792.
49. G. Lippmann, *Journal de Physique Théorique et Appliquée*, 1894, **3**, 97-107.
50. D. Gabor, *Proceedings of the Royal Society of London. Series A. Mathematical and Physical Sciences*, 1949, **197**, 454-487.



51. A. K. Yetisen, H. Butt, L. R. Volpatti, I. Pavlichenko, M. Humar, S. J. Kwok, H. Koo, K. S. Kim, I. Naydenova and A. Khademhosseini, *Biotechnology advances*, 2016, **34**, 250-271.
52. B. Shivananju, M. K. Priyadarshi, D. R. Mahapatra, G. Hegde and S. Asokan, presented in part at the Physics and Technology of Sensors (ISPTS), 2012 1st International Symposium on, 2012.
53. Y. Zhao, X. Zhao and Z. Gu, *Advanced Functional Materials*, 2010, **20**, 2970-2988.
54. J. H. Holtz and S. A. Asher, *Nature*, 1997, **389**, 829-832.
55. S. A. Asher, S. F. Peteu, C. E. Reese, M. Lin and D. Finegold, *Analytical and bioanalytical chemistry*, 2002, **373**, 632-638.
56. A. C. Sharma, T. Jana, R. Kesavamoorthy, L. Shi, M. A. Virji, D. N. Finegold and S. A. Asher, *Journal of the American Chemical Society*, 2004, **126**, 2971-2977.
57. K. Ueno, K. Matsubara, M. Watanabe and Y. Takeoka, *Advanced Materials*, 2007, **19**, 2807-2812.
58. C. I. Aguirre, E. Reguera and A. Stein, *Advanced Functional Materials*, 2010, **20**, 2565-2578.
59. C. Ma, Y. Jiang, X. Yang, C. Wang, H. Li, F. Dong, B. Yang, K. Yu and Q. Lin, *ACS applied materials & interfaces*, 2013, **5**, 1990-1996.
60. S. J. Yeo, F. Tu, S.-h. Kim, G.-R. Yi, P. J. Yoo and D. Lee, *Soft Matter*, 2015, **11**, 1582-1588.
61. J. H. Holtz, J. S. Holtz, C. H. Munro and S. A. Asher, *Analytical Chemistry*, 1998, **70**, 780-791.
62. Z. Samavati, T. N. Borhani, A. Samavati, A. F. Ismail, M. A. Rahman, M. H. D. Othman and M. Soleymani, *Optical Fiber Technology*, 2021, **67**, 102730.
63. S. Sharma and R. Verma, *Journal of Optics*, 2022, 1-6.
64. P. Panda and S. Chakroborty, *International Journal of Environmental Analytical Chemistry*, 2022, 1-16.
65. J. Jang, K. Kang, N. Raeis-Hosseini, A. Ismukhanova, H. Jeong, C. Jung, B. Kim, J. Y. Lee, I. Park and J. Rho, *Advanced Optical Materials*, 2020, **8**, 1901932.
66. I. Kasik, J. Mrazek, O. Podrazky, M. Seidl, J. Aubrecht, P. Tobiska, M. Pospisilova, V. Matejec, B. Kovacs and A. Markovics, *Sensors and Actuators B: Chemical*, 2009, **139**, 139-142.
67. N. H. Mack, J. W. Wackerly, V. Malyarchuk, J. A. Rogers, J. S. Moore and R. G. Nuzzo, *Nano letters*, 2007, **7**, 733-737.
68. M. Nuopponen and H. Tenhu, *Langmuir*, 2007, **23**, 5352-5357.
69. P. Wang, L. Zhang, Y. Xia, L. Tong, X. Xu and Y. Ying, *Nano letters*, 2012, **12**, 3145-3150.
70. Y. Li and L. Tong, *Opt. Lett.*, 2008, **33**, 303-305.
71. L. Tong, R. R. Gattass, J. B. Ashcom, S. He, J. Lou, M. Shen, I. Maxwell and E. Mazur, *Nature*, 2003, **426**, 816-819.
72. L. Tong and E. Mazur, *Journal of Non-Crystalline Solids*, 2008, **354**, 1240-1244.
73. S. K. Mishra and B. D. Gupta, *Analytical Methods*, 2014, **6**, 5191-5197.
74. A. K. Mallik, G. Farrell, D. Liu, V. Kavungal, Q. Wu and Y. Semenova, *Journal of Lightwave Technology*, 2018, **36**, 2667-2674.
75. Z. F. Zhang and Y. Zhang, *Optics & Laser Technology*, 2015, **74**, 16-19.
76. H. Luo, L. Liang, X. Ma, N. Liu, S. Huang and H. Sun, *IEEE Sensors Journal*, 2018, **18**, 8022-8027.
77. A. Suzuki and T. Tanaka, *Nature*, 1990, **346**, 345-347.

78. M. Choi, J. W. Choi, S. Kim, S. Nizamoglu, S. K. Hahn and S. H. Yun, *Nature photonics*, 2013, **7**, 987-994.
79. V. S. Raghuvanshi and G. Garnier, *Advances in Colloid and Interface Science*, 2019, **274**, 102044.
80. M. S. Akram, R. Daly, F. d. Cruz Vasconcellos, A. K. Yetisen, I. Hutchings and E. A. Hall, *Lab-on-a-chip devices and micro-total analysis systems*, 2015, 161-195.
81. C. D. Chin, V. Linder and S. K. Sia, *Lab on a Chip*, 2012, **12**, 2118-2134.
82. S. Shabahang, S. Kim and S. H. Yun, *Advanced functional materials*, 2018, **28**, 1706635.
83. J. K. Kim, H. J. Kim, J.-Y. Chung, J.-H. Lee, S.-B. Young and Y.-H. Kim, *Archives of pharmacal research*, 2014, **37**, 60-68.
84. J. P. Maranchi, M. M. Trexler, Q. Guo and J. H. Elisseeff, *International materials reviews*, 2014, **59**, 264-296.
85. J. L. Drury and D. J. Mooney, *Biomaterials*, 2003, **24**, 4337-4351.
86. F. Abbasi, H. Mirzadeh and A. A. Katbab, *Journal*, 2001.
87. T. Niemelä and M. Kellomäki, in *Bioactive Glasses*, Elsevier, 2011, pp. 227-245.
88. A. K. Manocchi, P. Domachuk, F. G. Omenetto and H. Yi, *Biotechnology and bioengineering*, 2009, **103**, 725-732.
89. D. Shan, C. Zhang, S. Kalaba, N. Mehta, G. B. Kim, Z. Liu and J. Yang, *Biomaterials*, 2017, **143**, 142-148.
90. J. Guo, X. Liu, N. Jiang, A. K. Yetisen, H. Yuk, C. Yang, A. Khademhosseini, X. Zhao and S. H. Yun, *Advanced Materials*, 2016, **28**, 10244-10249.
91. S. J. Kwok, S. Forward, C. M. Wertheimer, A. C. Liapis, H. H. Lin, M. Kim, T. G. Seiler, R. Birngruber, I. E. Kochevar and T. Seiler, *Investigative ophthalmology & visual science*, 2019, **60**, 2563-2570.
92. S. P. Sivaraman and A. M. Mohan, *Microporous and Mesoporous Materials*, 2021, **326**, 111390.
93. T. Liu, W. Wang, D. Jian, J. Li, H. Ding, D. Yi, F. Liu and S. Wang, *Sensors and Actuators B: Chemical*, 2019, **301**, 127168.
94. A. K. Yetisen, I. Naydenova, F. da Cruz Vasconcellos, J. Blyth and C. R. Lowe, *Chemical reviews*, 2014, **114**, 10654-10696.
95. R. B. Figueira, J. M. de Almeida, B. Ferreira, L. Coelho and C. J. Silva, *Materials Advances*, 2021.
96. Y. Jiang, J. Ma, J. Lv, H. Ma, H. Xia, J. Wang, C. Yang, M. Xue, G. Li and N. Zhu, *ACS sensors*, 2018, **4**, 152-160.
97. M. Saleem and K. H. Lee, *Rsc Advances*, 2015, **5**, 72150-72287.
98. N. J. Goddard and R. Gupta, *Sensors and Actuators B: Chemical*, 2020, **309**, 127776.
99. R. Gupta and N. J. Goddard, *Analyst*, 2021, **146**, 4964-4971.
100. T. Okamoto and I. Yamaguchi, *Optical Review*, 1997, **4**, 354-357.
101. J. P. Hulme, N. J. Goddard and C. Lu, *Sensors and Actuators B: Chemical*, 2011, **160**, 1508-1513.
102. V. Lazarova, P. Savoye, M. L. Janex, E. R. Blatchley and M. Pommepuy, *Water Science and Technology*, 1999, **40**, 203-213.
103. Y. Tang, Y. Su, N. Yang, L. Zhang and Y. Lv, *Analytical Chemistry*, 2014, **86**, 4528-4535.
104. G. Connell, *Water Disinfection Series: The Chlorination/Chloramination Handbook*, American Water Works Association, Denver, 1996.
105. N. A. George, A. M. Paul and M. S. Saranya, *Optik*, 2014, **125**, 301-303.

106. M. Tikkanen, *Guidance Manual for disposal of chlorinated water*, American Water Works Association, 2001.
107. M. Tachikawa, C. Sayama, K. Saita, M. Tezuka and R. Sawamura, *Water Research*, 2002, **36**, 2547-2554.
108. M. Szili, I. Kasik, V. Matejec, G. Nagy and B. Kovacs, *Sensors and Actuators B: Chemical*, 2014, **192**, 92-98.
109. C. Piraud, E. Mwarania, G. Wylangowski, J. Wilkinson, K. O'Dwyer and D. J. Schiffrin, *Analytical Chemistry*, 1992, **64**, 651-655.
110. M. Franson, A. Greenberg, R. Trussel and L. S. Clesceri, *Standard Methods for the Examination of Water and Wastewater*, American Public Health Association, Washington, 1985.
111. A. T. Palin, *J Inst Water Eng*, 1967, **21**, 537-545.
112. M. Szili, I. Kasik, V. Matejec, G. Nagy and B. Kovacs, *Sensors and Actuators, B: Chemical*, 2014, **192**, 92-98.
113. T. Soundappan, K. Haddad, S. Kavadiya, R. Raliya and P. Biswas, *Applied Nanoscience*, 2017, **7**, 645-653.
114. J.-H. Shim, J.-S. Lee, G.-S. Cha and H.-H. Nam, *Bulletin of the Korean Chemical Society*, 2010, **31**, 1583-1588.
115. R. A. Potyrailo, W. G. Morris, R. Wroczynski, L. Hassib, P. Miller, B. Dworken, A. M. Leach, S. Boyette and C. Xiao, *Sensors and Actuators B: Chemical*, 2009, **136**, 203-208.
116. L. X. Kong, A. Perebikovskiy, J. Moebius, L. Kulinsky and M. Madou, *Journal of laboratory automation*, 2016, **21**, 323-355.
117. M. Belz, W. J. Boyle, K.-F. Klein and K. T. Grattan, *Sensors and Actuators B: Chemical*, 1997, **39**, 380-385.
118. G. Robinson, J. Attridge, J. Deacon and S. Whiteley, *Sensors and Actuators B: Chemical*, 1993, **11**, 235-238.
119. Z.-F. Zhang, H. Cui, C.-Z. Lai and L.-J. Liu, *Analytical chemistry*, 2005, **77**, 3324-3329.
120. M. Yuqing, C. Jianrong and F. Keming, *Journal of Biochemical and Biophysical Methods*, 2005, **63**, 1-9.
121. L. Van der Schueren and K. De Clerck, *Coloration Technology*, 2012, **128**, 82-90.
122. pH Electrode Cleaning & Maintenance Guide, [www.hach.com/asset-get.download.jsa?id=11147536803](http://www.hach.com/asset-get.download.jsa?id=11147536803), (accessed 12-12-17, 2017).
123. D. Wencel, M. Barczak, P. Borowski and C. McDonagh, *Journal of Materials Chemistry*, 2012, **22**, 11720-11729.
124. D. Jankowska, M. Bannwarth, C. Schulenburg, G. Faccio, K. Maniura-Weber, R. Rossi, L. Scherer, M. Richter and L. Boesel, *Biosensors and Bioelectronics*, 2017, **87**, 312-319.
125. Z. Zhang and S. Achilefu, *Chemical Communications*, 2005, 5887-5889.
126. R. Heydari, M. Hosseini, A. Amraei and A. Mohammadzadeh, *Materials Science and Engineering: C*, 2016, **61**, 333-337.
127. N. Chamkouri, A. Niazi and V. Zare-Shahabadi, *Spectrochimica Acta Part A: Molecular and Biomolecular Spectroscopy*, 2016, **156**, 105-111.
128. J. Geltmeyer, G. Vancoillie, I. Steyaert, B. Breyne, G. Cousins, K. Lava, R. Hoogenboom, K. De Buysser and K. De Clerck, *Advanced Functional Materials*, 2016, **26**, 5987-5996.
129. S. Cerveny, J. Colmenero and A. Alegría, *Macromolecules*, 2005, **38**, 7056-7063.

130. M. de Dood, J. Kalkman, C. Strohhofer, J. Michielsen and J. Elsken, *Journal of Physical Chemistry B - J PHYS CHEM B*, 2003, **107**.
131. H. Wang, J. Wei and G. P. Simon, *Environmental Science & Technology*, 2014, **48**, 4214-4215.
132. S. Zhao, *Environmental Science & Technology*, 2014, **48**, 4212-4213.
133. C. Shen and C. Zhong, *Sensors and Actuators A: Physical*, 2011, **170**, 51-54.
134. X. Sang, C. Yu, T. Mayteevarunyoo, K. Wang, Q. Zhang and P. L. Chu, *Sensors and Actuators B: Chemical*, 2007, **120**, 754-757.
135. I. Yulianti, A. S. M. Supa'at and S. M. Idrus, 2014.
136. M.-L. Zhang, F. Jin, M.-L. Zheng and X.-M. Duan, *Rsc Advances*, 2014, **4**, 20567-20572.
137. J.-T. Zhang, Z. Cai, D. H. Kwak, X. Liu and S. A. Asher, *Analytical Chemistry*, 2014, **86**, 9036-9041.
138. Y. Zhao, X. Zhao, B. Tang, W. Xu and Z. Gu, *Langmuir*, 2010, **26**, 6111-6114.
139. N. Sai, B. Ning, G. Huang, Y. Wu, Z. Zhou, Y. Peng, J. Bai, G. Yu and Z. Gao, *Analyst*, 2013, **138**, 2720-2728.
140. K. I. MacConaghy, D. M. Chadly, M. P. Stoykovich and J. L. Kaar, *Analytical Chemistry*, 2015, **87**, 3467-3475.
141. J.-D. Colladon, *Comptes Rendus*, 1842, **15**.
142. J. Hecht, *Optics and Photonics News*, 1999, **10**, 26.
143. M. Popovic, T. Barwicz, E. Ippen and F. Kärtner, 2006, DOI: 10.1109/CLEO.2006.4628157.
144. M. Chin, *Opt. Express*, 2003, **11**, 1724-1730.
145. C. Zhou, M. K. Hedayati and A. Kristensen, *Opt. Express*, 2018, **26**, 24372-24383.
146. A. Kumar, C. Wang, F.-Y. Meng, C.-P. Jiang, G.-F. Yan, M. Zhao, C.-Q. Jing and L. Wang, *ACS Sensors*, 2020, **5**, 3939-3948.
147. H. Tsuda, *Measurement Science and Technology*, 2006, **17**, 645.
148. B. MacCraith, V. Ruddy, C. Potter, B. O'Kelly and J. McGilp, *Electronics letters*, 1991, **27**, 1247-1248.
149. F. Goos and H. Hänchen, *Annalen der Physik*, 1947, **436**, 333-346.
150. E. Hecht, *Optics*, Pearson Education, Incorporated, 2017.
151. K. Y. Bliokh and A. Aiello, *Journal of Optics*, 2013, **15**, 014001.
152. D. Nguyen, *Undergraduate Journal of Mathematical Modeling: One + Two*, 2020, **11**.
153. J. Homola, S. S. Yee and G. Gauglitz, *Sensors and Actuators B: Chemical*, 1999, **54**, 3-15.
154. H. H. Nguyen, J. Park, S. Kang and M. Kim, *Sensors*, 2015, **15**, 10481-10510.
155. R. Gupta and N. J. Goddard, *Sensors and Actuators B: Chemical*, 2017, **244**, 549-558.
156. R. Gupta, B. Bastani, N. J. Goddard and B. Grieve, *Analyst*, 2013, **138**, 307-314.
157. P. Lu and Y.-L. Hsieh, *Polymer*, 2009, **50**, 3670-3679.
158. I. Y. Dmitriev, P. V. Vlasov, M. F. Lebedeva, I. V. Gofman, V. Y. Elokhovskiy, E. N. Popova, M. S. Lozhkin, E. N. Vlasova, I. S. Kuryndin and M. A. Smirnov, *Materials Chemistry and Physics*, 2017, **187**, 88-95.
159. C. A. Grattoni, H. H. Al-Sharji, C. Yang, A. H. Muggeridge and R. W. Zimmerman, *Journal of Colloid and Interface Science*, 2001, **240**, 601-607.
160. W. J. Im, B. B. Kim, J. Y. Byun, H. M. Kim, M.-G. Kim and Y.-B. Shin, *Sensors and Actuators B: Chemical*, 2012, **173**, 288-294.
161. A. Mizutani, S. Urakawa and H. Kikuta, *Appl. Opt.*, 2015, **54**, 4161-4166.

162. D. C. Schoenmakers, A. E. Rowan and P. H. J. Kouwer, *Nature Communications*, 2018, **9**, 2172.
163. M. G. Cascone, L. Lazzeri, E. Sparvoli, M. Scatena, L. P. Serino and S. Danti, *J Mater Sci Mater Med*, 2004, **15**, 1309-1313.
164. Q. Ling, W. Liu, J. Liu, L. Zhao, Z. Ren and H. Gu, *ACS Applied Materials & Interfaces*, 2022, **14**, 24741-24754.
165. M. Baklanov, K. Mogilnikov, V. Polovinkin and F. Dultsev, *J. Vac. Sci. Technol. B*, 2000, **18**, 1385-1391.
166. T. Lü, G. Shan and S. Shang, *Journal of Applied Polymer Science*, 2010, **118**, 2572-2581.
167. H. Zuo, Z.-B. Li, B.-X. Zhao, J.-Y. Miao, L.-J. Meng, K.-W. Jang, C.-J. Ahn, D.-H. Lee and D.-S. Shin, *Highly Efficient Microwave-assisted Aminolysis of Epoxides in Water*, 2011.
168. X. Wu, Y. Li, N. Li, J. Zhou and X. Hao, *High Performance Polymers*, 2017, **29**, 1165-1174.
169. F. Colangelo, P. Russo, F. Cimino, R. Cioffi, I. Farina, F. Fraternali and L. Feo, *Composites Part B: Engineering*, 2017, **126**, 100-107.
170. L. Matějka, *Macromolecules*, 2000, **33**, 3611-3619.
171. Shivani, B. Pujala and A. K. Chakraborti, *The Journal of organic chemistry*, 2007, **72**, 3713-3722.
172. I. Dmitriev, I. Kuryndin, N. Bobrova and M. Smirnov, *Materials Today Communications*, 2015, **4**, 93-100.
173. S. Fouad, N. Sabri, Z. A. Zahid Jamal and P. Poopalan, *Surface plasmon resonance sensor sensitivity enhancement using gold-dielectric material*, 2017.
174. S. Neiser, K. I. Draget and O. Smidsrød, *Food Hydrocolloids*, 1999, **13**, 445-458.
175. N. Biçak, N. Açıkkaya and G. Koza, *Polymer Bulletin*, 1997, **39**, 459-464.
176. A. S. P. Azzouz and R. D. Sulayman, *Iraqi National Journal of Chemistry*, 2012, **46**, 215-228.
177. J. Clayden, N. Greeves and S. Warren, *Organic Chemistry*, OUP Oxford, 2012.
178. H. Dong, H. Du and X. Qian, *The Journal of Physical Chemistry B*, 2009, **113**, 12857-12859.
179. E. Turan and T. Çaykara, *Journal of Applied Polymer Science*, 2007, **106**, 2000-2007.
180. C. Wang, Y. Bu, S. Guo, Y. Lu, B. Sun and Z. Shen, *Cement and Concrete Composites*, 2019, **96**, 154-162.
181. C. Kroh, R. Wuchrer, M. Günther, T. Härtling and G. Gerlach, *Journal of Sensors and Sensor Systems*, 2018, **7**, 51-55.
182. T. Boyaci and N. Orakdogan, *Advances in Polymer Technology*, 2017, **36**, 442-454.
183. N. S. Okten, C. C. Canakci and N. Orakdogan, *European Polymer Journal*, 2019, **114**, 176-188.
184. A. Bhat, B. Smith, C.-Z. Dinu and A. Guiseppi-Elie, *Materials Science and Engineering: C*, 2019, **98**, 89-100.
185. M. A. Mohammed, J. T. M. Syeda, K. M. Wasan and E. K. Wasan, *Pharmaceutics*, 2017, **9**, 53.
186. J. L. O'Conner, M. F. Wade and Y. Zhou, *Biotechniques*, 1991, **10**, 300-302.
187. M. Beaumont, R. Tran, G. Vera, D. Niedrist, A. Rousset, R. Pierre, V. P. Shastri and A. Forget, *Biomacromolecules*, 2021, **22**, 1027-1052.
188. P. Zucca, R. Fernandez-Lafuente and E. Sanjust, *Molecules*, 2016, **21**, 1577.
189. R. Gupta and N. J. Goddard, *Sensors and Actuators B: Chemical*, 2016, **237**, 1066-1075.

190. R. R. Melo, R. C. Alnoch, A. F. L. Vilela, E. M. Souza, N. Krieger, R. Ruller, H. H. Sato and C. Mateo, *Molecules*, 2017, **22**.
191. G. Buhus, M. Popa and J. Desbrieres, *Journal of Bioactive and Compatible Polymers - J BIOACT COMPAT POLYM*, 2009, **24**, 525-545.
192. Y. Yang, G. Chen, P. Murray and H. Zhang, *SN Applied Sciences*, 2020, **2**, 435.
193. C. Ryan, E. Alcock, F. Buttimer, M. Schmidt, D. Clarke, M. Pemble and M. Bardosova, *Sci Technol Adv Mater*, 2017, **18**, 528-540.
194. R. Gupta and N. Goddard, *17th International Conference on Miniaturized Systems for Chemistry and Life Sciences, MicroTAS 2013*, 2013, **3**, 1490-1492.
195. T. Hunter, *Philosophical Transactions of the Royal Society B: Biological Sciences*, 2012, **367**, 2513-2516.
196. M. Malmqvist, *Carbohydrate Research*, 1978, **62**, 337-348.
197. J. Brandrup, E. H. Immergut, E. A. Grulke, A. Abe and D. R. Bloch, *Polymer handbook*, Wiley New York, 1999.
198. Y. Huang, P. Yong, Y. Chen, Y. Gao, W. Xu, Y. Lv, L. Yang, R. L. Reis, R. P. Pirraco and J. Chen, *RSC Advances*, 2017, **7**, 28711-28722.
199. S. Guo, Y. Qiao, W. Wang, H. He, L. Deng, J. Xing, J. Xu, X.-J. Liang and A. Dong, *Journal of Materials Chemistry*, 2010, **20**, 6935-6941.
200. S. Hajebi, A. Abdollahi, H. Roghani-Mamaqani and M. Salami-Kalajahi, *Polymer*, 2019, **180**, 121716.
201. G. Demirel and R. Klitzing, *Chemphyschem : a European journal of chemical physics and physical chemistry*, 2013, **14**.
202. A. Mignon, D. Devisscher, J. Vermeulen, D. Snoeck, P. Dubruel, S. Van Vlierberghe and N. De Belie, *Bio-based pH-responsive superabsorbent polymers for self-healing cracks in concrete*, 2016.
203. T. Kulkarni and G. Slaughter, 2017.
204. E. Omidinia, N. Shadjou and M. Hasanzadeh, *Applied Biochemistry and Biotechnology*, 2014, **172**, 2070-2080.
205. J. Zhang, W. Li, J. Lee, K.-C. Loh, Y. Dai and Y. W. Tong, *Energy*, 2017, **137**, 479-486.
206. K. Podual, F. J. Doyle and N. A. Peppas, *Polymer*, 2000, **41**, 3975-3983.
207. B. Kang, Y.-d. Dai, X.-h. Shen and D. Chen, *Materials Letters*, 2008, **62**, 3444-3446.
208. F. Sher, A. Malik and H. Liu, *Journal of Environmental Chemical Engineering*, 2013, **1**, 684-689.
209. C. J. Crook, A. Smith, R. A. Jones and A. J. Ryan, *Physical Chemistry Chemical Physics*, 2002, **4**, 1367-1369.
210. A. Rodriguez-Sanchez, J. C. Leyva-Diaz, J. Gonzalez-Lopez and J. M. Poyatos, *Chemical Engineering Journal*, 2018, **336**, 102-111.
211. L. Zhang, J. Wang, G. Fu and Z. Zhang, *Journal of Cleaner Production*, 2020, **276**, 123203.
212. Q. He, H. Wang, L. Chen, S. Gao, W. Zhang, J. Song and J. Yu, *Journal of Hazardous Materials*, 2020, **384**, 121454.
213. G. Colacicco, *Nature*, 1963, **198**, 583-584.
214. H. Yuan, Z. Qiu, H. Qiu and R. Zhang, *Polymer Engineering & Science*, 2017, **57**, 69-77.
215. R. L. Mikkelsen, *Fertilizer research*, 1994, **38**, 53-59.
216. R. L. Mikkelsen, A. Behel and H. Williams, *Fertilizer research*, 1993, **36**, 55-61.

217. E. A. López-Maldonado, M. T. Oropeza-Guzman, J. L. Jurado-Baizaval and A. Ochoa-  
Terán, *Journal of Hazardous Materials*, 2014, **279**, 1-10.
218. M. Mohammadian, R. Sahraei and M. Ghaemy, *Chemosphere*, 2019, **225**, 259-269.
219. M. Busch, N. Simic and E. Ahlberg, *Phys Chem Chem Phys*, 2019, **21**, 19342-19348.